

**Strontium Isotope Stratigraphy of the Platreef at Turfspruit, Northern Limb,
Bushveld Igneous Complex**

by

Cedric Mayer

A thesis submitted in partial fulfillment
of the requirements for the degree of
Master of Science (MSc) in Geology

The Faculty of Graduate Studies
Laurentian University
Sudbury, Ontario, Canada

© Cedric Mayer, 2018

THESIS DEFENCE COMMITTEE/COMITÉ DE SOUTENANCE DE THÈSE
Laurentian University/Université Laurentienne
 Faculty of Graduate Studies/Faculté des études supérieures

Title of Thesis Titre de la thèse	Strontium Isotope Stratigraphy of the Platreef at Turfspruit, Northern Limb, Bushveld Complex	
Name of Candidate Nom du candidat	Mayer, Cedric Claude Joseph	
Degree Diplôme	Master of Science	
Department/Program Département/Programme	Geology	Date of Defence Date de la soutenance October 25, 2018

APPROVED/APPROUVÉ

Thesis Examiners/Examineurs de thèse:

Dr. Pedro Jugo
(Supervisor/Directeur(trice) de thèse)

Dr. Matt Leybourne
(Committee member/Membre du comité)

Dr. Danie Grobler
(Committee member/Membre du comité)

Dr. Wolfgang Maier
(External Examiner/Examineur externe)

Approved for the Faculty of Graduate Studies
 Approuvé pour la Faculté des études supérieures
 Dr. David Lesbarrères
 Monsieur David Lesbarrères
 Dean, Faculty of Graduate Studies
 Doyen, Faculté des études supérieures

ACCESSIBILITY CLAUSE AND PERMISSION TO USE

I, **Cedric Claude Joseph Mayer**, hereby grant to Laurentian University and/or its agents the non-exclusive license to archive and make accessible my thesis, dissertation, or project report in whole or in part in all forms of media, now or for the duration of my copyright ownership. I retain all other ownership rights to the copyright of the thesis, dissertation or project report. I also reserve the right to use in future works (such as articles or books) all or part of this thesis, dissertation, or project report. I further agree that permission for copying of this thesis in any manner, in whole or in part, for scholarly purposes may be granted by the professor or professors who supervised my thesis work or, in their absence, by the Head of the Department in which my thesis work was done. It is understood that any copying or publication or use of this thesis or parts thereof for financial gain shall not be allowed without my written permission. It is also understood that this copy is being made available in this form by the authority of the copyright owner solely for the purpose of private study and research and may not be copied or reproduced except as permitted by the copyright laws without written authority from the copyright owner.

Abstract

The origin of the Platreef in the Northern Limb of the Bushveld Igneous Complex (BIC) and its correlation as the stratigraphic equivalent of the Merensky Reef in the Eastern and Western limbs has been long debated. Strontium isotope stratigraphy across the Platreef was completed on drillcore from the Turfspruit farm to test a possible correlation with the Merensky Reef. The results show a significant $^{87}\text{Sr}/^{86}\text{Sr}_i$ shift from ~ 0.7060 to 0.7090 through the mineralized section of the Upper Platreef, which decreases to 0.7074 and then increases again and stabilize at ~ 0.708 in the Main Zone. This matches the isotopic shift previously documented through the Merensky and Bastard Cyclic units in the Eastern and Western limbs of the BIC. This coincident shift in $^{87}\text{Sr}/^{86}\text{Sr}_i$ is substantive evidence to confirm that the mineralized intervals in the Upper Platreef are the stratigraphic equivalent to the Merensky and Bastard Cyclic units. This thesis also documents the presence of micro-cycles within magmatic units (up to 350 cycles identified through 215 meters). Working hypotheses linking the micro-cycles to thickness of mineralization are suggested. Testing those hypotheses are outside of the main scope of this study and are suggested for future work.

Keywords

Bushveld Igneous Complex, Northern Limb, Platreef, Strontium Isotope Stratigraphy, Magmatic Cycles.

Co-Authorship Statement

Several collaborators contributed to the work presented. The project was conceived by Dr. Jugo and fine-tuned with feedback from Dr. Grobler and Dr. Leybourne. Drill core logging and sample selection was completed by the candidate under supervision of Dr. Jugo. Whole-rock sample preparation was completed by the candidate and outsourced to ALS Geochemistry, Vancouver, Canada. Sample preparation for whole rock strontium isotope analyses were completed by the candidate guided by Dr. Voinot, Dr. Chipley and Dr. Kyser. Analyses were completed by Dr. Voinot at Queen's Facilities for Isotope Research (QFIR). Data reduction and corrections were completed by the candidate with the assistance of Dr. Voinot. Sample preparation, analyses and data correction for *in-situ* strontium isotope analyses on plagioclase were completed by the candidate. Laboratory protocols (calibration, fine-tuning) for *in-situ* Sr isotope analyses at QFIR were completed by the candidate and Dr. Voinot. Initial interpretation for the isotope data was completed by the candidate with input from Drs. Jugo, Leybourne and Grobler. Subsequently, the advisors edited subsequent drafts of the thesis and provided scientific input. The collaborators provided guidance and supervision with laboratory analyses.

Acknowledgements

Dr. Jugo and Dr. Leybourne are acknowledged for providing me with the chance to work on this project. They both provided their expertise, guidance and instruction throughout the entire project. Dr. Grobler's expertise in the Bushveld Igneous Complex, specifically the Northern Limb, was of great help throughout the project. This project was financially supported by the Queen Elizabeth II Diamond Jubilee Scholarship, Ivanplats, and NSERC. Logistical support was provided by the Goodman School of Mines, especially M. Adibpour, D. Leroy and B. Jago. Also, logistical support by Ivanplats while in South Africa is greatly appreciated, especially from D. du Plessis, A. Crossingham and T. Dunnet. Analytical work on strontium isotopes at Queen's University could not have been completed without the help of D. Chipley, A. Voinot and K. Kyser. D. Crabtree is acknowledged for his help with electron probe microanalyses at the Ontario Geolabs and J. Petrus for his help in completing the LA-ICP-MS element distribution maps. Lastly, E. Keir-Sage for his help collecting some of the samples at Ivanplats.

Table of Contents

Abstract	iii
Co-Authorship Statement	iv
Acknowledgements	v
List of Figures	ix
List of Tables	xi
1. Introduction to thesis	1
1.1 General background and outline of the research problem.....	1
1.2 Research question and significance.....	1
1.3 Structure of thesis.....	2
1.4 Statement of responsibilities	2
1.5 Statement of original contributions	3
2. Background	5
2.1 Bushveld Igneous Complex	5
2.1.1 Magmatic stratigraphy of the RLS	5
2.2 Northern Limb geology	8
2.3 Mineralization in the Rustenburg Layered Suite.....	11
2.3.1 The Merensky Reef	11
2.3.2 The UG2 chromitite	12
2.3.3 The Pseudoreef.....	12
2.3.4 Platreef	13
2.4 Strontium isotopic stratigraphy of the transition from the Upper Critical Zone to the Main Zone.....	13

2.4.1 Eastern and Western limbs	13
2.4.2 Northern Limb	16
3. Methods	18
3.1. Core logging and sampling	18
3.2 Petrography	19
3.3 Sample preparation for whole-rock geochemistry	19
3.4 Electron probe microanalyses	20
3.5 Element distribution maps (LA-ICP-MS)	20
3.6 Whole-rock strontium isotopes	21
3.7 <i>In-situ</i> strontium isotopes in plagioclase by LA-MC-ICP-MS	22
4. Results	26
4.1 Core logging	26
4.2 Petrography	28
4.3 Plagioclase composition	31
4.4 Whole-rock strontium isotopes	32
4.5 <i>In-situ</i> strontium isotopes in plagioclase	32
4.6 Cr/MgO	33
5. Discussion	34
5.1 Strontium isotope stratigraphy of the Northern Limb	34
5.2 Magmatic stratigraphy	36
5.3 Comparison of Turfspruit results to the Eastern and Western limbs	39
5.4 Comparison of Turfspruit results to the Northern Limb	41
5.5 The Platreef	41
6. Conclusions	43

7. Recommendations for future work.....	45
8. References	46
9. Figure Captions	52
10. Figures	57
11. Tables	74
12. Appendices	92
Appendix A: Element distribution maps	92
A.1 Alteration.....	92
A.2 Cumulate vs. intercumulate	92
A.3 Plagioclase zonation	93
A.4 Pyroxene	93
A.5 Interpretation	94
A.6 References	96
A.7 Figures	97
Appendix B: Whole-rock geochemistry.....	101
Appendix C: Thin section descriptions	115

List of Figures

Figure 1. Geological map of the Rustenburg Layered Suite	57
Figure 2. Comparison of the different stratigraphic units used in the Northern Limb.....	58
Figure 3. Geological map of the Northern Limb.....	59
Figure 4. Magmatic stratigraphy at Turspruit (Grobler et al. 2018)	60
Figure 5. Summary of initial strontium isotope data in the BIC. A) Main BIC limbs, from Kruger (1994) ; B) Northern Limb of the BIC, from Mangwegape et al. (2016)	61
Figure 6. Magmatic stratigraphy logged from UMT094.....	62
Figure 7. Full cycle stratigraphy with sections displaying micro-cycles	63
Figure 8. Micro-cycles displayed in core boxes from UMT094.....	64
Figure 9. Anorthite content of plagioclase through the stratigraphy in UMT094.....	65
Figure 10. Whole-rock initial strontium isotope analyses of plagioclase (core, rim and whole plagioclase) from UMT094	66
Figure 11. <i>In-situ</i> initial strontium isotope analyses of plagioclase (core, rim and whole plagioclase) from UMT094.....	67
Figure 12. Cr/MgO values through the stratigraphy in UMT094	68
Figure 13. <i>In-situ</i> initial strontium isotope analyses comparing cumulus vs. intercumulus plagioclase.....	69
Figure 14. <i>In-situ</i> initial strontium isotope values with 3PGE (Pt+Pd+Rh), Cr, Ni and Cu/Pd	70
Figure 15. Possible correlation between the different stratigraphic units of the Northern Limb	71
Figure 16. Three-dimensional model of the geology from the Northern Limb.....	72

Figure 17. Comparison of in-situ initial strontium isotope values to values from Seabrook et al. (2005)	73
Figure A 1. Element distribution maps of sample UMT094-1311 (by LA-ICP-MS).....	97
Figure A 2. LA-ICP-MS elemental maps of sample 094-1238.....	98
Figure A 3. LA-ICP-MS elemental maps of sample 094-1285.....	99
Figure A 4. LA-ICP-MS elemental maps of sample 094-1282.....	100
Figure C 1. Scanned thin sections associated with thin section descriptions.....	115

List of Tables

Table 1. Summary of strontium isotope studies throughout the Bushveld Igneous Complex.	74
Table 2. Mineralogical abundances throughout magmatic units within UMT094.	79
Table 3. Plagioclase composition and anorthite (An) content (by EPMA-WDS).	80
Table 4. Whole-rock strontium isotope data.	84
Table 5. Strontium isotope data from <i>in-situ</i> analyses of plagioclase.	85
Table 6. Cr/Mgo values with depth in UMT094.	90
Table C 1. Summary of thin section mineralogy of samples studied.	117
Table C 2. Summary of petrography (rock classification, mineral textures and alteration) of samples studied.	118

1. Introduction to thesis

1.1 General background and outline of the research problem

This thesis documents the magmatic stratigraphy, geochemistry and Sr isotopic signatures through the upper part of the Platreef in the Northern Limb of the Bushveld Igneous Complex as sampled at Turfspruit (near Mokopane, Limpopo Province, Republic of South Africa). The Bushveld Igneous Complex (BIC) is the largest layered mafic intrusion in the world (60,000 km²) and hosts the world's largest reserves of platinum-group elements (PGE; [Maier 2005](#); [Scoates and Friedman 2008](#); [Maier et al. 2013 and references therein](#); [Oberthür et al. 2016](#)). Three stratigraphic units contain most of the PGE mineralization: the Merensky Reef and the UG2 chromitite, both located in the Eastern and Western limbs of the BIC, and the Platreef, which is located in the Northern Limb of the BIC ([Mungall and Naldrett 2008](#); [Cawthorn 2010](#); [Peck and Huminicki 2016](#)). Although the Merensky Reef and Platreef are situated roughly at the same stratigraphic position (near the base of the Main Zone), they have been thought to be different units due, in part, to mineralization within the Platreef being much thicker than the Merensky Reef (up to ~90 m vs. ~1.5 m) and style of mineralization (contact-style vs. reef; [Schouwstra et al. 2000](#); [Manyeruke et al. 2005 and references therein](#); [Maier et al. 2008](#); [Grobler et al. 2018](#)). The purpose of this study is to test the hypothesis that the upper part of the Platreef might be the stratigraphic equivalent of the Merensky Reef.

1.2 Research question and significance

Is there a strontium isotopic shift across the Platreef that matches the isotopic shift documented for the Merensky Reef in the Eastern and Western limbs of the BIC?

Although the Platreef is roughly at the same stratigraphic position as the Merensky Reef (Maier et al. 2008 and references therein), it has been interpreted mostly as a contact-type mineralization and not reef-type mineralization. This interpretation is mostly historical and due to the fact that initially, the documented Platreef consisted of magmatic units heavily intermingled with footwall (sedimentary rocks and granitic basement), suggesting a strong influence of sediments in the mineralization processes. However, magmatic stratigraphy, with negligible footwall assimilation, down-dip at Turfspruit indicates that the mineralization might be reef-type and might therefore correlate with the Merensky Reef (Grobler et al. 2018). The goal of this project is to use Sr isotopes to establish whether or not the upper part of the Platreef correlates with the Merensky and Bastard cyclic units.

1.3 Structure of thesis

This dissertation is presented in a traditional thesis layout. A publication will be submitted to Mineralium Deposita based on a condensed version of this thesis, focusing on the in-situ strontium isotope analyses of plagioclase.

1.4 Statement of responsibilities

The project was initially conceived by P. Jugo, who highlighted the lack of strontium isotope stratigraphy within the Northern Limb, especially in mineralized magmatic units unaffected by assimilation.

Field work and sample collection was completed by the candidate in the spring and summer of 2016. D. Grobler and the Ivanplats geologists (T. Dunnet, A. Brits, A. Crossingham) assisted in selecting the ideal drill core for the project and getting familiarized with the magmatic

stratigraphy of the Bushveld Igneous Complex, with special interest to the Northern Limb. P. Jugo and M. Leybourne supervised the sampling and assisted with selecting the ideal core samples for the project. Some of the samples used were collected by E. Keir-Sage and N. Makohliso.

All samples were cut on site to quarter core or half core at Ivanplats, Mokopane, South Africa. Thirty-six samples were cut for thin sections with the help of M. Langa and were then prepared by W. Desjardins at Laurentian University. Portions of all samples were later crushed and pulverized by the candidate at Laurentian University and sent for analysis at ALS Geochemistry, Vancouver, Canada. Sample selection and preparation for whole-rock Sr isotope analyses were completed by the candidate with the exception of three samples selected and prepared by E. Keir-Sage. Whole-rock strontium isotope analyses were completed by D. Chipley and A. Voinot at Queen's Facility for Isotope Research (QFIR). P. Jugo initiated the push for better data using LA-MC-ICP-MS because of large uncertainties in the Sr isotopic values in some samples. Thirty-seven samples were cut for 100 μm thick thin section for LA-MC-ICP-MS and prepared by W. Desjardins at Laurentian University. S. Mkhonto provided four additional thin sections, which were initially prepared by N. Makohliso. Analytical protocols for the *in-situ* analyses at QFIR were tested and implemented by the candidate, A. Voinot and M. Leybourne. Sample selection and preparation for *in-situ* strontium isotope analyses in plagioclase, as well as data reduction/corrections were completed by the candidate. Samples for EPMA were selected by the candidate and analyzed with the help of D. Crabtree at the Ontario Geoscience laboratories. Element distribution maps by LA-ICP-MS were acquired with the help of M. Leybourne and J. Petrus at Laurentian University.

1.5 Statement of original contributions

The original contributions made by this study are:

- Documentation of the first strontium isotope stratigraphy through the mineralized unit in the Northern Limb of the BIC (the upper part of the Platreef) in a drill core seemingly unaffected by assimilation. To our knowledge no previous studies have successfully avoided footwall assimilation in the Platreef.
- Documentation of a clear shift in Sr isotopic ratios within the upper part of the Platreef in the Northern Limb of the BIC that match those documented in the main limbs (E and W) of the BIC; thus, providing a way to correlate the mineralization in the upper part of the Platreef with the Merensky and Bastard cyclic units.
- Documentation of small-scale cycles ('micro-cycles') in the magmatic stratigraphy of the Northern Limb. To our knowledge such cyclicity had not been documented previously.
- Provides a large geochemical data set for magmatic units unaffected by assimilation through the Platreef.
- Proposes a working hypothesis that links micro-cyclicity to the thickness of mineralization, which could help explain why the mineralization in the Northern Limb is much thicker in comparison to the Merensky Reef in the Eastern and Western limbs.

2. Background

2.1 Bushveld Igneous Complex

The Bushveld Magmatic Province (BMP) is located in northern South Africa and encompasses an extrusive sequence (Rooiberg Group) and an intrusive sequence (Bushveld Igneous Complex - BIC; e.g. [Kinnaird et al. 2004](#)). The BIC intruded into the Rooiberg Group, Transvaal Supergroup and Archean basement, and is composed of three main suites: (1) the Rustenburg Layered Suite (RLS; [Fig. 1](#)), a sequence of mafic to ultramafic layered cumulate rocks; (2) the Lebowa Granite Suite, a series of granites overlying the RLS; and (3) the Rashedoop Granophyre Suite, interpreted as the late felsic phase of the BIC ([Kinnaird et al. 2004](#); [Kruger 2005](#)). There are five limbs to the BIC: the Eastern, Western, Far-Western, Southern (or Bethal) and Northern Limbs ([Fig. 1](#); [Maier et al. 2013](#)). This research focuses on the Northern Limb and comparisons to the Eastern and Western limbs of the BIC. The Eastern and Western limbs of the BIC are the largest in area and have been the most researched, explored and mined of all limbs over the past century.

2.1.1 Magmatic stratigraphy of the RLS

The reference geology of the Rustenburg Layered Suite is based on studies of the magmatic units within the Eastern and Western Limbs of the Bushveld Igneous Complex. The magmatic stratigraphy of the RLS is well defined and has five main zones: Marginal Zone, Lower Zone, Critical Zone, Main Zone, and Upper Zone ([Fig. 2](#) - Eastern and Western limbs; [Maier et al. 2013](#) and references therein).

The Marginal Zone typically occurs between the footwall and the Lower or Critical Zones or as sills within the footwall and is considered to be the quenched phase of the intrusion or a late

crystallization of residual liquid derived from within the magma chamber (Kruger 2005; Cawthorn et al. 2006; Barnes et al. 2010; Maier et al. 2013 and references therein). The Marginal Zone is considered to represent a rapid crystallization of the initial magma, which was highly contaminated by assimilation of the footwall (Cawthorn et al. 2006). This norite-dominant sequence, with minor pyroxenites, can be up to 800 meters thick and host xenoliths of dolostone, quartzite and anorthosite (Cawthorn et al. 2006).

The Lower Zone (LZ) is mainly composed of harzburgite, dunite and orthopyroxenite with minor norite layers. It is up to 1300 m thick but varies throughout the Rustenburg Layered Suite due to variations in floor topography (Wilson 2012). In the Western Limb, the lowermost part of the LZ contains an equal proportion of pyroxenite and harzburgite. By contrast, the uppermost section of the LZ contains a higher proportion of harzburgite than pyroxenite. In some locations, cycles can be observed in the LZ such as the Far-Western Limb, which shows up to nine cyclic units containing dunite-harzburgite-pyroxenite, respectively, in that order. Throughout the Lower Zone, less than 1% chromite is present through the magmatic stratigraphy (Cawthorn et al. 2006; Maier et al. 2013).

The Critical Zone (CZ) is of interest for mining because it hosts multiple chromitite layers, some of them containing PGE, and mineralized horizons or 'reefs'. The chromite layers are grouped into three distinct clusters: up to seven Lower Group (LG) chromitites, up to four Middle Group (MG) chromitites and up to three Upper Group (UG) chromitites (Maier et al. 2013 and references therein). Of significant interest is the UG2 chromitite, which hosts significant PGE mineralization (e.g. ~2000 ppb Pt, ~1200 ppb Pd ~360 ppb Ru and ~100 ppb Ir over 66 cm; Maier and Barnes 2008). The CZ can be separated into two: (1) the Lower Critical Zone (LCZ) and the Upper Critical Zone (UCZ). The LCZ is dominantly pyroxenite with some olivine-rich intervals and hosts all of the LG and half of the MG chromitites (Kruger 2005). The appearance

of an anorthosite layer located between the MG2 and MG3 chromitites is used to separate the LCZ from the UCZ. The UCZ is dominantly norite and pyroxenite but also has major chromite seams, including the PGE-rich UG2 chromitite. The UCZ hosts the MG3, MG4 and all of the UG chromitites including the UG1 and UG2. Chromite is a trace mineral in most units of the UCZ (excluding most anorthosites and norites) that occur in between the major MG and UG chromite seams, but also appears as small chromite seams (centimeters to millimeters in thickness; [Veksler et al. 2014](#)). In the uppermost UCZ, PGE mineralization is found within the Merensky Reef but also the Pseudoreef, Bastard Reef and Boulder Bed, all occurring above the UG chromitites. The Pseudoreef is a mineralized reef that occurs stratigraphically above the UG chromite seams but below the Merensky Cyclic Unit (MCU) within small cyclic units in the northwestern BIC ([e.g. Maier et al. 2013](#)). Above the MCU is the Bastard Reef, which in the Western and Eastern Limb is typically 1-5 cm thick but can be up to 30 cm thick and defines the bottom of the Bastard Cyclic Unit (BCU; [Maier et al. 2013 and references therein](#)). In most locations in the BIC, the Bastard Reef contains little PGE mineralization but is commonly mistaken for the Merensky Reef (due to the presence of a chromitite seam and sulfides; [Maier and Barnes 2008](#)), hence the name. The BCU is the uppermost unit of the Critical Zone just below the Main Zone of the RLS.

The 2-3 km thick Main Zone (MZ) occurs above the Critical Zone and is dominated by gabbronorite and norite with minor occurrences of pyroxenite. Placement of the contact between the MZ and CZ was suggested to be the top of the uppermost unit of the Bastard Cyclic Unit, which is a mottled anorthosite ([Maier et al. 2013](#)). The MZ is dominated by gabbronorite-norite cycles in the lower part of the MZ. These cycles are separated by small pyroxenite units. The first appearance of magnetite has been used to identify the boundary between the MZ and the UZ ([e.g. Maier et al. 2013](#)).

The Upper Zone (UZ) is the uppermost unit of the RLS and typically is between 1-2 km thick. The UZ is dominated by layers of gabbro-norite, anorthosite, diorite and magnetite. There are 26 magnetite layers in the Upper Zone of the Eastern and Western Limbs. The magnetite layers are typically between a few centimeters to a few meters thick but can be thicker than 10 m and commonly contain anorthosite xenoliths (Cawthorn et al. 2006). Cumulate olivine and apatite appear in the uppermost section of the Upper Zone (Cawthorn et al. 2006).

2.2 Northern Limb geology

The stratigraphy of the Northern Limb is roughly similar to that of the Eastern and Western limbs. Within the RLS, the Main Zone and Upper Zone are present, the Lower Zone is locally present as satellite bodies in parts of the Northern Limb, and the Platreef occurs at the stratigraphic level of the Critical Zone.

The Platreef in the Northern Limb of the Bushveld Igneous Complex is host to the thickest Pt-Pd deposits in the world (Kinnaird et al. 2005; Holwell et al. 2006), with a maximum thickness of ~90 m averaging 4.5 g/t PGE (TMT006 at Turfspruit; Grobler et al. 2018). The Platreef is north of the Planknek Fault (Fig. 3) and was defined by Kinnaird and McDonald (2005; p. 196) as: “Mafic units enriched in Ni-Cu-PGE that occur between the Archean granite-gneiss basement or the Transvaal Supergroup and gabbros-gabbro-norites of the Main Zone”. Although this definition seemingly depicts the Platreef as mineralized from the Main Zone to the footwall, it is not the case; PGE mineralization occurs within distinct sections of the Platreef and is not continuous throughout the whole stratigraphy. In most areas, the Platreef occurs in proximity to the footwall and forms an interaction zone or assimilation zone between the magmatic units and the Transvaal Supergroup in the southern part of the Northern Limb, or the Archean granitic gneiss in the northern part (Fig. 3). Although the Platreef has been suggested to

be the stratigraphic equivalent to the Merensky Reef in the Eastern and Western Limbs of the BIC, it is significantly thicker than the Merensky Reef (50-400 m thick vs. ~1 m on average; Schouwstra, et al. 2000; Manyeruke et al. 2005 and references therein; Kinnaird 2005; Grobler et al. 2018).

The magmatic stratigraphy of the Critical Zone in the Northern Limb was variably affected by assimilation of different footwall lithologies (Harris and Chaumba 2001; Holwell et al. 2007; Maier et al. 2008; Smith et al. 2016). This footwall assimilation resulted in the development of many different interpretations of the magmatic stratigraphy (Fig. 2). The most common stratigraphic interpretations are: (1) the widely-used Platreef stratigraphy (described above); (2) the A, B, C reef nomenclature (Barton et al. 1986; Kruger 2010); (3) the Grasvally norite-pyroxenite-anorthosite (GNPA) member, used south of the Planknek Fault (Fig. 3; McDonald et al. 2005); (4) the T1 and T2 reefs at the Waterberg Project (Kinnaird et al. 2017); (5) units 1, 2 and 3 used at the Aurora Project (McDonald et al. 2017); and (6) the stratigraphy used at Turfspruit by Ivanplats (Grobler et al. 2018). Figure 1 shows the locations where some of the different stratigraphic schemes are used within the Northern Limb.

The A, B, C reef stratigraphy was mainly used to describe multiple mineralized reefs occurring within a series of pyroxenites in the Platreef (Barton et al. 1986; Fig. 2). Stratigraphically, the lowermost reef is the A-reef (heterogenous feldspathic pyroxenite), followed by the B-reef (medium- to coarse-grained pyroxenite with minor chromite), and the C-reef (feldspathic pyroxenite) occurring just below the Main Zone (Barton et al. 1986; Manyeruke et al. 2005; Kruger 2010). The term “GNPA member” (Fig. 2) is used for stratigraphy South of the Planknek Fault (Fig. 3) and consists of 2 sections: (1) the lower sub-zone dominated by cumulate orthopyroxene and clinopyroxene with minor chromite and plagioclase; and (2) the upper sub-zone is dominated by units containing cumulate plagioclase (McDonald et al. 2005).

The stratigraphy at the Waterberg project (Fig. 2) consists of a mineralized zone (T1 and T2 reefs) occurring between the Upper Zone and a troctolite-gabbro-norite-anorthosite unit (TGA; Kinnaird et al. 2017). Below the TGA sequence is an ultramafic unit also containing mineralization, underlain by granofels or granite (Kinnaird et al. 2017). At the Aurora Project, Cu-Ni-PGE mineralization is hosted in the Upper Main Zone of the Northern Limb (e.g. Maier et al. 2008; McDonald et al. 2017). The Aurora stratigraphy (Fig. 2) is separated into three main units: Unit 3, the lowermost unit, composed of peridotite and mela-gabbro-norite with meter-sized calc-silicate rafts; Unit 2, a sequence of gabbro-norite to leuco-gabbro-norite with minor units of olivine-gabbro-norite and minor pegmatoidal units containing sulfides and magnetite (~10 cm to 5 m-thick); and Unit 1, composed of pigeonite gabbro-norite (McDonald et al. 2017).

The magmatic stratigraphy established by Ivanplats is summarized in figure 4 and has been developed to take account of units seen throughout over 700 000 m of drill core. Grobler et al. (2018) observed that, at Turfspruit, the Platreef seems to represent the Upper Critical Zone and parts of the Lower Critical Zone, which include two higher grade reefs (the Bastard and Merensky reefs). Minor magmatic units throughout Turfspruit pinch and swell along strike but major units can be followed throughout the property (Grobler et al. 2018). The Main Zone gabbro-norite (HW3) is the uppermost unit in every hole down-dip at Turfspruit. Below the Main Zone there are four main cyclic units that can be observed: (1) the Bastard Cyclic Unit (BCU); (2) the Merensky Cyclic Unit (MCU); (3) the Footwall Cyclic Unit (FCU); and (4) the UG2 Cyclic Unit (UG2CU). Within the BCU there are a total of three possible sub-units, which are a mottled-spotted anorthosite (HW2), pyroxenite-norite cyclic units (HW1) and a mineralized feldspathic pyroxenite (BAR). A small chromite stringer occurs rarely at the top or the bottom of the mineralized feldspathic pyroxenite. The MCU can have up to five different units: (1) pyroxenite-norite cyclic units (MD2), (2) feldspathic orthopyroxenite (MD1), (3) mineralized

feldspathic pyroxenite (M2), (4) mineralized pegmatoidal feldspathic orthopyroxenite (M1U) and, (5) mineralized pegmatoidal feldspathic harzburgite (M1L). A chromite stringer occurs between M2 and M1U. The top of the M2 marks the start of the Merensky Reef equivalent. Below the MCU is the FCU, which can contain up to three units: (1) pyroxenite-norite cyclic units (FW3), (2) norite resulting from shale or hornfels assimilation (HW2) and (3) para-harzburgite resulting from dolomite or calc-silicate assimilation (HW1). The UG2CU follows the FCU and is composed of feldspathic pyroxenite (UG2HW), the UG2 chromitite and pyroxenite or harzburgite (UG2FW). Below the UG2CU is Lower Zone followed by the footwall, which is mainly the Duitshland Formation at Turfspruit. Xenoliths of the footwall are mainly found in the eastern portion of the Turfspruit farm; further down-dip to the west only minor xenoliths are found and typically occur within 50 meters of the footwall contact. The Ivanplats stratigraphy was modelled based on primary magmatic units seen at Turfspruit but also considers the units found within the assimilation zone (Grobler et al. 2018).

2.3 Mineralization in the Rustenburg Layered Suite

Platinum-Group Element mineralization within the Rustenburg Layered Suite of the Eastern and Western limbs is hosted in four main units: (1) the Merensky Reef, (2) the UG2 chromitite, (3) the Pseudoreef and (4) the Platreef.

2.3.1 The Merensky Reef

The Merensky Reef is located at the base of the Merensky Cyclic Unit throughout the Eastern and Western limbs. In the Eastern and Western limbs, mining is focused on the Merensky Reef because of thick mineralization (up to ~1.5 m) and high PGE concentrations (5-7 g/t PGE; Osbahr et al. 2013) in comparison to other units within the RLS of the Eastern and Western

limbs. The Merensky Reef is typically a feldspathic pyroxenite bounded by a lower and upper chromite stringer (~1-2 cm thick) and occurs at the base of the MCU of the BIC (Osbaahr et al. 2013). The mineralization of the Merensky reef is typically a few decimeters up to two meters in thickness and the mineralized feldspathic pyroxenite can be pegmatoidal (typically between 4 cm and 2.5 m), composed of pegmatitic pyroxenes with intercumulate plagioclase and minor sulfide (~3%) that contain PGE mineralization (~5-7 g/t PGE; Naldrett et al. 2009; Osbaahr et al. 2013). Although facies variations of the Merensky Reef occur throughout the BIC, and within individual mines (Smith et al. 2003), the Merensky Reef mineralization is always located at the base of the MCU and almost always associated with a pegmatoid and two chromite stringers.

2.3.2 The UG2 chromitite

The UG2 chromitite is located at the base of the UG2 Cyclic Unit throughout the Eastern and Western limbs of the BIC. It is on average a 70 cm-thick chromitite containing 75-90% chromite (Mondal and Mathez 2007) and hosts PGE mineralization (~6 ppm; Maier et al. 2013). Mineralization typically occurs within the base and the upper part of the UG2 chromitite, but is commonly also hosted within the upper part of the pegmatoidal feldspathic pyroxenite located below the chromitite (Maier and Barnes 2008).

2.3.3 The Pseudoreef

The Pseudoreefs occur below the Merensky Reef and above the UG2 chromitite mainly in the northwestern region of the BIC, north of Pilanesberg. Their mineralization is typically hosted within a small (~10 cm thick) sulfide-bearing pegmatoidal harzburgite unit (Naldrett et al. 1986), but can be within a sulfide-bearing pyroxenite or troctolite (Maier and Barnes 2008). Pseudoreefs are typically poorly developed or absent but can contain up to ~5-6 ppm of PGE (Maier and Barnes 1999; Naldrett et al. 2009).

2.3.4 Platreef

The Platreef mineralization is located below the Main Zone in the Northern Limb of the BIC (Kinnaird and McDonald 2005). Ni-Cu-PGE mineralization is erratically distributed throughout the Platreef but the main high-grade mineralization is typically located near the upper contact (Kinnaird et al. 2005). The Platreef may contain similar PGE grades as the Merensky Reef, with some intersections that are above 10 g/t PGE (Kinnaird et al. 2005). However, most mineralization in the Platreef is typically ~1-2 g/t PGE over several tens of meters (Kinnaird et al. 2005). One of the best mineralized intersections through the Platreef is drill hole TMT006, drilled by Ivanplats, with ~90 m averaging 4.5 g/t PGE (Grobler et al. 2018).

2.4 Strontium isotopic stratigraphy of the transition from the Upper Critical Zone to the Main Zone

Strontium isotope stratigraphy in the BIC uses the initial strontium isotope ratio ($^{87}\text{Sr}/^{86}\text{Sr}_i$) calculated from whole-rock or mineral separates (e.g., plagioclase or pyroxene) to distinguish isotopically different magmatic sequences through the stratigraphy. The $^{87}\text{Sr}/^{86}\text{Sr}_i$ is calculated using a known age of crystallization of the Bushveld (2054.89 ± 0.37 Zeh et al. 2015) and a decay constant ($\lambda = 1.393 \pm 0.004 \times 10^{-11} \text{ y}^{-1}$; Nebel et al. 2011) with measured $^{87}\text{Sr}/^{86}\text{Sr}$ and $^{87}\text{Rb}/^{86}\text{Sr}$. The strontium isotopic system is used in layered mafic intrusions mainly for interpretations of processes occurring at the time of formation and for stratigraphic correlation of magmatic units across the intrusion.

2.4.1 Eastern and Western limbs

Strontium isotope stratigraphy has previously been used in the Eastern and Western limbs and documents isotopic shifts through the magmatic stratigraphy, which have been related to new

pulses of magma into the magma chamber (Hamilton 1977; Yang et al. 2013 and references therein). Table 1 is a summary of the available studies documenting strontium isotope stratigraphy throughout the BIC. The first study on strontium isotopes in the BIC was conducted by Hamilton (1977), who identified different $^{87}\text{Sr}/^{86}\text{Sr}_i$ signatures throughout the different zones of the BIC. The strontium isotopic shift associated with the Merensky Reef was initially identified in the Western Limb of the RLS by Kruger and Marsh (1982). The shift in initial Sr isotope ratio, from 0.7064 to 0.7075, starts at the base of the Merensky Reef and occurs through the Merensky and Bastard cyclic units, which are a combined total of 20 meters in thickness. Two scenarios were suggested to explain the increase in initial strontium isotopic ratios ($^{87}\text{Sr}/^{86}\text{Sr}_i$): (1) contamination of the magma by country rocks at the level of emplacement (because the footwall rocks would have higher $^{87}\text{Sr}/^{86}\text{Sr}_i$); or (2) crystallization triggered by a new contaminated influx of magma (higher $^{87}\text{Sr}/^{86}\text{Sr}_i$ due to assimilation of crustal material in a preceding staging chamber), which interacts with the resident magma in the magma chamber causing an increase in the initial Sr isotope ratio (Kruger and Marsh 1982). Two main shifts were identified by Sharpe (1985) in the strontium isotope stratigraphy from the Upper Critical Zone to the Upper Zone of the Eastern Limb. The largest is the shift occurring through the Merensky and Bastard Cyclic units (0.7065 to 0.7085), analogous to the shift identified by Kruger and Marsh (1982), and the second occurs at the Main Zone-Upper Zone boundary, also known as the Pyroxenite Marker ($^{87}\text{Sr}/^{86}\text{Sr}_i = 0.7085$ to 0.7073; Sharpe 1985). A study at the Atok section in the Eastern Limb showed similar results across the Merensky Reef in the strontium isotopic profile to the Western Limb (Lee and Butcher 1990). Although there are variations in pegmatoids, Pt-Pd mineralization, chromite stringers and magmatic units between the Eastern and Western limbs, the strontium isotopic profiles suggest that the Bushveld magma chamber was homogenized at the time of formation of the MCU and BCU. Lee and Butcher (1990) also

documented a shift between the Merensky and Bastard Cyclic units and hypothesized that the Merensky Reef and the Bastard Reef could have formed from a sill-like intrusion based on four main points: (1) the Merensky and Bastard Reef bifurcate along strike; (2) contacts between the reefs and the underlying units are sharp; (3) the thickness of the Merensky and Bastard pyroxenite fluctuates along strike, indicating that they might have assimilated the lower unit; and (4) the $^{87}\text{Sr}/^{86}\text{Sr}_i$ shift seen through the Merensky and Bastard Cyclic units might be associated with the interaction of the intrusion with an underlying low $^{87}\text{Sr}/^{86}\text{Sr}_i$ source (~0.706 - Critical Zone) and an overlying higher $^{87}\text{Sr}/^{86}\text{Sr}_i$ source (~0.708 - Main Zone; [Lee and Butcher 1990](#)). The most commonly cited strontium isotope stratigraphic profile of the BIC was compiled by [Kruger \(1994; Fig. 5A\)](#). [Kruger \(1994\)](#) compiled the strontium isotope stratigraphy from the Lower Zone into the Upper Zone of the Western Limb of the BIC, representing the first complete strontium isotope stratigraphy of the Rustenburg Layered Suite. According to [Kruger \(1994\)](#), the Sr isotope profile of the RLS has two main stages: the Integration Stage and the Differentiation Stage. The Integration Stage occurs through the Lower Zone, Critical Zone and Lower Main Zone and documents an open system with multiple pulses of magma feeding a magma chamber. Interaction with the resident magma caused many isotopic shifts throughout the lower stratigraphy of the RLS. The Differentiation Stage encompasses the Upper Main Zone and Upper Zone and documents a closed system fractional crystallization sequence. This stage does not have many Sr isotopic shifts and reflects a lack of new magmatic activity. The only shift recorded through the Differentiation Stage is the shift that occurs at the Pyroxenite Marker ([Sharpe 1985; Kruger 1994](#)).

In the early 2000s, the focus of studies shifted towards the bimodal population of chemically and isotopically distinct minerals within the Merensky and Bastard Cyclic units ([Seabrook et al. 2005; Chutas et al. 2012; Yang et al. 2013](#)). Orthopyroxene and plagioclase were determined to

have different trace element compositions in the Critical Zone magma compared to the Main Zone. Through the MCU and BCU, a mixture of chromium-rich orthopyroxene (> 2500 ppm) from the Critical Zone and chromium-poor orthopyroxene (< 1000 ppm) from the Main Zone can be found (Seabrook et al. 2005). Likewise, plagioclase showed a similar chemical trend with strontium-rich plagioclase (> 450 ppm) in samples from the Critical Zone and strontium-poor plagioclase (< 390 ppm) in samples from the Main Zone (Seabrook et al. 2005). Because the difference in Sr content between the MCU and BCU also coincides with the strontium isotope shift and a Cr/MgO shift seen in whole-rock analyses, Seabrook et al. (2005) considered the MCU and BCU as Transitional Units between the Upper Critical Zone and the Lower Main Zone. The Sr isotopic values show that there is isotopic disequilibrium between minerals within the Lower and Critical Zone but the Upper Zone is isotopically uniform (Chutas et al. 2012). Disequilibrium of strontium isotopes from core to rim within individual plagioclase grains has also been reported (from 0.706 at the rim to 0.708 at the core within the MCU; Yang et al. 2013).

2.4.2 Northern Limb

In the Northern Limb, Kruger (2005) recorded values for $^{87}\text{Sr}/^{86}\text{Sr}_i$ of the Platreef on the Turfspruit Farm. These values average ~ 0.7109 , with a maximum $^{87}\text{Sr}/^{86}\text{Sr}_i$ of 0.71459 (Kruger 2005). Other studies in the Platreef record values of $^{87}\text{Sr}/^{86}\text{Sr}_i$ ranging from 0.7054 to 0.7226 at Overysel and Sandsloot (Barton et al. 1986). Such values are much higher than typical isotopic values in the Eastern and Western limbs, and were therefore inconsistent with a correlation between the Northern Limb and the rest of the BIC. Mangwegape et al (2016) published the strontium isotope stratigraphy of the Upper and Main zones of the Northern Limb using *in-situ* strontium isotope analyses of plagioclase (Fig. 5B). Data collected by Mangwegape et al (2016) shows relatively constant Sr isotopic ratios (~ 0.7073 to 0.7078) in the Upper Zone and Upper

Main Zone with small fluctuations. Strontium isotope data documented in [Mangwegape et al. 2016](#) only covers stratigraphy above the Platreef, likely because of footwall assimilation, therefore cannot be used to test the existence of an isotopic shift across the mineralization or correlation with the rest of the BIC. Lastly, [Huthmann et al. \(2017\)](#) published data from the Waterberg Project in the far Northern Limb, which show relatively consistent $^{87}\text{Sr}/^{86}\text{Sr}_i$ values between 0.7065 to 0.7075 throughout the magmatic stratigraphy.

3. Methods

3.1. Core logging and sampling

Drill hole UMT094 is located further southwest, compared to most holes drilled by Ivanplats, which are located closer to the exposed contact between the Northern Limb of the RLS and the Transvaal sequence. UMT094 was selected because it is located down dip from the Flatreef (a section of mineralization that is relatively flat-lying; [Grobler et al. 2018](#)) and drill core shows magmatic stratigraphy with limited footwall interaction compared to core from holes located up dip, in the assimilation zone. Hole UMT094 is 1602 meters in depth and intersects 1185 meters of Main Zone gabbro-norite before intersecting mineralized cyclic units (BCU, MCU, FCU and UG2CU).

Samples were collected from drill core available as either full (if previously unsampled) or half core (if sampled previously by other workers). Samples were selected based on the lack of alteration/assimilation textures and distance from what was interpreted as the possible base of the Merensky Cyclic Unit (identified by significant increase in Pt, Pd, Rh, Ni, Cu, Cr content in whole-rock geochemistry and the presence of magmatic cycles). Because the main focus of the thesis is to document the possible existence of shifts in $\text{Sr}^{87}/\text{Sr}^{87}_i$ across this unit, sample density was higher across this boundary. Other samples were taken around the possible Pseudoreef and the Bastard Reef to document possible changes in $\text{Sr}^{86}/\text{Sr}^{87}_i$ through these stratigraphic units. Sections of core that were selected were then cut in half on site at Ivanplats. Intervals for thin section were specifically chosen to be representative of major units, to be on contacts, chromite stringers or other areas of interest. Samples were then cut to small thin section slabs and used for thin section preparation at Laurentian University.

3.2 Petrography

Petrography was completed at Laurentian University using a polarizing microscope. Thirty-six representative samples were chosen for petrography and prepared as standard-thickness polished sections (30 μm thick). The focus of petrography was to identify and document mineralogy, alteration, veining, grain size and shape, with special attention to plagioclase within the samples for later *in-situ* plagioclase analyses. An additional set of 36 polished sections (100 μm thick) was prepared for *in-situ* strontium isotope analyses (to ensure laser ablation did not hit the glass support of the polished sections during analyses).

3.3 Sample preparation for whole-rock geochemistry

Some of the sample preparation was completed at Laurentian University. Samples were firstly crushed with a hammer. To avoid contamination, samples were placed in thick sample bags before hammering. In addition, the steel plate and hammer used to crush the samples were wiped with ethanol between samples. Samples were hammered until all pieces were small enough to be inserted into the low Cr-Mo steel ring mill, in which they were pulverized. To avoid contamination between samples, clean quartz was pulverized between samples, commonly more than once, and then the container, lid, ring and puck were wiped with ethanol. The pulverized sample was put into plastic vials. Pulverized samples were split and half was sent to ALS Geochemistry, Vancouver, BC, Canada for geochemical analyses with reference materials (MRG-1 and SY-3) labelled as unknown samples for quality control. Analyses performed at ALS Geochemistry included the following: 1) major elements were analyzed by inductively coupled plasma atomic emission spectroscopy (ICP-AES) following lithium metaborate fusion; 2) trace elements (Ba, Cr, Cs, Ga, Hf, Nb, Rb, Sr, Ta, Th, U, V, Y, Zr and the REE) by ICP mass

spectrometry (ICP-MS) following lithium metaborate fusion (Method ME-MS81) to include elements within phases resistant to acid digestion (zircon, chromite, monazite); 3) trace and some major elements (Ag, Al, As, Ba, Be, Bi, Ca, Cd, Ce, Co, Cr, Cs, Cu, Fe, Ga, Ge, Hf, In, K, La, Li, Mg, Mn, Mo, Na, Nb, Ni, P, Pb, Rb, Re, S, Sb, Sc, Se, Sn, Sr, Ta, Te, Ti, Tl, U, V, W, Y, Zn, Zr) by an ultra-trace four-acid digestion (HF, HClO₄, HCl, HNO₃) method (ME-MS61L) followed by a mixture of ICP-AES and ICP-MS analysis, to allow lower detection limits on elements not incorporated in resistant phases; 4) lead oxide fire assay was used to preconcentrate and collect Au, Pt and Pd, with subsequent analysis by ICP-MS and ICP-AES (method PGM-MS23L or PGM-ICP27 where contents were over range by ICP-MS).

3.4 Electron probe microanalyses

Electron probe microanalyses (EPMA) were performed at the Geoscience Laboratories (GeoLabs) of the Ontario Geological Survey, Sudbury. Individual plagioclase grains were selected from 24 samples representative of the magmatic stratigraphy. Plagioclase were analyzed at the core and care was taken to avoid zones with evident alteration. Seven analyses per sample were collected and used to calculate an average anorthite content (and associated quartiles with maximum and minimum values) of plagioclase per sample. Analytical conditions used for the WDS acquisition were a rastered beam diameter of 8 µm, a probe current of 20 nA and an acceleration voltage of 20 kV. Elements analyzed, presented as weight percent oxides, with detection limits were SiO₂ (0.024), TiO₂ (0.018), Al₂O₃ (0.019), MgO (0.009), CaO (0.018), MnO (0.027), FeO_t (0.026), SrO (0.071), Na₂O (0.012) and K₂O (0.014).

3.5 Element distribution maps (LA-ICP-MS)

Elemental distribution maps laser ablation (LA)-ICP-MS were completed at Laurentian University in the Chemical Fingerprinting Lab. Areas of interests for mapping were selected based on plagioclase type (cumulate or intercumulate) to assess whether there was any significant contrast in trace element chemistry. Further, samples and areas of interest within samples were selected based on the amount of alteration present to assess changes in element content and element mobility due to alteration. A Resonetics M50 193 nm excimer laser interfaced with an ICP-MS was used for the analyses. The parameters used were: a laser energy of 4 J/cm², a pulse frequency of 8 Hz, a beam diameter of 36 μm, a scan velocity of 18 μm/s and a round spot size. Glass standards (GSC-1, GSE-1G, GSD-1G and NIST610) were used for calibration and quality control. The masses analyzed to calculate concentrations correspond to: ²³Na, ²⁴Mg, ²⁷Al, ²⁹Si, ³⁹K, ⁴⁴Ca, ⁴⁵Sc, ⁴⁷Ti, ⁵¹V, ⁵²Cr, ⁵⁵Mn, ⁵⁷Fe, ⁶⁰Ni, ⁷¹Ga, ⁷²Ge, ⁸⁵Rb, ⁸⁸Sr, ⁸⁹Y, ⁹⁰Zr, ¹³³Cs, ¹³⁷Ba, ¹³⁹La, ¹⁴⁰Ce, ¹⁴¹Pr, ¹⁴⁶Nd, ¹⁴⁷Sm, ¹⁵³Eu, ¹⁵⁷Gd, ¹⁵⁹Tb, ¹⁶³Dy, ¹⁶⁵Ho, ¹⁶⁶Er, ¹⁶⁹Tm, ¹⁷²Yb, ¹⁷⁵Lu, ²⁰⁴Pb, ²⁰⁶Pb, ²⁰⁷Pb and ²⁰⁸Pb.

3.6 Whole-rock strontium isotopes

Samples for strontium isotope analyses were chosen based on stratigraphic position relative to the base of the Merensky Cyclic Unit. Samples were chosen to cover a few meters below the base of the MCU, across both the MCU and BCU, and ~100 m into the MZ. Sample weights for analyses were decided based on concentrations of Rb-Sr within the sample. Spike AVI (Sr) and spike AVIII (Rb) were added to the samples prior to digestion, which act as internal standards. Blanks and reference material (BHVO-1, JB-2 and BIR-1) were included in the process as quality control. The amount of the spike added was determined by the concentration of Sr and Rb within the sample based on whole-rock geochemistry. The sample was then digested with 5 mL of

hydrofluoric (29 M), nitric (15 M) and hydrochloric acid (10 M) at a 3:2:1 ratio, respectively. The samples were dried following 3-4 days of digestion on a hot plate. If fluorides formed during digestion, the samples were allowed to dry completely and 1 to 2 mL of boric acid and hydrochloric acid at a 1:1 ratio were added to the samples to dissolve the fluorides. Once all fluorides were dissolved the sample was dried once more. Some samples were not completely dissolved after this step (likely chromite grains in the residue); therefore, aqua regia was added to the samples. Once samples were completely dissolved and dried, 1 mL of 3 M nitric acid was added to the samples to prepare them for automated chromatography (using a prepFAST system). If not completely dissolved, 2-2.5 mL of 3 M nitric acid was added to attempt dissolving minor chromite grains. Some samples still had chromite grains following this process but chromite does not contain any Sr-Rb and therefore does not affect the Sr-Rb isotopic system. All samples were then placed in a centrifuge to separate minor undissolved particles. Samples were then put through the prepFAST 15 samples at a time, including blanks and certified reference materials (BHVO-1, JB-2 and BIR-1). Following this, sample aliquots of Sr and Rb were analysed with the Neptune multi-collector (MC)-ICP-MS.

The isotope dilution correction calculation was modelled after [Cheong et al. \(2014\)](#). Based on the calculated strontium ratios, including the $^{87}\text{Sr}/^{86}\text{Sr}$, from the equations in [Cheong et al. \(2014\)](#), the strontium and rubidium concentrations, the $^{87}\text{Rb}/^{85}\text{Rb}$, the $^{87}\text{Rb}/^{86}\text{Sr}$ and finally the $^{87}\text{Sr}/^{86}\text{Sr}_i$ could be calculated. An age of 2054.89 ± 0.37 ([Zeh et al. 2015](#)) and a decay constant of $1.393 \times 10^{-11} \text{ y}^{-1}$ ([Nebel et al. 2011](#)) was used for the initial strontium isotope calculation. Uncertainties were calculated using a Monte Carlo simulation.

3.7 In-situ strontium isotopes in plagioclase by LA-MC-ICP-MS

The analytical protocol used for *in-situ* analyses in plagioclase was based on the procedures documented in [Yang et al. \(2013\)](#), [Mangwegape et al. \(2016\)](#) and [Wilson et al. \(2017\)](#). Thirty-seven samples representative of the magmatic stratigraphy, above the assimilation zone, were selected from drill core UMT094 at Turfpruit ([Fig. 3](#)). Polished 100 μm thick sections were prepared for each sample. Plagioclase grains (rim, core or whole plagioclase) were selected prior to analysis. *In-situ* Sr isotope analyses were performed by laser ablation multi-collector inductively coupled plasma mass spectrometry (LA-MC-ICP-MS) at the Queen's Facility for Isotope Research (QFIR) using a 193 nm excimer laser (Elemental Scientific NWR193) interfaced with a Thermo-Finnigan Neptune MC-ICP-MS. A laser beam of circular section and 150 μm diameter was used with a repetition rate of 10 Hz, a beam energy density of $\sim 2.3 \text{ J/cm}^2$ and a duration of 120 s per analysis preceded by a 60 s blank analysis. The masses analyzed were ^{82}Kr , ^{83}Kr , ^{84}Sr , ^{85}Rb , ^{86}Sr , ^{87}Sr , ^{88}Sr , $^{44}\text{CaPO}$, as well as double charged REE ($^{163}\text{Dy}^{++}$, $^{167}\text{Er}^{++}$, $^{171}\text{Yb}^{++}$, $^{173}\text{Yb}^{++}$ and $^{175}\text{Lu}^{++}$) using dynamic mode (centre mass jumping from 86 to 86.5). The idle time was set to 3.0 s to allow for magnet and amplifiers to settle. The integration time was set to 2.0 s for Kr, Rb, Sr and CaPO, and 1.0 s for doubly charged REE. After analysis, all data that resulted in a negative value were nulled (mainly Kr and REE). Five to ten spot analyses were completed per sample with one reference material (BHVO-2G, BIR-1G or TB-1G) analyzed after every two spot analyses on plagioclase. Spot analyses were done on the rim or core of plagioclase grains; commonly both on the same grain if the grains were large enough. If the grains were too small to analyze the rim or core, the points were labeled as a "whole plagioclase". After acquisition, data were corrected for Kr interference (^{84}Kr on ^{84}Sr and ^{86}Kr on ^{86}Sr , calculated from ^{82}Kr and ^{83}Kr) using the blank analysis for each individual sample (background counts), and then corrected for doubly charged REE interference on Rb and Sr (^{85}Rb was corrected for

interference of $^{170}\text{Er}^{++}$ and $^{170}\text{Yb}^{++}$; ^{86}Sr was corrected for interference of $^{172}\text{Yb}^{++}$; ^{87}Sr was corrected for interference of $^{174}\text{Yb}^{++}$; and ^{88}Sr was corrected for interference of $^{176}\text{Yb}^{++}$ and $^{176}\text{Lu}^{++}$). The $^{87}\text{Rb}/^{85}\text{Rb}$ mass bias was calculated using the Sr mass bias ($^{86}\text{Sr}/^{88}\text{Sr}$ measured relative to the $^{86}\text{Sr}/^{88}\text{Sr}$ natural value = 0.1196). The $^{87}\text{Sr}/^{86}\text{Sr}$ values were then corrected for interference of ^{87}Rb on ^{87}Sr . At that stage, the calculated $^{87}\text{Sr}/^{86}\text{Sr}$ values were not in agreement with the certified values of the reference materials. Therefore, a time-dependent function was used to correct for the certified values of $^{87}\text{Sr}/^{86}\text{Sr}$ values of the standards. This correction was completed using the $^{85}\text{Rb}/^{88}\text{Sr}$ measured (y) and $^{87}\text{Sr}/^{86}\text{Sr}$ measured subtracted by the certified value of $^{87}\text{Sr}/^{86}\text{Sr}$ for the reference materials (TB-1G and BHVO-2G) analyzed at the start and end of each analytical session (typically includes four samples). BIR-1G was not used for the correction because of lower Sr-Rb concentrations (larger analytical uncertainties) but is used to check the accuracy of the correction calculation. Using linear regressions, the slope (m) and intercept (b) were calculated for each individual analysis, then used to correct for drift over time and differences in the standard $^{87}\text{Sr}/^{86}\text{Sr}$ measured values to the true $^{87}\text{Sr}/^{86}\text{Sr}$ values. The certified value of $^{87}\text{Rb}/^{86}\text{Sr}$ in TB-1G was used to correct for $^{87}\text{Rb}/^{86}\text{Sr}$ in the samples. This was calculated using natural ratios and average published concentrations of Sr (1322 ± 52 ppm) and Rb (140 ± 10 ppm) for TB-1G (Norman et al. 2004; Elburg et al. 2005; Lucassen et al. 2011; Kimura and Chang 2012; Norman et al. 2016). Based on the difference between the value measured and the true $^{87}\text{Rb}/^{86}\text{Sr}$ in TB-1G empirical correction factors were calculated for each analysis (~2.3 to 2.0) and applied to the $^{87}\text{Rb}/^{86}\text{Sr}$ measured. In total, 131 analyses of BHVO-2G were completed with an average $^{87}\text{Sr}/^{86}\text{Sr}$ of 0.70347 ± 0.00022 (1σ), 55 analyses of BIR-1G gave an average $^{87}\text{Sr}/^{86}\text{Sr}$ of 0.7029 ± 0.0017 (1σ) and 56 analyses of TB-1G gave an average $^{87}\text{Sr}/^{86}\text{Sr}$ of 0.70565 ± 0.00011 (1σ). The standard deviation on BIR-1G is slightly higher because of lower

concentrations of both Sr and Rb within the reference material. Values obtained here i.e., BHVO-2G = 0.70345 to 0.70353, BIR-1G = 0.7030 to 0.7032, and TB-1G = 0.70558 to 0.70576 are within error of published ranges for these standards, available from the Georem database (<http://georem.mpch-mainz.gwdg.de>). The standard deviation was calculated individually for each analytical session based on the reproducibility of the standards within that sequence. The $^{87}\text{Sr}/^{86}\text{Sr}_i$ was calculated using the true values of $^{87}\text{Sr}/^{86}\text{Sr}$ and $^{87}\text{Rb}/^{86}\text{Sr}$ calculated and using an age of 2054.89 ± 0.37 Ma (Zeh et al. 2015) and a decay constant of 1.39×10^{-11} (Nebel et al. 2011).

4. Results

4.1 Core logging

Drill hole UMT094 is part of a sequence of drill holes located further down-dip on the central-western portion of Turfspruit (Fig. 3). The rocks sampled by these holes are considerably less affected by contamination with country rocks compared to other drill cores in the area. The magmatic stratigraphy established by Ivanplats (Fig. 4; Grobler et al. 2018) was used to log UMT094. Although not all units of the Ivanplats stratigraphy (Fig. 4; Grobler et al. 2018) are observed in UMT094, the drill core contains some of the best-preserved magmatic stratigraphy in the area. Figure 6 summarizes the magmatic stratigraphy logged in UMT094. Main Zone gabbro-norite (HW3) is the uppermost unit in UMT094 from 0 to 1186.66 meters. Below this, the four main cyclic units (BCU, MCU, FCU and UG2CU) are all present within UMT094. The BCU is composed of a mottled-spotted anorthosite (HW2 – 1186.66 to 1214.27 m) at the top, followed by pyroxenite-norite cyclic units (HW1 – 1214.27 to 1233.22 m) and a mineralized feldspathic pyroxenite (BAR – 1233.22 to 1239.13 m) at the base. A thin (~1 cm) chromite stringer is observed at the top of the mineralized feldspathic pyroxenite (1233.22 m). Following this, the MCU of UMT094 contains four of the six units in the MCU: feldspathic orthopyroxenite (MD1 – 1239.13 to 1252.34 m) occurs just below the BAR, followed by a mineralized feldspathic pyroxenite (M2 – 1252.34 to 1253.98 m), underlain by a mineralized pegmatoidal orthopyroxenite (M1U – 1253.98 to 1291.83 m) and lastly at the base, the mineralized pegmatoidal feldspathic harzburgites (M1L – 1291.83 to 1291.93 m). A chromite stringer occurs between M2 and M1U at 1253.98 meters. The FCU is located below the MCU and contains only two units: pyroxenite-norite cyclic units (FW3 – 1291.93 to 1335.95 m) and a weakly

mineralized interval (1335.95 to 1338.15 m), interpreted as a possible pseudoreef (PSDR). Although there is no pseudoreef unit within the Ivanplats stratigraphy (Fig. 4) because of inconsistent pseudoreef-type mineralization at Turfspruit, the pseudoreef unit was added in the stratigraphy of UMT094 due to similarities to other pseudoreefs in the BIC (PGE-mineralized olivine gabbro-norite/troctolite located between the Merensky Reef and UG2-equivalent chromitite). The UG2CU underlies the FCU and is composed of feldspathic pyroxenite (UG2HW – 1338.15 to 1364.77 m), the UG2 chromitite (1364.77 to 1365.42 m) and a pyroxenite or harzburgite (UG2FW – 1365.42 to 1404.03). Although most of the UG2CU in UMT094 is in part of the assimilation zone, the UG2 chromitite is still visible and the upper part of the UG2HW is unaffected by assimilation (Grobler et al. 2018). Another chromite seam (possibly the UG1-equivalent) is located within the assimilation zone at the bottom of the magmatic units in UMT094 (~1402 m).

Many major cyclic units (i.e., BCU, MCU, FCU and UG2CU) can be identified in drill core UMT094. Minor cyclic units (meter to 10s of meters scale) were identified within the major cyclic units and some seem to be composed of cycles smaller than one meter (micro-cyclic units).

The general stratigraphy of a cycle, where fully developed, grades from an olivine cumulate-bearing rock at the base to anorthosite at the top (Fig. 7). Although major cycles are developed within the stratigraphy, they do not typically include all units from a hypothetical fully developed cycle. Within these major cyclic units (i.e., BCU, MCU and FCU), minor and micro-cycles are also observed. More than 350 separate micro-cyclic units were identified through 215 m of drill core (Main Zone to UG2CU). At the meter scale, from below the Main Zone to the assimilation zone in UMT094, repetition of two to three units was observed (i.e., micro-cyclic units; Figs. 7-8). Figure 8 shows core box pictures of these micro-cyclic units within UMT094. Starting from just below the Main Zone, figure 8A shows norite to pyroxenite cycles from the HW2 of the

Bastard Cyclic Unit. The repetition of a pyroxenite and mela-gabbro-norite is also observed below the BAR in the MD1 of the MCU (Fig. 8B). These micro-cycles eventually grade into mineralized (sulfide-bearing) pyroxenites at the transition between the MD1 and M2 units. Repetition of micro-cyclic units is also found in the mineralized section of the MCU. Figure 8C shows alternating pegmatoidal feldspathic pyroxenite with a mineralized (sulfide-bearing) pyroxenite of the MCU. These micro-cycles are dominantly the pegmatoidal feldspathic pyroxenite in the lowermost part of the sequence of sub-cycles but gradually change upwards to dominantly pyroxenite with a small pegmatoidal feldspathic pyroxenite at the base of each small cycle. Repetition of micro-cycles constituting a pegmatoidal feldspathic pyroxenite containing disseminated-chromite at the base and a pegmatoidal feldspathic pyroxenite at the top, occurs in the lower part of the M1U (Fig. 8D). The most noticeable example of micro-cyclic units is in FW3 of the FCU (Fig. 8E), where repetition of small cycles (anorthosite at the top to pyroxenite at the bottom) at the tens of centimeters scale, and in some case at the meter scale, occur. This section is a repetition of the uppermost part of a fully developed cycle (Fig. 7-8E). In the Pseudoreef, an olivine-rich cumulate rock transitions to a pegmatoidal mineralized olivine-bearing feldspathic pyroxenite (Fig. 8F), containing an increase in intercumulus plagioclase and sulfides.

4.2 Petrography

Petrography was completed on 36 thin sections that were classified into groups based on their stratigraphic units. The main mineralogy of these stratigraphic units is displayed in Table 2.

The lowermost part of the preserved magmatic stratigraphy is mostly unaffected by assimilation is the UG2HW. This unit is mainly composed of mela-gabbro-norite containing ~60% orthopyroxene, ~16% clinopyroxene, and ~20% plagioclase (intercumulate). Minor

amounts of chromite (5-2%) are found within the UG2HW as well as trace amounts of white mica (~2%) and sulfides (~1%, dominantly pyrrhotite). Weak white mica alteration can be observed throughout the UG2HW.

The pseudoreef (PSDR), located just above the UG2HW, is mainly composed of an olivine gabbro/norite. The PSDR is dominantly composed of intercumulate plagioclase (40-20%), olivine (up to 25%), and orthopyroxene (~35%). Clinopyroxene is present in minor amounts (~4-8%). Chromite abundance is up to ~8%, whereas sulfide abundance (in a combination of pyrrhotite, chalcopyrite, pentlandite) account for up to ~4% of the sample. Some alteration is evident (white mica alteration of plagioclase, serpentinization of olivine).

Within the FW3, cycles from pyroxenite at the base to anorthosites at the top are present, therefore a large range in mineral abundance occurs through this unit. The FW3 is dominantly pyroxenite and mela-gabbro/norite at the base containing ~20-15% intercumulate plagioclase, with ~50% orthopyroxene and 35-25% clinopyroxene. In the upper part of the FW3, plagioclase is dominantly cumulate ranging from ~50-90%, with ~40-2% orthopyroxene and ~40-1% clinopyroxene. Sulfides are concentrated at the base of the FW3, ranging from 3-1% (pyrrhotite > chalcopyrite > pentlandite) at the base and ~2% (pyrrhotite > chalcopyrite = pentlandite) to trace amounts in the upper part of FW3. Alteration within these samples is usually weak to moderate white mica alteration with some localized alteration containing biotite, chlorite, magnetite, pyrite and gedrite.

The M1L, the lowest unit of the Merensky Cyclic Unit, is described as an olivine norite and is composed of ~20% cumulate olivine, ~15% clinopyroxene, ~8% intercumulate plagioclase, ~3% orthopyroxene, and alteration products (45%) mostly from serpentinization of olivine. Sulfides compose ~ 3% (pyrrhotite = chalcopyrite = pentlandite) of the M1L and chromite is

present up to ~3%. Strong alteration is found throughout the unit, including moderate white mica alteration of plagioclase, and minor magnetite stringers associated with serpentinization (~3%).

The M1U consist of a large range in rocks due to cyclicity between a pegmatoidal feldspathic pyroxenite to pyroxenite/orthopyroxenite to mela-gabbro. This section has a large range in mineral abundance where orthopyroxene can range from ~75 to 1% in abundance, clinopyroxene can range from ~80 to 1% and intercumulate plagioclase can range from ~25 to 10%. Chalcopyrite, pyrrhotite and pentlandite (Ccp = Po = Pn) can all reach ~2% in some sections but can also occur in trace amounts. Chromite can be present in up to ~3% but is absent in some sections of M1U. Strong alteration is present in some samples, mainly the pegmatoidal feldspathic pyroxenites, where up to ~15% white mica can be present with some chlorite, biotite, calcite, magnetite and gedrite.

In the MD1, the uppermost part of the Merensky Cyclic Unit, the samples are mainly mela-gabbro/norite and contain ~70% orthopyroxene, ~10-3% clinopyroxene and ~20-15% intercumulate plagioclase. Weak white mica alteration occurs within the plagioclase with some magnetite within these units. Only ~1% of pyrrhotite and trace amounts of chalcopyrite and pentlandite can be found in this section.

The BAR (Bastard Reef) ranges from an olivine-bearing mela-gabbro to mela-gabbro and contains roughly ~65% orthopyroxene, ~15-5% clinopyroxene, and ~25-15% intercumulate plagioclase. Some olivine (~5%) can be found associated with the chromite stringer at the top of the Bastard Reef. Chalcopyrite is the dominant sulfide in the Bastard Reef (~2-1%) but some pyrrhotite (~1%) and trace pentlandite are also present. Minor chromite sometimes occurs in the BAR up to ~1% in specific sections. The dominant alteration is white mica (~4-3%) of plagioclase but some biotite (~1% to trace), magnetite (trace) and chlorite (trace) is present.

Just above the BAR is the HW1, still part of the BCU, which is composed of cyclic units from mela-gabbro norite at the base to anorthosite at the top. The main unit within this sequence is gabbro norite that contains mostly cumulate plagioclase (~60-50%) with ~20% cumulate orthopyroxene and ~20% cumulate clinopyroxene. Some minor white mica (~3%) does occur and trace amounts of sulfides (pyrrhotite = chalcopyrite = pyrite) are present.

The uppermost unit of the BCU is the HW2, which is a mottled anorthosite. This unit is composed of mainly ~70% cumulate plagioclase with ~25% cumulate orthopyroxene and ~3% cumulate clinopyroxene. Minor white mica alteration occurs within the plagioclase and trace amounts of biotite, magnetite, pyrrhotite, chalcopyrite and pyrite occur throughout the unit.

Lastly, the Main Zone (HW3) is composed mainly of gabbro norite with minor pyroxenite units. The gabbro norite is composed of ~65-55% cumulate plagioclase, ~30% orthopyroxene and ~15% clinopyroxene.

4.3 Plagioclase composition

Data for An content of plagioclase are presented in [Table 3](#). As illustrated in [Fig. 9](#), the anorthite content of plagioclase changes through the magmatic stratigraphy of UMT094 but varies more significantly within some cyclic units than others. From the uppermost part of the UG2CU to the uppermost part of the FCU there is a gradual increase in anorthite content from ~An₆₉ to ~An₇₆, with little variation in An content within individual samples. The olivine gabbro norite of the MIL has the highest anorthite content at An₈₂. For the rest of the MCU and BCU, the median anorthite content fluctuates mainly between An₆₀ and An₇₆. Larger ranges of anorthite content within individual samples occur in the MCU and BCU. Significant ranges in An content can be observed at ~1282 m depth with samples ranging from An₄₅ to An₇₆. Most mineralized units within the BCU and MCU have a larger range in anorthite content compared to

the MZ and FCU. The anorthite content is relatively constant in the Main Zone, ranging between An₆₇ and An₇₄ but does shift slightly between individual units.

4.4 Whole-rock strontium isotopes

Whole-rock strontium isotope analyses, including uncertainties and $^{87}\text{Sr}/^{86}\text{Sr}_i$ values are presented in [Table 4](#). A total of 25 whole-rock sample analyses for strontium isotopes were completed throughout the magmatic stratigraphy ([Fig. 10](#)). The $^{87}\text{Sr}/^{86}\text{Sr}_i$ for samples below the MCU range from 0.7053 to 0.7071, increasing slightly towards the contact between the FCU and MCU. Throughout the MCU and BCU, $^{87}\text{Sr}/^{86}\text{Sr}_i$ values range from 0.7056 within the M1L to 0.7093 within the lower M1U. The $^{87}\text{Sr}/^{86}\text{Sr}_i$ values change between 0.7068 and 0.7090 throughout the rest of the MCU and BCU. Within the Main Zone, one sample at 126 m above the base of the MCU has a $^{87}\text{Sr}/^{86}\text{Sr}_i$ value of 0.7066. All other samples within the Main Zone are between 0.7081 and 0.7094.

4.5 In-situ strontium isotopes in plagioclase

Data for individual plagioclase analyses for strontium isotope are presented in [Table 5](#). A total of 251 plagioclase analyses (core, rim or whole grain) were completed on thirty-seven samples through the stratigraphy ([Fig. 11](#)). Below the MCU, $^{87}\text{Sr}/^{86}\text{Sr}_i$ values are between 0.7058 and 0.7069. Within the MCU, $^{87}\text{Sr}/^{86}\text{Sr}_i$ values increase from ~0.7062 at the bottom to ~0.7090 at ~1261 m, before decreasing to ~0.7072 at the top of the MCU. $^{87}\text{Sr}/^{86}\text{Sr}_i$ values within the BCU show considerable variation between 0.7070 to just above 0.7080. In the Main Zone, the initial Sr isotope ratios range from ~0.7075 in the lowermost sample, up to ~0.7085 at ~1135 m, and decreasing to ~0.7080 in the uppermost sample.

4.6 Cr/MgO

Cr/MgO values of UMT094 (Table 6) show a decreasing trend from the lower major cyclic units (FCU and UG2CU) to the Main Zone (Fig. 12). Within the UG2CU and FCU, Cr/MgO values are variable but are higher than values within the MCU, BCU and Main Zone. Values within the UG2CU peak at ~2450 and within the FCU Cr/MgO exceeds 500 in parts of the stratigraphy. Within the MCU there is a peak at Cr/MgO = ~500, followed by a sharp decrease to ~110-120 through the rest of the MCU and Lower BCU. The upper part of the BCU changes from Cr/MgO = 60 and increases to 75, which remains constant into the Main Zone. These variations are mostly controlled by the distribution of chromitite seams (which control the Cr content in the rocks).

5. Discussion

5.1 Strontium isotope stratigraphy of the Northern Limb

The whole-rock strontium isotope profile of UMT094 (Fig. 10) demonstrates a similar trend to the well-known $^{87}\text{Sr}/^{86}\text{Sr}_i$ shift, from 0.7065 to 0.7080, that occurs at the stratigraphic height of the Merensky Reef initially identified by Kruger & Marsh (1982) in the Eastern and Western limbs of the BIC (Fig. 5A). In UMT094 the shift is from $^{87}\text{Sr}/^{86}\text{Sr}_i = 0.706$ at the base of the FCU, to $^{87}\text{Sr}/^{86}\text{Sr}_i = 0.708$ in the Main Zone. Minor fluctuations can be observed throughout the isotopic profile (Fig. 10). Although the transition from the Critical Zone to the Main Zone in the Eastern and Western limbs is typically sharp or gradational without many smaller shifts, the isotope profile in the Northern Limb is different (Fig. 10). Smaller shifts can be observed throughout the Transitional Units (MCU and BCU) and Footwall Cyclic Unit. The shifts commonly coincide with some minor-cycles, smaller than the Bastard, Merensky and Footwall Cyclic units, but are most likely associated with increased alteration within some of the samples especially through the MCU and BCU. The large variation (largest from 45 to 76) and decrease in An content of plagioclase through the MCU and BCU confirms that there is an increase in alteration through these cyclic units (Fig. 9). Although some uncertainties on the strontium isotope analyses for whole-rock are much larger than the *in-situ* analyses (mainly in the MCU due to high whole-rock Rb/Sr values) the main shift can still be identified. Samples within the assimilation zone (below 1355 m) have more radiogenic signatures (> 0.710) and therefore have inherited part of the footwall isotopic signature, making them unusable for developing a strontium isotope stratigraphy of the primary magmas (see Table 4 for additional samples within the assimilation zone and footwall). The high $^{87}\text{Sr}/^{86}\text{Sr}_i$ coincide with values published by Kruger

(2005; average of 0.7109 at Turfspruit) and Barton et al. (1986; range from 0.7054 to 0.7226 at Overysel and Sandsloot) indicating that both of these studies sampled magmatic stratigraphy affected by footwall assimilation. Additionally, with the new stratigraphy from Grobler et al. (2018) one can identify the location of the samples analysed by Kruger (2005) in relation to the Merensky Reef.

Due to the high uncertainties of some of the whole-rock strontium isotope sample analyses, *in-situ* strontium isotope analyses on plagioclase were completed on the same set of samples, including additional samples to fill gaps within the whole rock strontium isotope stratigraphy (Fig. 11). These data are similar to the whole-rock strontium isotope data but show some significant differences. Firstly, the uncertainties on the *in-situ* analyses are much smaller (~0.0002) than the uncertainties of the samples completed for whole-rock strontium isotopes (up to ~0.0013). Fluctuations in strontium isotope stratigraphy within major cyclic units are seen in the whole-rock data; however, such fluctuations are absent in the strontium isotope stratigraphy based on *in-situ* analyses in plagioclase. This is attributed to the addition of radiogenic Sr because of increased alteration within the MCU and BCU, which is the stratigraphic location for most of the fluctuations occurring in the stratigraphy (Fig. 10). Use of *in-situ* analyses in plagioclase allow for selection of unaltered plagioclase grains (grains with evident alteration were not analyzed). Additionally, the *in-situ* analyses for the Main Zone, FCU and UG2CU are much more consistent throughout the units compared to the samples completed by whole-rock analyses. This is likely because of the whole-rock data consisting of a mixture of three main sources within the rock: (1) plagioclase, (2) pyroxene and (3) alteration. Although alteration was avoided as much as possible during sampling and selection of samples for whole-rock strontium isotope analyses, alteration through some sections of the stratigraphy was unavoidable. Nonetheless, the whole-rock data indicate that the Northern Limb stratigraphy shows a similar shift, at a similar

stratigraphic position, to the shift occurring at the Merensky Reef in the Eastern and Western limbs.

The *in-situ* analyses assist in inferring processes, from the mineral scale to the scale of the whole magma chamber, occurring at the time of formation of the Northern Limb and the rest of the BIC. Firstly, the comparison between core, rim and whole-plagioclase analyses give some insight on magmatic processes occurring at the time of formation. Through the UG2CU, FCU, MCU and BCU, there is no clear distinction between the core, rim and whole-plagioclase values. In the three uppermost samples of the Main Zone, there is a clear distinction between the rim and core values. The mean of the rims is more radiogenic than the cores in samples 1096, 1111 and 1135 (1096 – core of 0.70784 ± 21 and rim of 0.70796 ± 8 ; 1111 – core of 0.70781 ± 27 and rim of 0.70817 ± 9 ; 1135 – core of 0.70813 ± 2 and rim of 0.70861 ± 8). Although there was no visual evidence of zonation in plagioclase (EMPA and LA-ICPMS element distribution maps; [Appendix A](#)), there was evidence of isotopic zonation within the Main Zone plagioclase ([Fig. 11](#)). Both cumulate and intercumulate plagioclase was analyzed for *in-situ* strontium isotopes but there was no significant difference between the two types in the same major cyclic unit ([Fig. 13](#)). As the whole-rock strontium isotopes showed, the shift occurring through the Transitional Units in the Eastern and Western limbs is also present through mineralization in the Upper Platreef. The shifts towards higher $^{87}\text{Sr}/^{86}\text{Sr}_i$ through the stratigraphy (lower sections of the MCU and BCU) correlate with significant Pt-Pd mineralization ([Fig. 14](#)) indicating that mineralization and the isotopic shift are likely related to the same process (e.g., influx of contaminated magma into the chamber).

5.2 Magmatic stratigraphy

Different stratigraphic schemes have been used across the Northern Limb (e.g. GNPA member, A-B-C Reefs, Platreef, Aurora and Waterberg; [Fig. 15](#)). Unfortunately, the use of different stratigraphic units has made it challenging to correlate lithologies throughout the Northern Limb and to test correlations with the Eastern and Western limbs. The lack of correlation is mostly due to the disturbance of magmatic stratigraphy in proximity to the footwall as a result of extensive assimilation. In the Northern Limb there are distinct differences between Bushveld rocks located relatively close to the footwall (in outcrop and up-dip) compared to Bushveld rocks further down-dip ([Fig. 16](#)). In the assimilation zone (up to several hundreds of meters above the footwall) all magmatic units have textures reflecting assimilation of Transvaal rocks but textures vary depending on proximal footwall lithologies ([Fig. 16](#)). Most units have sporadic intervals of vari-textured norite, gabbronorite, pyroxenite or harzburgite. Within this zone, cyclic units are indistinguishable from one another and magmatic cumulate textures are almost lost. The presence of calc-silicate xenoliths within the magmatic stratigraphy is indicative of assimilation within those specific units. Xenoliths are common within the assimilation zone and are remnants of footwall assimilation, but they can also be found outside of the assimilation zone. Xenoliths typically occur at the bottom of larger cyclic units, possibly indicating that they were transported into the magma chamber with new pulses of magma or dislodged from the footwall or hanging wall to the chamber during the emplacement of new pulses of magma. At the Aurora project, calc-silicate xenoliths are present throughout all units ([McDonald et al. 2017](#)), indicating that these magmatic units are likely all part of the assimilation zone. I suggest that at the Aurora Project, Unit 3 can be correlated to the Main Zone, Unit 2 contains the Bastard, Merensky and Footwall Cyclic Units, and Unit 1 represents the Critical Zone ([Fig. 15](#)). Similarly, throughout the Platreef calc-silicate xenoliths have been identified in most of the magmatic stratigraphy ([Holwell and McDonald 2006](#); [Hutchinson and McDonald 2008](#); [Maier et al. 2008](#);

Ihlenfeld and Keays 2011). Although individual units are lost within the assimilation zone, chromitite layers such as the UG2-equivalent, can typically be observed within the assimilation zone and are relatively undisturbed (Grobler et al. 2018). The Pt-Pd mineralization of the Bastard Reef and Merensky Reef also progresses through the assimilation zone but becomes more dispersed due to mingling between the magmatic units and footwall rocks. Although assimilation affects the consistency of mineralization, the main reefs can typically be located with the highest grade in Pt-Pd-Rh-Au (Grobler et al. 2018).

The down-dip stratigraphy of the Northern Limb has many similarities to the Eastern and Western limbs. As proposed by Grobler et al. (2018), the Bastard and Merensky Cyclic Units are present but are thicker in comparison to equivalent cyclic units in the Eastern and Western limbs. The stratigraphy documented at Turfspruit can be applied throughout the magmatic units located out of the assimilation zone in the Northern Limb. Figure 15 shows the stratigraphy at Turfspruit with potential correlations between the A-B-C reef described by Barton et al. (1986) and other stratigraphic units used through the Northern Limb (Platreef, GNPA Member, Aurora, Waterberg). The Platreef is a combination of all the major cyclic units stacked together and can be much thicker than 100 m (Kinnaird et al. 2005), seemingly showing erratic mineralization throughout the whole unit (Fig. 15).

The micro-cyclicity present within UMT094 (Fig. 8) could indicate processes related to mineralization in the Northern Limb. Although outside the scope of this study, the presence of these micro-cyclic units could provide clues to explain the thicker mineralization of the Northern Limb. The stacking of multiple micro-cycles containing mineralization at the bottom of individual cycles could lead to a thicker mineralization compared to the single reef seen in the Eastern and Western limbs of the BIC. One hypothesis could be that the presence of these cycles is related to the proximity of a major feeder, which some have suggested is located in the vicinity

of Mokopane (Kruger 2005; van der Merwe 2008 and references therein; Finn et al. 2015). The relation between the thickness of mineralization, micro-cycles and the proximity of a feeder is simply a hypothesis and more work needs to be done.

5.3 Comparison of Turfspruit results to the Eastern and Western limbs

In the Western Limb of the BIC at Rustenburg Platinum Mines, Kruger and Marsh (1982) identified a shift in $^{87}\text{Sr}/^{86}\text{Sr}_i$ at the stratigraphic location of the Merensky pegmatoid. Elsewhere in the BIC, the shift at this stratigraphic level comprises of a shift through the MCU (~10 m thick) from ~0.7064 at the base to ~0.7075 at the top. This shift continues through the BCU and the $^{87}\text{Sr}/^{86}\text{Sr}_i$ value increases to ~0.7080. Kruger and Marsh (1982) suggested that this isotopic shift is related to a new magma influx and magma mixing. Additionally, the MCU and BCU are thought to represent proportions of mixing between the resident magma and the new magma influx, which was homogenized throughout the Bushveld magma chamber (Kruger and Marsh 1982; Kruger 1992). Seabrook et al. (2005) compiled different Sr isotope studies through the Transitional Units (MCU and BCU) across the BIC (Fig. 17; Western Limb localities: Amandelhult, Union, Rustenburg, Brits; Eastern Limb localities: Richmond, Atok). Throughout the BIC, the $^{87}\text{Sr}/^{86}\text{Sr}_i$ shift is present through the Transitional Units, although it varies from a sharp shift at the base of the MCU to a gradual shift through the Transitional Units.

Data collected during this project show a similar shift in the upper part of the Platreef in UMT094. The shift occurs through the MCU and BCU (Fig. 11). In the UG2CU and FCU, the $^{87}\text{Sr}/^{86}\text{Sr}_i$ values are consistently near ~0.7064 on average. The MCU contains the main isotopic shift, which is also seen in the rest of the BIC but increases up to ~0.709 within the MCU. The $^{87}\text{Sr}/^{86}\text{Sr}_i$ values at the top of the BCU in UMT094 are ~0.7075 on average and increase to just under 0.7080 in the Main Zone. Thus, the Transitional Units of the Northern Limb show the same

shift as that of the Eastern and Western limbs (Fig. 17). In addition, the Cr/MgO values (Cr content mainly controlled by chromite and clinopyroxene; MgO content mainly controlled by orthopyroxene) from UMT094 (Fig. 12) shows a similar transition from the Critical Zone to the Main Zone than that of Seabrook et al. (2005) in the Eastern and Western limbs. I conclude that the mineralized sections of the Platreef in the Northern Limb can be correlated with the Merensky and Bastard reefs in the Eastern and Western limbs and, therefore, the stratigraphy used in the Eastern and Western limbs is applicable to the Northern Limb.

The magnitude of the excursion up to $^{87}\text{Sr}/^{86}\text{Sr}_i \sim 0.7090$ at ~1261 m in the MCU has yet to be documented elsewhere in the BIC. However, some samples with $^{87}\text{Sr}/^{86}\text{Sr}_i$ values of 0.7090 have been measured within the Transitional Units at Brits and Atok (Seabrook et al. 2005; Fig. 17). In the Northern Limb, increases in $^{87}\text{Sr}/^{86}\text{Sr}_i$ values occur only through the mineralized units of the MCU. Another subtle increase in $^{87}\text{Sr}/^{86}\text{Sr}_i$ is located through the mineralization at the base of the BCU. Thus, reef mineralization is coincident with increasing $^{87}\text{Sr}/^{86}\text{Sr}_i$ values, which I interpret as linking new pulses of different or contaminated magma to PGE mineralization. The $^{87}\text{Sr}/^{86}\text{Sr}_i$ of 0.7090 could be a closer representation of the isotopic signature from the contaminated pulse of magma that entered the magma chamber at the stratigraphic location of the Merensky Reef. Furthermore, the thickness of the MCU and BCU in the Northern Limb is also consistent with a thicker interval over which the $^{87}\text{Sr}/^{86}\text{Sr}_i$ shift occurs compared to locations in the Eastern and Western limbs of the BIC. Therefore, the proximity to the feeder could play a role in the magnitude of the excursion being thicker at Turfspruit Farm and thinner further away in the Eastern and Western limbs. The presence of a gradual isotopic shift through the Transitional Units compared to a sharp shift could possibly also be explained by the proximity of a feeder to Mokopane, which Finn et al. (2015) identified as the possible location of the feeder to the BIC.

5.4 Comparison of Turfspruit results to the Northern Limb

Only a few studies on strontium isotopes have been completed in the Northern Limb of the BIC. [Barton et al. \(1996\)](#) and [Kruger \(2005\)](#) analysed samples from the Platreef but these were within the assimilation zone, resulting in more radiogenic $^{87}\text{Sr}/^{86}\text{Sr}_i$ values (> 0.710). The *in-situ* Sr isotopic data documented by [Mangwegape et al. \(2016\)](#) in the Upper and Main zones of the Northern Limb show similar trends to the compilation by [Kruger \(1994\)](#) in the Western Limb ([Fig. 5A](#)). However, correlation between all limbs was still unclear primarily because [Mangwegape et al. \(2016\)](#) did not document samples in the Critical Zone that were not heavily influenced by footwall assimilation. The data presented from the Main Zone here are consistent and overlap with data in [Mangwegape et al. 2016](#), but the main contribution of the work documented in this thesis pertains to data stratigraphically below (i.e., within the Critical Zone). Some samples (e.g. 1111, 1135, 1165; [Table 5](#)) in the Main Zone show similar $^{87}\text{Sr}/^{86}\text{Sr}_i$ values to the least radiogenic samples in [Mangwegape et al. \(2016\)](#) but direct correlation is difficult without detailed logging of magmatic units. [Huthmann et al. \(2017\)](#) published data from the Waterberg Project, which show consistent $^{87}\text{Sr}/^{86}\text{Sr}_i$ values between 0.7065 to 0.7075 throughout the whole sequence. There is no large shift within the mineralization of the Waterberg Project, further indicating that the Waterberg magmatic sequence might be disconnected from the rest of the BIC, as suggested by [Huthmann et al. \(2017\)](#).

5.5 The Platreef

The Platreef is renowned to be the mineralized unit located in the Northern Limb of the BIC between the Main Zone and the footwall, and has been suggested to be the stratigraphic equivalent to the Merensky Reef in the Eastern and Western limbs ([Schouwstra et al. 2000](#);

[Manyeruke et al. 2005 and references therein; Grobler et al. 2018](#)). The data presented here confirms a direct correlation between the units containing mineralization in the upper Platreef and the Merensky Reef. Therefore, the magmatic stratigraphy presented by [Grobler et al. \(2018; Fig. 4\)](#) should be applicable to the rest of the Northern Limb and the term “Platreef” should be used with caution. The term is valid to describe sections in which footwall assimilation has destroyed recognizable magmatic stratigraphy but not to imply that the Platreef has a different origin than the MCU. The term Platreef has been used because it was thought that the magmatic units containing mineralization in the Northern Limb were of a different origin than the magmatic units hosting the Merensky Reef in the Eastern and Western limbs. This interpretation (i.e., the Platreef having a different origin than the Upper Critical Zone in the rest of the BIC) is likely due to the deceiving overprinting assimilation textures disrupting the magmatic stratigraphy, which texturally makes the Platreef seem like one magmatic unit. However, the Platreef consists of multiple magmatic units within the assimilation zone of the Northern Limb ([Grobler et al. 2018](#)). The Platreef is not a reef itself but contains multiple mineralized reefs within its stratigraphy, which are interlayered with magmatic units containing no mineralization. Although assimilation of the footwall might disrupt minor magmatic units and textures, major cyclic units can still be distinguished from one another ([Grobler et al. 2018; this study](#)).

6. Conclusions

The strontium isotope stratigraphy through the upper part of the UCZ and the lower MZ in the Northern Limb of the BIC exhibits a gradual shift in $^{87}\text{Sr}/^{86}\text{Sr}_i$ from 0.7064 at the top of the FCU to 0.7090 in the MCU. This main shift is followed by a decrease to 0.7074 at the base of the BCU, which finally increases through the BCU and stabilizes at 0.7080 within the MZ (Fig. 11). The main $^{87}\text{Sr}/^{86}\text{Sr}_i$ shift coincides with the mineralized interval in the drill core investigated. Thus, the Sr isotope shift provides strong evidence that mineralization in the Platreef correlates with the Merensky Reef in the Eastern and Western limbs of the Bushveld Igneous Complex. This is consistent with the stratigraphy proposed in Grobler et al. (2018) defining the mineralized units in the Northern Limb as the Merensky Cyclic Unit. This correlation has been obscured in other areas in the Northern Limb due to the proximity and extensive assimilation of footwall rocks in outcropping and shallow mineralized areas. Additionally, the isotopic correlation validates that the stratigraphy of the Northern Limb is similar to that of the Eastern and Western Limbs. Therefore, the magmatic stratigraphy proposed by Grobler et al. (2018) should be applicable throughout the Northern Limb, with exception to the magmatic stratigraphy of the Waterberg Project because of different magmatic and strontium isotope stratigraphy. The strontium isotope shifts towards more radiogenic $^{87}\text{Sr}/^{86}\text{Sr}_i$ values, at the base of the MCU and BCU, are directly linked to significant Pt-Pd mineralization indicating that the mineralization may be linked to the processes causing the shift in $^{87}\text{Sr}/^{86}\text{Sr}_i$ (Fig. 14). Also, the thickness of the interval across which the $^{87}\text{Sr}/^{86}\text{Sr}_i$ changes in the Northern Limb is much thicker than the Sr isotopic shift occurring elsewhere in the BIC. Lastly, micro-cyclicality within the magmatic units of the Northern Limb could provide new evidence that could help unravel the origin of the thick mineralization, although more work is needed to explore this hypothesis.

7. Recommendations for future work

Although this research has answered some major questions about the Northern Limb and the correlation of the Northern Limb to the rest of the BIC, there are still some unanswered questions and new questions that have surfaced over the course of this research:

(1) Strontium isotope stratigraphy

- a) Are there pristine magmatic units down-dip away from assimilation along the whole Northern Limb? Looking at drill core further down-dip away from assimilation is key to identifying magmatic units undisturbed by assimilation.
- b) Can the strontium isotopic shift be documented throughout the Northern Limb? Strontium isotopic stratigraphy has a very good potential to assess the extent of the MCU and BCU towards the northernmost sections of the Northern Limb.

(2) Micro-cyclic units

- a) Are the micro-cyclic units only in the Northern Limb or can some be observed throughout the Bushveld? Documentation in this thesis of micro-cyclic units has been described in detail and needs to be documented by others during future work for comparison across the BIC.

8. References

- Barnes S-J, Maier WD and Curl EA. (2010) *Composition of the Marginal Rocks and Sills of the Rustenburg Layered Suite, Bushveld Complex, South Africa: Implications for the Formation of the Platinum-Group Element Deposits*. *Economic Geology* 105 (8): 1491-1511.
- Barton JM, Cawthorn RG and White J. (1986) *The Role of Contamination in the Evolution of the Platreef of the Bushveld Complex*. *Economic Geology* 81 (5): 1096-1104.
- Carr HW, Kruger FJ, Groves DI and Cawthorn RG. (1999) *The Petrogenesis of Merensky Reef Potholes at the Western Platinum Mine, Bushveld Complex: Sr-Isotopic Evidence for Synmagmatic Deformation*. *Mineralium Deposita* 34 (4): 335-47.
- Cawthorn, RG, Eales HV, Walraven F, Uken R and Watkeys MK. (2006) *The Bushveld Complex*. In: Johnson MR, Anhaeusser CR and Thomas RJ. (editors) *The Geology of South Africa*, First edition. Geological Society of South Africa, Johannesburg: 261-281.
- Cawthorn, RG and Walraven F. (1998) *Emplacement and Crystallization Time for the Bushveld Complex*. *Journal of Petrology* 39 (9): 1669-87.
- Cawthorn, RG. (2010) *The Platinum Group Element Deposits of the Bushveld Complex in South Africa*. *Platinum Metals Review* 54 (4): 205-15.
- Cheong C, Jeong Y-J and Kwon S-T. (2014) *Correction of spike contribution for strontium isotopic measurement by thermal ionization mass spectrometry: a test for spike-standard mixed solutions*. *Journal of Analytical Science and Technology* 5 (26): 1-4.
- Chutas NI, Bates E, Prevec SA, Coleman DS and Boudreau AE. (2012) *Sr and Pb Isotopic Disequilibrium between Coexisting Plagioclase and Orthopyroxene in the Bushveld Complex, South Africa: Microdrilling and Progressive Leaching Evidence for Sub-Liquidus Contamination within a Crystal Mush*. *Contributions to Mineralogy and Petrology* 163 (4): 653-68.
- Eales HV, Marsh JS, Mitchell AA, de Klerk WJ, Kruger FJ and Field M. (1986) *Some Geochemical Constraints upon Models for the Crystallization of the Upper Critical Zone-Main Zone Interval, Northwestern Bushveld Complex*. *Mineralogical Magazine* 50: 567-82.
- Eales HV, de Klerk WJ, Butcher AR and Kruger FJ. (1990) *The Cyclic Unit beneath the UG1 Chromitite (UGIFW Unit) at RPM Union Section Platinum Mine-Rosetta Stone of the Bushveld Upper Critical Zone?*. *Mineralogical Magazine* 54 (March): 23-43.
- Eales HV, de Klerk WJ and Teigler B. (1990) *Evidence for Magma Mixing Processes within the Critical and Lower Zones of the Northwestern Bushveld Complex, South Africa*. *Chemical Geology* 88: 261-78.
- Elburg M, Vroon P, van der Wagt B and Tchalikian A. (2005) *Sr and Pb isotopic composition of five USGS glasses (BHVO-2G, BIR-1G, BCR-2G, TB-1G, NKT-1G)*. *Chemical Geology* 223: 196-207.
- Finn CA, Bedrosian PA, Cole JC, Khoza TD and Webb SJ. (2015) *Mapping the 3D extent of the Northern Lobe of the Bushveld layered mafic intrusion from geophysical data*. *Precambrian Research* 268: 279-294.
- Gao Y, Hoefs J, Hellebrand E, von der Handt A and Snow JE. (2007) *Trace Element Zoning in Pyroxenes from ODP Hole 735B Gabbros: Diffusive Exchange or Synkinematic Crystal Fractionation?* *Contributions to Mineralogy and Petrology* 153: 429-42.
- Godel B, Barnes S-J and Maier WD. (2007) *Platinum-Group Elements in Sulphide Minerals, Platinum-Group Minerals, and Whole-Rocks of the Merensky Reef (Bushveld Complex, South Africa): Implications for the Formation of the Reef*. *Journal of Petrology* 48 (8): 1569-1604.

- Grobler DF, Brits JAN, Maier WD and Crossingham A. (2018) *Litho- and chemostratigraphy of the Flatreef PGE deposit, northern Bushveld Complex*. Mineralium Deposita 2018: <https://doi.org/10.1007/s00126-018-0800-x>.
- Hamilton J. (1977) *Sr Isotope and Trace Element Studies of the Great Dyke and Bushveld Mafic Phase and Their Relation to Early Proterozoic Magma Genesis in Southern Africa*. Journal of Petrology 18 (1): 24–52.
- Harmer RE and Sharpe MR. (1985) *Field Relations and Strontium Isotope Systematics of the Marginal Rocks of the Eastern Bushveld Complex*. Economic Geology 80 (4): 813–37.
- Harris C and Chaumba JB. (2001) *Crustal Contamination and Fluid–rock Interaction during the Formation of the Platreef, Northern Limb of the Bushveld Complex, South Africa*. Journal of Petrology 42 (7): 1321–47.
- Holwell DA, Boyce AJ and McDonald I. (2007) *Sulfur Isotope Variations within the Platreef Ni-Cu-PGE Deposit: Genetic Implications for the Origin of Sulfide Mineralization*. Economic Geology 102 (6): 1091–1110.
- Holwell DA and McDonald I. (2007) *Distribution of Platinum-Group Elements in the Platreef at Overysel, Northern Bushveld Complex: A Combined PGM and LA-ICP-MS Study*. Contributions to Mineralogy and Petrology 154 (2): 171–90
- Holwell DA, McDonald I and Armitage PEB. (2006) *Platinum-Group Mineral Assemblages in the Platreef at the Sandsloot Mine, Northern Bushveld Complex, South Africa*. Mineralogical Magazine 70 (1): 83–101.
- Holwell DA, Armitage PEB and McDonald I. (2005) *Observations on the Relationship between the Platreef and Its Hangingwall*. Transactions of the Institutions of Mining and Metallurgy, Section B: Applied Earth Science 114 (4): 199–207.
- Holwell DA and McDonald I. (2006) *Petrology, Geochemistry and the Mechanisms Determining the Distribution of Platinum-Group Element and Base Metal Sulphide Mineralisation in the Platreef at Overysel, Northern Bushveld Complex, South Africa*. Mineralium Deposita 41 (6): 575–98.
- Hutchinson D and McDonald I. (2008) *Laser Ablation ICP-MS Study of Platinum-Group Elements in Sulphides from the Platreef at Turfspruit, Northern Limb of the Bushveld Complex, South Africa*. Mineralium Deposita 43 (6): 695–711.
- Huthmann FM, Kinnaird JA, Yudovskaya MA and Elburg M. (2017) *The Sr isotopic stratigraphy of the far northern Bushveld Complex*. South African Journal of Geology 120 (4): 499–510.
- Ihlenfeld C and Keays RR. (2011) *Crustal Contamination and PGE Mineralization in the Platreef, Bushveld Complex, South Africa: Evidence for Multiple Contamination Events and Transport of Magmatic Sulfides*. Mineralium Deposita 46 (7): 813–32.
- Junge M, Oberthür T and Melcher F. (2014) *Cryptic Variation of Chromite Chemistry, Platinum Group Element and Platinum Group Mineral Distribution in the UG-2 Chromitite: An Example from the Karee Mine, Western Bushveld Complex, South Africa*. Economic Geology 109 (3): 795–810.
- Keays RR, Ihlenfeld C, Foster J and Jowitt S. (2011) *Crustal Contamination and PGE Mineralization in the Platreef, Bushveld Complex, South Africa: Evidence for Multiple Contamination Events and Transport of Magmatic Sulfides*. Mineralium Deposita 46 (7): 813–32.
- Kimura J-I and Chang Q. (2012) *Origin of the suppressed matrix effect for improved analytical performance in determination of major and trace elements in anhydrous silicate samples using 200 nm femtosecond laser ablation sector-field inductively coupled plasma mass spectrometry*. Journal of Analytical Atomic Spectrometry 27: 1549–1559.

- Kinnaird JA, Yudovskaya M, Mccreesh M, Huthmann F and Botha TJ. (2017) *The Waterberg Platinum Group Element Deposit: Atypical Mineralization in Mafic-Ultramafic Rocks of the Bushveld Complex, South Africa*. *Economic Geology* 112: 1367-1394.
- Kinnaird JA, Kruger FJ, Nex PAM and Cawthorn RG. (2002) *Chromitite Formation — a Key to Understanding Processes of Platinum Enrichment*. *Applied Earth Science*, no. 1: 23–35.
- Kinnaird JA, Yudovskaya M, Mccreesh M, Huthmann F and Botha TJ. (2017) *The Waterberg Platinum Group Element Deposit: Atypical Mineralization in Mafic-Ultramafic Rocks of the Bushveld Complex, South Africa*. *Economic Geology* 112: 1367–94.
- Kinnaird JA (2005) *Geochemical evidence for multiphase emplacement in the southern Platreef*. *Applied Earth Science* 114 B: 225-242
- Kinnaird JA. (2005) *The Bushveld Large Igneous Province*. Large Igneous Provinces Commission. <http://www.largeigneousprovinces.org/05may>. Accessed January 2018.
- Kinnaird JA and McDonald I. (2005) *An Introduction to Mineralisation in the Northern Limb of the Bushveld Complex*. *Applied Earth Science* 114 (4): 194–98.
- Kinnaird JA, Hutchinson D, Schurmann D, Nex PAM and de Lange R. (2005) *Petrology and Mineralisation of the Southern Platreef: Northern Limb of the Bushveld Complex, South Africa*. *Mineralium Deposita* 40 (5): 576–97.
- Kinnaird JA, Kruger FJ and Cawthorn RG. (2004) *Rb-Sr and Nd-Sm Isotopes in Fluorite Related to the Granites of the Bushveld Complex*. *South African Journal of Geology* 107 (3): 413–30.
- Kruger FJ and Marsh JS. (1985) *The Mineralogy, Petrology, and Origin of the Merensky Cyclic Unit in the Western Bushveld Complex*. *Economic Geology* 80 (4): 958–74.
- Kruger FJ and Marsh JS. (1982) *Significance of $^{87}\text{Sr}/^{86}\text{Sr}$ ratios in the Merensky cyclic unit of the Bushveld Complex*. *Nature* 298: 53-55.
- Kruger FJ. (2010) *The Merensky and Bastard Cyclic Units and the Platreef of the Bushveld Complex: Consequences of Main Zone Magma Influxes and Dynamics*. The 4th International Platinum Conference, Platinum in Transition “Boom or Bust,” no. The Southern African Institute of Mining and Metallurgy: 43–46.
- Kruger FJ. (1994). *The Sr-Isotopic Stratigraphy of the Western Bushveld Complex*. *South African Journal of Geology* 97 (4): 393–98.
- Kruger FJ. (1992) *The Origin of the Merensky Cyclic Unit: Sr-Isotopic and Mineralogical Evidence for an Alternative Orthomagmatic Model*. *Australian Journal of Earth Sciences* 39 (3): 255–61.
- Kruger FJ, Cawthorn RG and Walsh KL. (1987) *Strontium Isotopic Evidence against Magma Addition in the Upper Zone of the Bushveld Complex*. *Earth and Planetary Science Letters* 84: 51–58.
- Kruger FJ. (2005) *Filling the Bushveld Complex Magma Chamber: Lateral Expansion, Roof and Floor Interaction, Magmatic Unconformities, and the Formation of Giant Chromitite, PGE and Ti-V-Magnetitite Deposits*. *Mineralium Deposita* 40 (5): 451–72.
- Latypov R, Chistyakova S, Barnes ST and Hunt EJ. (2017) *Origin of Platinum Deposits in Layered Intrusions by In-situ Crystallization: Evidence from Undercutting Merensky Reef of the Bushveld Complex*. *Journal of Petrology* 58 (4): 715–62.
- Lee CA and Butcher AR. (1990) *Cyclicity in the Sr Isotope Stratigraphy Through the Merensky and Bastard Reef Units, Atok Section, Eastern Bushveld Complex*. *Economic Geology* 85: 877–83.
- Lucassen F, Franz G, Dulski P, Romer RL and Rhede D. (2010) *Lithos Element and Sr isotope signatures of titanite as indicator of variable fluid composition in hydrated eclogite*. *Lithos* 121 (1-4): 12-24.

- Maier WD. (2005) *Platinum-Group Element (PGE) Deposits and Occurrences: Mineralization Styles, Genetic Concepts, and Exploration Criteria*. *Journal of African Earth Sciences* 41 (9): 165–91.
- Maier WD, de Klerk L, Blaine J, Manyeruke T, Barnes SJ, Stevens MVA and Mavrogenes JA. (2008) *Petrogenesis of Contact-Style PGE Mineralization in the Northern Lobe of the Bushveld Complex: Comparison of Data from the Farms Rooipoort, Townlands, Drenthe and Nonnenwerth*. *Mineralium Deposita* 43 (3): 255–80.
- Maier WD and Barnes S-J. (2008) *Platinum-group elements in the UG1 and UG2 chromitites, and the Bastard Reef, at Impala platinum mine, western Bushveld Complex, South Africa: Evidence for late magmatic cumulate instability and reef constitution*. *South Africa Journal of Geology* 111: 159-176.
- Maier WD and Barnes S-J. (1999) *Platinum-Group Elements in silicate rocks of the Lower, Critical and Main zones at Unione Section, Western Bushveld Complex*. *Journal of Petrology* 40 (11): 1647-1671.
- Maier WD, Barnes S-J and Groves DI. (2013) *The Bushveld Complex, South Africa: Formation of Platinum– Palladium, Chrome- and Vanadium-Rich Layers via Hydrodynamic Sorting of a Mobilized Cumulate Slurry in a Large, Relatively Slowly Cooling, Subsiding Magma Chamber*. *Mineralium Deposita* 48: 1–56.
- Mangwegape M, Roelofse F, Mock T and Carlson RW. (2016) *The Sr-Isotopic Stratigraphy of the Northern Limb of the Bushveld Complex, South Africa*. *Journal of African Earth Sciences* 113: 95–100.
- Manyeruke TD, Maier WD and Barnes S-J. (2005) *Major and trace element geochemistry of the Platreef on the farm Townlands, northern Bushveld Complex*. *South African Journal of Geology* 108 (3): 381-396.
- Manyeruke TD, Maier WD and Barnes S-J. (2005) *Major and Trace Element Geochemistry of the Platreef on the Farm Townlands, Northern Bushveld Complex*. *South African Journal of Geology* 108 (3): 381–96.
- McDonald I, Harmer REJ, Holwell DA, Hughes HSR and Boyce AJ. (2017) *Cu-Ni-PGE mineralisation at the Aurora Project and potential for a new PGE province in the Northern Bushveld Main Zone*. *Ore Geology Reviews* 80: 1135-1159.
- McDonald I, Holwell DA and Armitage PEB. (2005) *Geochemistry and Mineralogy of the Platreef and ‘Critical Zone’ of the Northern Lobe of the Bushveld Complex, South Africa: Implications for Bushveld Stratigraphy and the Development of PGE Mineralisation.* *Mineralium Deposita* 40 (5): 526–49.
- Mitchell AA. (1986) *The Petrology, Mineralogy and Geochemistry of the Main Zone of the Bushveld Igneous Complex at Rustenburg Platinum Mines, Union Section*. PhD thesis, Rhodes University.
- Mondal SK and Mathez EA. (2007) *Origin of the UG2 chromitite layer, Bushveld Complex*. *Journal of Petrology* 48 (3): 495-510.
- Mungall JE, Kamo SL and McQuade S. (2016) *U-Pb geochronology documents out-of-sequence emplacement of ultramafic layers in the Bushveld Igneous Complex of South Africa*. *Nature Communications* 7: 13385.
- Mungall JE and Naldrett AI. (2008) *Ore Deposits of the Platinum-Group Elements*. *Elements* 4 (4): 253–58.
- Naldrett AJ, Gasparrini EC, Barnes SJ, Von Gruenewaldt G and Sharpe MR. (1986) *The Upper Critical Zone of the Bushveld Complex and the origin of the Merensky-type ores*. *Economic Geology* 81: 1105-1117.

- Naldrett AJ, Wilson A, Kinnaird J and Chunnett G. (2009) *PGE Tenor and Metal Ratios within and below the Merensky Reef, Bushveld Complex: Implications for its Genesis*. *Journal of Petrology* 50 (4): 625-659.
- Nebel O, Scherer EE and Mezger K. (2011) *Evaluation of the ^{87}Rb decay constant by age comparison against the U–Pb system*. *Earth and Planetary Science Letter* 301 (1-2): 1-8.
- Norman MD, Garcia MO and Bennett VC. (2004) *Rhenium and chalcophile elements in basaltic glasses from Ko'olau and Moloka'i volcanoes: Magmatic outgassing and composition of the Hawaiian plume*. *Geochimica et Cosmochimica Acta*. 68 (18): 3761-3777.
- Norman MD, Taylor LA, Shih C and Nyquist LE. (2016) *Crystal accumulation in a 4.2 Ga lunar impact melt*. *Geochimica et Cosmochimica Acta*. 172: 410-429.
- Oberthür T, Junge M, Rudashevsky N, de Meyer E and Gutter P. (2016) *Platinum-Group Minerals in the LG and MG Chromitites of the Eastern Bushveld Complex, South Africa*. *Mineralium Deposita* 51 (1): 71–87.
- Osbaht I, Klemd R, Oberthür T, Brätz H and Schouwstra R. (2013) *Platinum-group element distribution in base-metal sulfides of the Merensky Reef from the eastern and western Bushveld Complex, South Africa*. *Mineralium Deposita* 48: 211-232.
- Peck DC and Huminicki MAE. (2016) *Value of Mineral Deposits Associated with Mafic and Ultramafic Magmatism: Implications for Exploration Strategies*. *Ore Geology Reviews* 72: 269–98.
- Prevec SA, Ashwal LD and Mkaza MS. (2005) *Mineral Disequilibrium in the Merensky Reef, Western Bushveld Complex, South Africa: New Sm-Nd Isotopic Evidence*. *Contributions to Mineralogy and Petrology* 149 (3): 306–15.
- Roelofse F, Ashwal LD and Romer RL. (2015) *Multiple, Isotopically Heterogeneous Plagioclase Populations in the Bushveld Complex Suggest Mush Intrusion*. *Chemie Der Erde - Geochemistry* 75 (3): 357–64.
- Schouwstra RP, Kinloch ED and Lee CA. (2000) *A Short Geological Review of the Bushveld Complex*. *Platinum Metals Review* 44 (1): 33–39.
- Scoates JS and Friedman RM. (2008) *Precise Age of the Platiniferous Merensky Reef, Bushveld Complex, South Africa, by the U-Pb Zircon Chemical Abrasion ID-TIMS Technique*. *Economic Geology* 103 (3): 465–71.
- Seabrook CL, Cawthorn RG and Kruger FJ. (2005) *The Merensky Reef, Bushveld Complex: Mixing of Minerals Not Mixing of Magmas*. *Economic Geology* 100 (6): 1191–1206.
- Sharpe MR. (1985) *Strontium Isotope Evidence for Preserved Density Stratification in the Main Zone of the Bushveld Complex, South Africa*. *Nature* 316 (6024): 119–26.
- Smith DS, Basson IJ and Reid DL. (2003) *Normal reef subfacies of the Merensky Reef at Northam Platinum Mine, Zwartklip facies, Western Bushveld Complex, South Africa*. *The Canadian Mineralogist* 42: 243-260.
- Smith JW, Holwell DA, McDonald I and Boyce AJ. (2016) *The Application of S Isotopes and S/Se Ratios in Determining Ore-Forming Processes of Magmatic Ni-Cu-PGE Sulfide Deposits: A Cautionary Case Study from the Northern Bushveld Complex*. *Ore Geology Reviews* 73: 148–74.
- Tegner C, Cawthorn RG and Kruger FJ. (2006) *Cyclicality in the Main and Upper Zones of the Bushveld Complex, South Africa: Crystallization from a Zoned Magma Sheet*. *Journal of Petrology* 47 (11): 2257–79.
- van der Merwe MJ. (2008) *The Geology and Structure of the Rustenburg Layered Suite in the Potgietersrus/Mokopane Area of the Bushveld Complex, South Africa*. *Mineralium Deposita* 43 (4): 405–19.

- Veksler IV, Reid DL, Dulski P, Keiding JK, Schannor M, Hecht L and Trumbull RB. (2014) *Electrochemical Processes in a Crystal Mush: Cyclic Units in the Upper Critical Zone of the Bushveld Complex, South Africa*. *Journal of Petrology* 56 (6): 1229–50.
- Wilson AH, Zeh A and Gerdes A. (2017) *In-situ Sr isotopes in Plagioclase and Trace Element Systematics in the Lowest Part of the Eastern Bushveld Complex: Dynamic Processes in an Evolving Magma Chamber*. *Journal of Petrology* 58 (2): 327-360.
- Wilson AH. (2012) *A Chill Sequence to the Bushveld Complex: Insight into the First Stage of Emplacement and Implications for the Parental Magmas*. *Journal of Petrology* 53 (6): 1123–68.
- Yang S-H, Maier WD, Lahaye Y and O'Brien H. (2013) *Strontium Isotope Disequilibrium of Plagioclase in the Upper Critical Zone of the Bushveld Complex: Evidence for Mixing of Crystal Slurries*." *Contributions to Mineralogy and Petrology* 166 (4): 959–74.
- Yudovskaya M, Belousova E, Kinnaird J, Dubinina E and Grobler DF. *Re-Os and S isotope evidence for the origin of Platreef mineralization (Bushveld Complex)*. *Geochimica et Cosmochimica Acta*. 214: 282-307.
- Yudovskaya MA, Kinnaird JA, Grobler DF, Costin G, Abramova VD and Dunnett T. (2017) *Zonation of Merensky-Style Platinum-Group Element Mineralization in Turfspruit Thick Reef Facies (Northern Limb of the Bushveld Complex)*. *Economic Geology* 112: 1333-1365.
- Yudovskaya MA and Kinnaird JA. (2010) *Chromite in the Platreef (Bushveld Complex, South Africa): Occurrence and Evolution of Its Chemical Composition*. *Mineralium Deposita* 45 (4): 369–91.
- Yudovskaya M, Kinnaird J, Naldrett AI, Mokhov AV, McDonald I and Reinke C. (2011) *Facies Variation in PGE Mineralization in the Central Platreef of the Bushveld Complex, South Africa*. *Canadian Mineralogist* 49 (6): 1349–84.
- Zeh A, Ovtcharova M, Wilson AH and Schaltegger U. (2015) *The Bushveld Complex was emplaced and cooled in less than one million years - results of zirconology, and geotectonic implications*. *Earth and Planetary Science Letters* 418: 103-114.

9. Figure Captions

Figure 1. Geological map of the Rustenburg Layered Suite (modified from [Mungall et al. 2016](#)) showing locations of sites for the compiled strontium isotope stratigraphy in the Eastern and Western Limb ([Seabrook et al. 2005](#)) and locations of strontium isotope stratigraphy studies in the Northern Limb. Inset shows the locations of the Bushveld Igneous Complex.

Figure 2. Summary of the magmatic stratigraphy of the Eastern and Western Limbs of the Bushveld Igneous Complex ([Maier et al. 2013](#)) and comparison with the stratigraphic units used by different studies in Northern Limb. References: GNPA Member, [McDonald et al. 2005](#); A-B-C Reef, [Barton et al. 1986](#); Turfspruit, [Grobler et al. 2018](#); Platreef, [Kinnaird et al. 2005](#); Aurora Project, [McDonald et al. 2017](#); Waterberg Project, [Kinnaird et al. 2017](#).

Figure 3. Geological map of the central part of the Northern Limb of the Bushveld Igneous Complex (see insert in top right corner), the location of the Turfspruit and Macalacaskop farms, and the location of drill hole UMT094. Map modified from [McDonald et al. \(2017\)](#).

Figure 4. General magmatic stratigraphy at Turfspruit ([Grobler et al. 2018](#)), including rock-types generally associated with the different stratigraphic units within the major cyclic units (BCU, MCU, FCU and UG2CU).

Figure 5. A) Strontium isotope stratigraphy of the Western Limb (modified from [Kruger 1994](#)). B) Strontium isotope stratigraphy of the Upper Zone and Main Zone of the Northern Limb (modified from [Mangwegape et al. 2016](#)). The largest shift in the strontium isotope profile of the

Western Limb is at the stratigraphic height of the Merensky Reef. In the Northern Limb, data from [Mangwegape et al. \(2016\)](#) stops just above the Platreef, likely because of footwall assimilation (as inferred from values higher than 0.710).

Figure 6. Magmatic stratigraphy logged from UMT094 using the magmatic units described by [Grobler et al. 2018](#).

Figure 7. Sketch summarizing the micro-cycles documented in UMT094. The diagram on the left represents a full cycle commencing from a cumulate olivine-bearing rock (not always present) at the base to anorthosites at the top. Stratigraphic columns on the right are examples of five-meter sections of core with multiple micro-cycles (mineralization is shown in red on the left of the columns). Letters and arrows to the left of the legend indicate the lithologies present in each example. Micro-cycles are displayed as blue arrows on the right of the stratigraphic columns.

Figure 8. Sections of core showing micro-cyclicity: (A) anorthosite to pyroxenite within the Bastard Cyclic Unit; (B) mela-gabbro to pyroxenite also within the Merensky Cyclic Unit ; (C) pyroxenite to pegmatoidal feldspathic pyroxenite in also the Merensky Cyclic Units; (D) pegmatoidal feldspathic pyroxenite to chromite-bearing pegmatoidal feldspathic pyroxenite in the Merensky Cyclic Unit; (E) anorthosite to pyroxenite within the Footwall Cyclic Unit; and (F) pyroxenite to cumulate olivine-bearing rock in the Pseudoreef.

Figure 9. Variation in the anorthite content ($\text{Ca}/[\text{Ca}+\text{Na}+\text{K}]$) in plagioclase with depth in drill core UMT094. Black squares are medians of multiple analyses (minimum 7), black circles are first and third quartile and error bars are maximum and minimum values. MZ = Main Zone, BCU = Bastard Cyclic Unit, MCU = Merensky Cyclic Unit, FCU = Footwall Cyclic Unit, U2CU = UG2 Cyclic Unit.

Figure 10. Whole rock strontium isotopic stratigraphy of the Platreef (from this study – red; uncertainties are 2σ STD) compared to available data from the Main Zone (blue – [Mangwegape et al. 2016](#)) and the Eastern Limb (orange – [Seabrook et al. 2005](#)). BCU = Bastard Cyclic Unit, MCU = Merensky Cyclic Unit, FCU = Footwall Cyclic Unit, UG2CU = UG2 Cyclic Unit, CZ = Critical Zone.

Figure 11. $^{87}\text{Sr}/^{86}\text{Sr}_i$ values of core (red), rim (blue) and whole plagioclase (green) throughout the magmatic stratigraphy at Turfspruit Farm in UMT094 (uncertainties are 1σ STD). Cyclic units are displayed for reference. BCU = Bastard Cyclic Unit, MCU = Merensky Cyclic Unit, FCU = Footwall Cyclic Unit, U2CU = UG2 Cyclic Unit.

Figure 12. Downhole Cr/MgO to show the transition between the Critical Zone and Main Zone. A gradual decrease in Cr/MgO can be seen through the transitional Units (BCU and MCU). Large spikes at 1370 and 1400 meters are due to chromitite units. BCU = Bastard Cyclic Unit, MCU = Merensky Cyclic Unit, FCU = Footwall Cyclic Unit, UG2CU = UG2 Cyclic Unit, TV = Transvaal Supergroup.

Figure 13. $^{87}\text{Sr}/^{86}\text{Sr}_i$ values of cumulate (red) and intercumulate (blue) plagioclase throughout the magmatic stratigraphy of UMT094. BCU = Bastard Cyclic Unit, MCU = Merensky Cyclic Unit, FCU = Footwall Cyclic Unit, U2CU = UG2 Cyclic Unit.

Figure 14. Comparison of stratigraphic variations in $^{87}\text{Sr}/^{86}\text{Sr}_i$ (this work) with whole rock content in 3PGE (Pt+Pd+Rh), Cr, Ni and Cu/Pd (data provided by Ivanplats). The comparison highlights the relationship between increased 3PGE content within the MCU and increasing $^{87}\text{Sr}/^{86}\text{Sr}_i$.

Figure 15. Magmatic stratigraphy of the Eastern and Western limbs of the Bushveld Igneous Complex (Maier et al. 2013) and possible correlation with the stratigraphic units used by different studies in Northern Limb. Although different nomenclature has been used throughout the Northern Limb (mainly due to assimilation obscuring magmatic lithologies), the units can be correlated through mineralization, chromitite seams and chromium content. Thickness displayed are from the interpreted top of the Bastard Cyclic Unit to the base of the Critical Zone (if present). Dashed line shows possible correlation between different nomenclature in the Northern Limb and to the stratigraphy in the Eastern and Western Limbs. References: GNPA Member, McDonald et al. (2005); A-B-C Reef, Barton et al. (1986); Turfspruit, Grobler et al. (2018); Platreef, Kinnaird et al. (2005); Aurora Project, McDonald et al. (2017); Waterberg Project, Kinnaird et al. (2017).

Figure 16. Geological interpretation of the mineralization in the Northern Limb showing the transition from the up-dip section closer to the footwall to the down-dip region where the

magmatic sequence is less affected by footwall assimilation. The mineralization up-dip is mostly within the assimilation zone compared to down-dip, where mineralization is mostly above the assimilation zone. The location of drill hole UMT094 is also displayed. Most of the early research on the Platreef focused on outcropping lithologies or sections up-dip, where footwall assimilation is pervasive. The surface geology is based on a geological map from [McDonald et al. \(2017\)](#); the front face of the diagram was modified from an interpretation completed by Ivanplats ([Grobler et al. 2018](#)). The side of the diagram has been interpreted based on the surface geology. Descriptions are observations from different sources (B - [McDonald et al. 2017](#); D – [Barnes et al. 2017](#); C, G and H – [Grobler et al. 2017](#)).

Figure 17. Comparison of $^{87}\text{Sr}/^{86}\text{Sr}_i$ data from this study (Northern Limb) to data summarized in [Seabrook et al. \(2005\)](#) for different sections of the Eastern and Western limbs. [Seabrook et al. \(2005\)](#) is shown in sections 10 meters below the contact between the Critical Zone and the Merensky Cyclic Unit and 40 meters above it. With the exception of the section at Brits, the MCU is no thicker than 20 m. In contrast in UMT094 the MCU is more than 50 m thick.

10. Figures

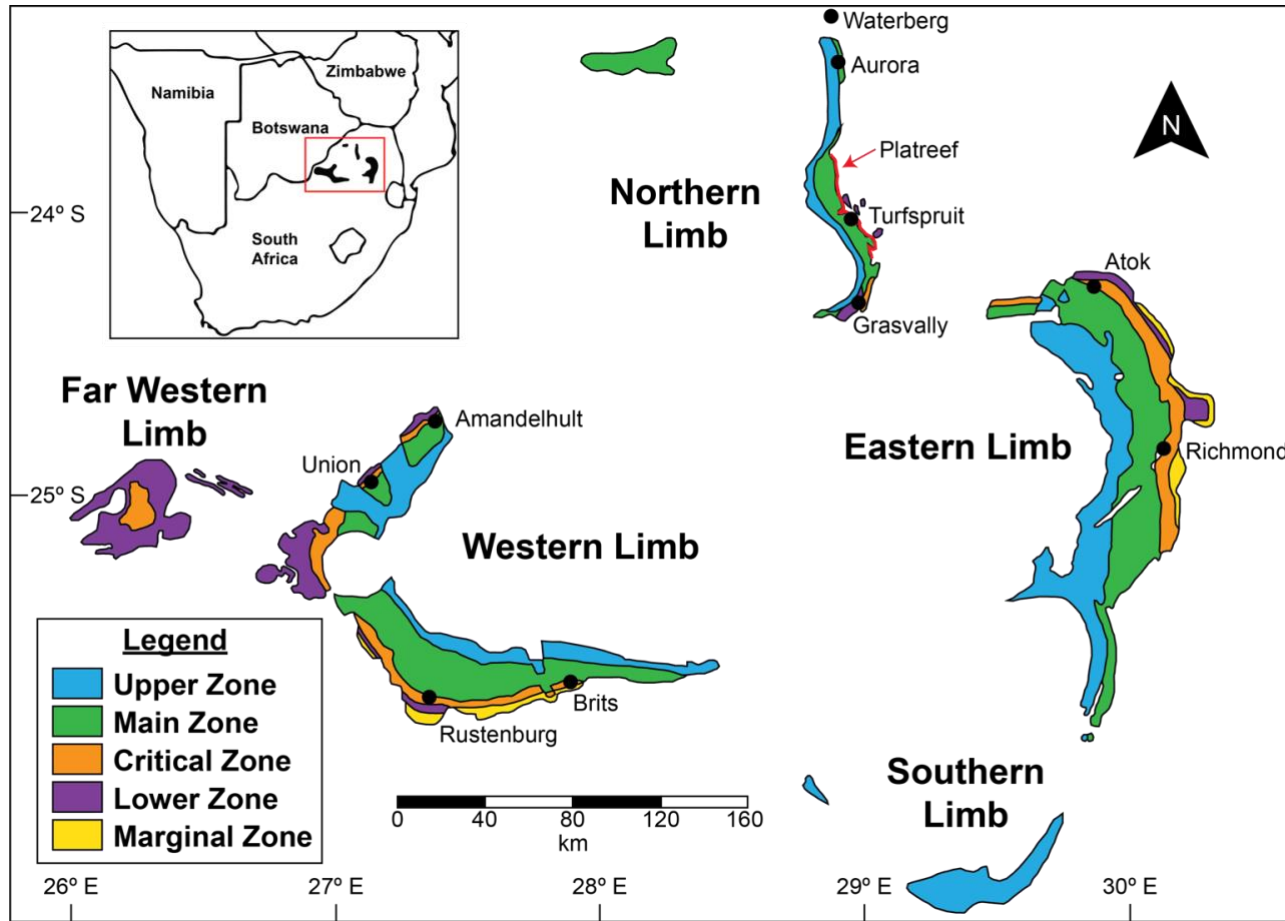


Figure 1

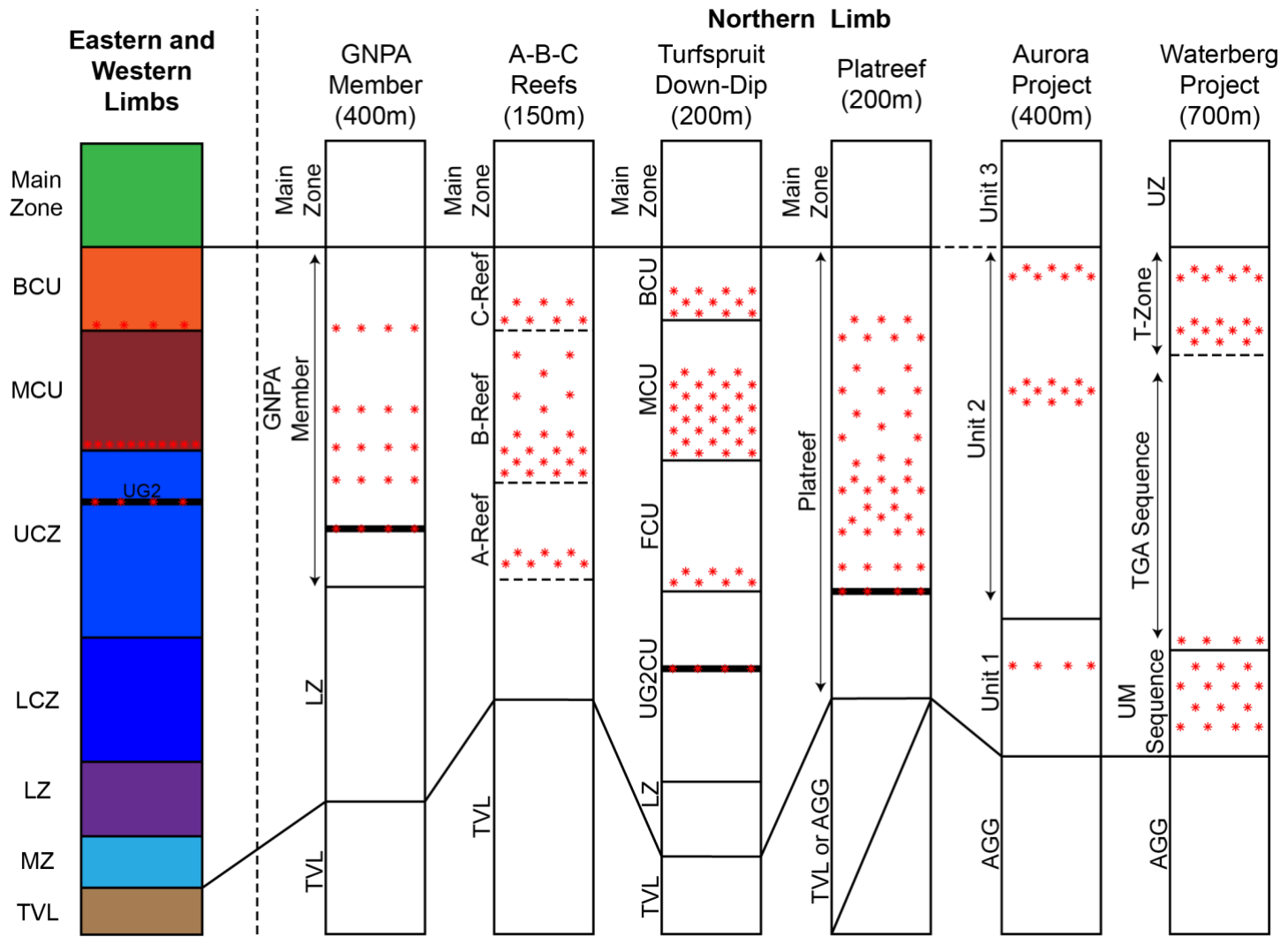


Figure 2

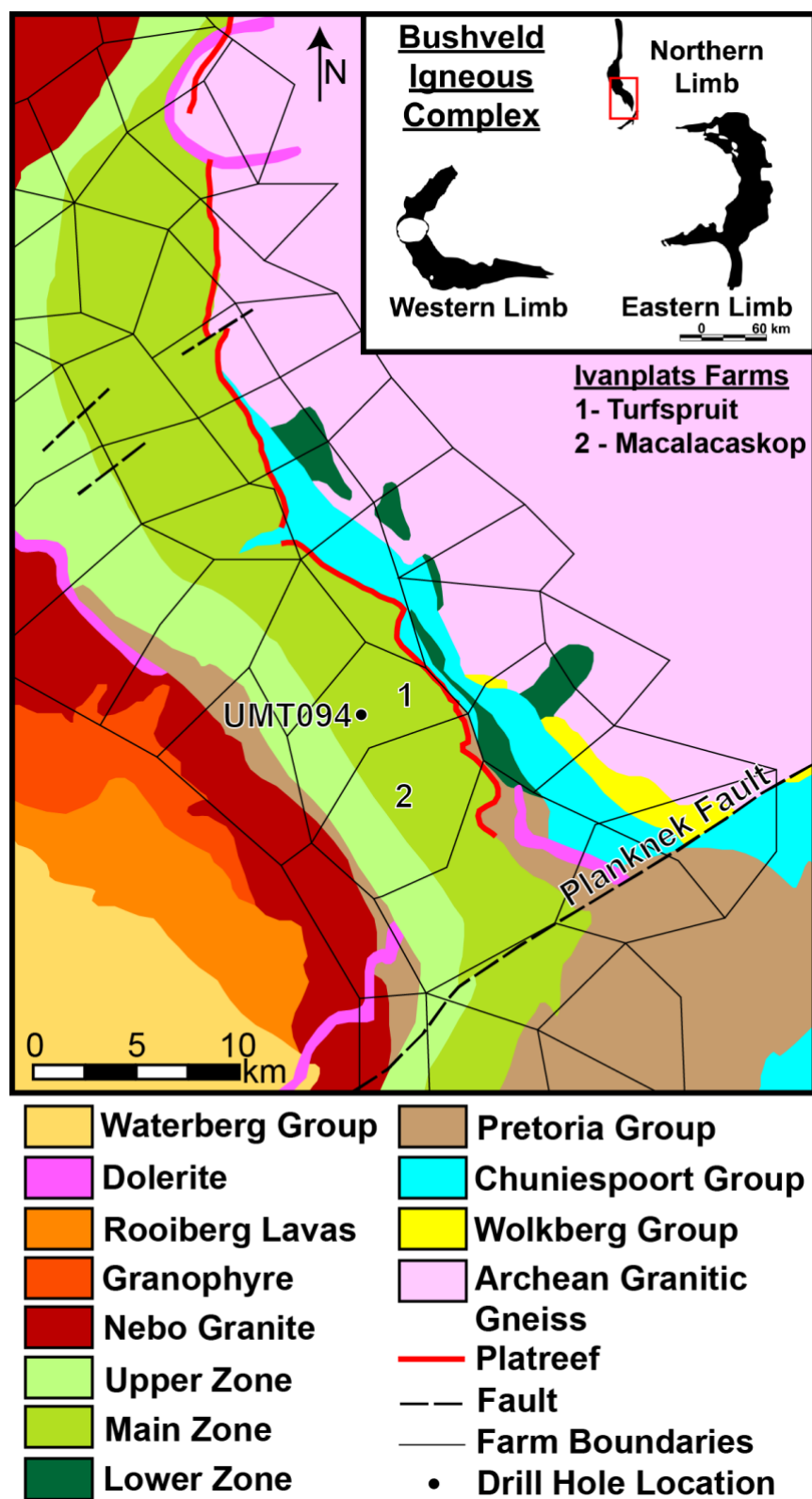


Figure 3

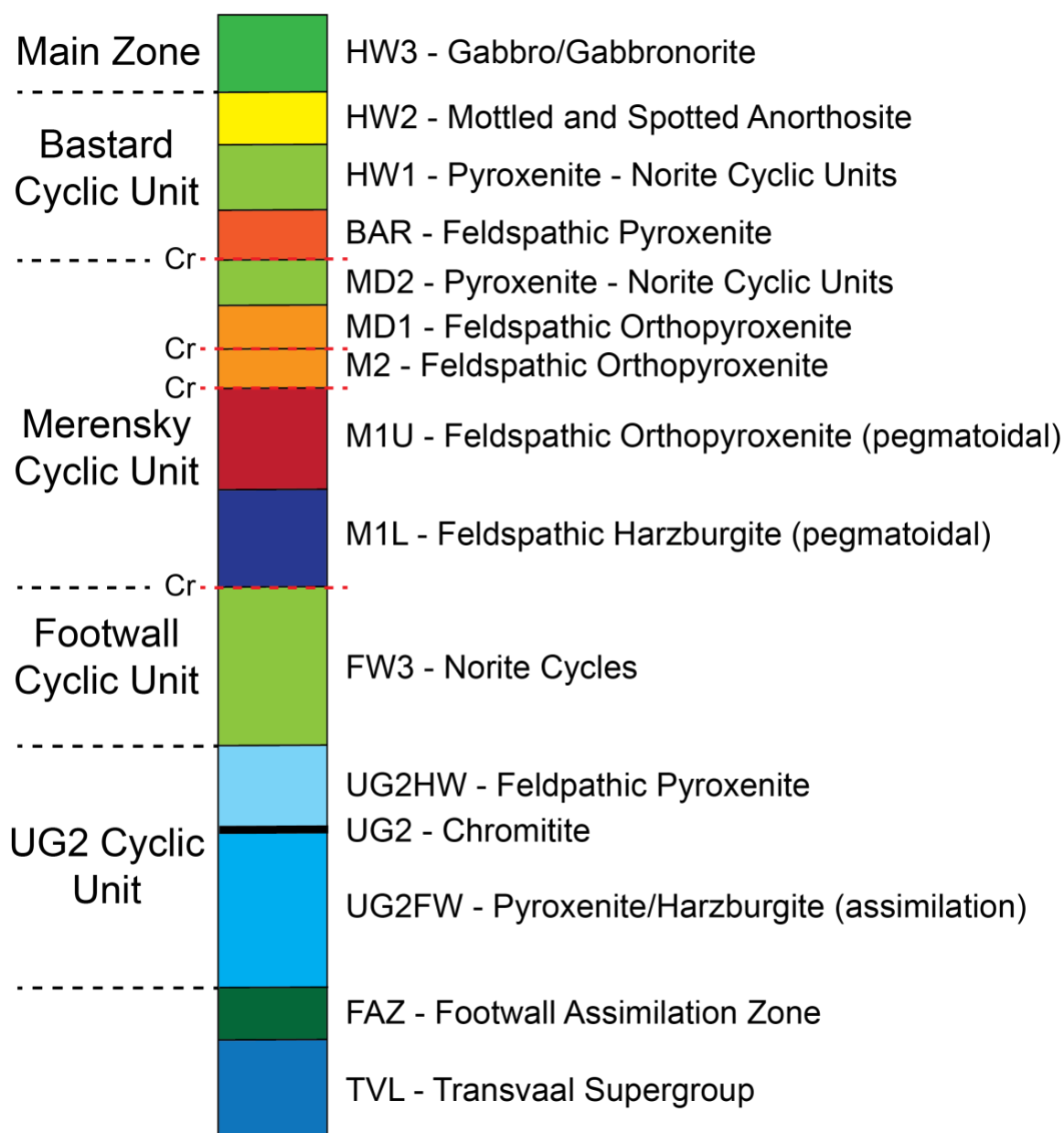


Figure 4

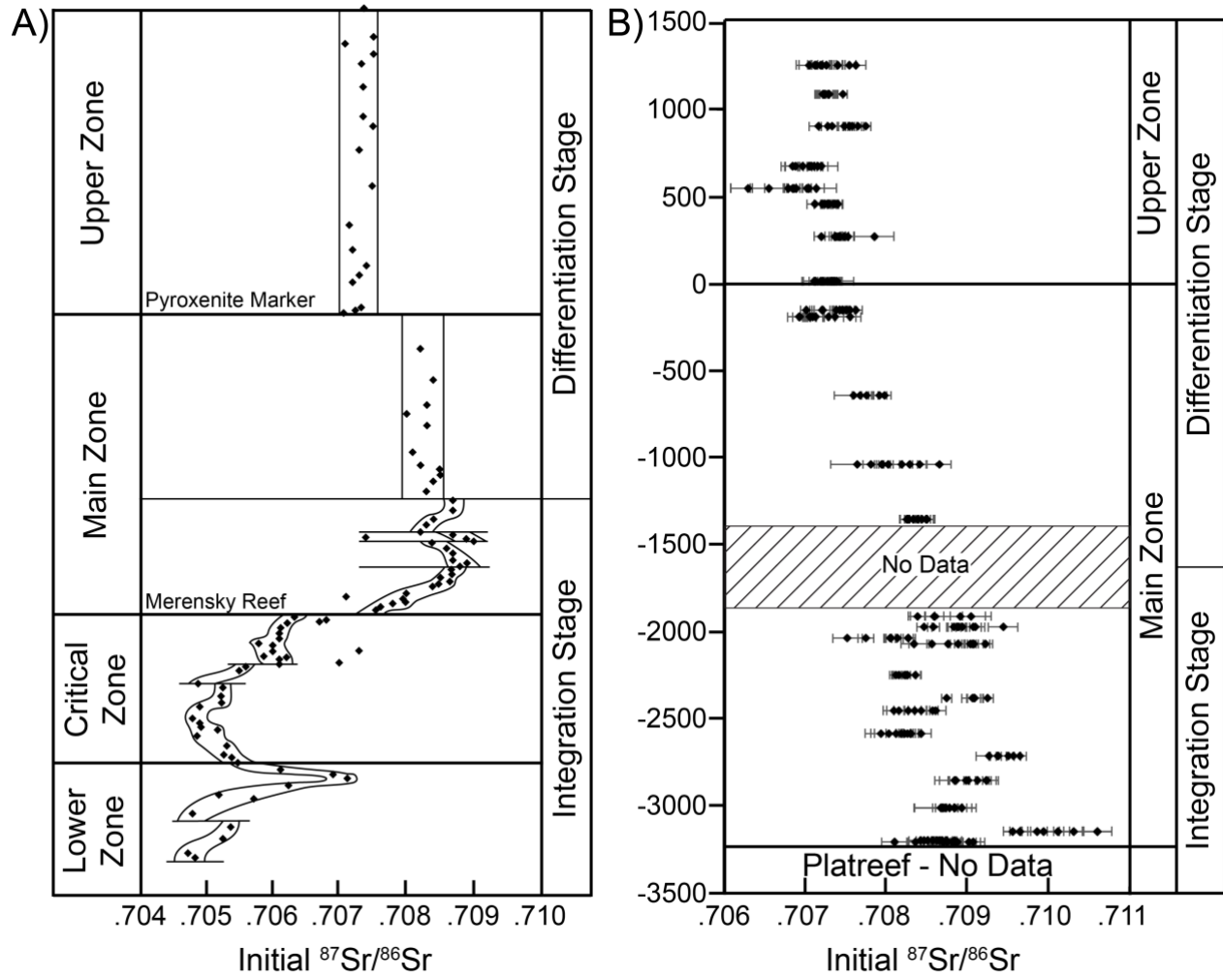


Figure 5

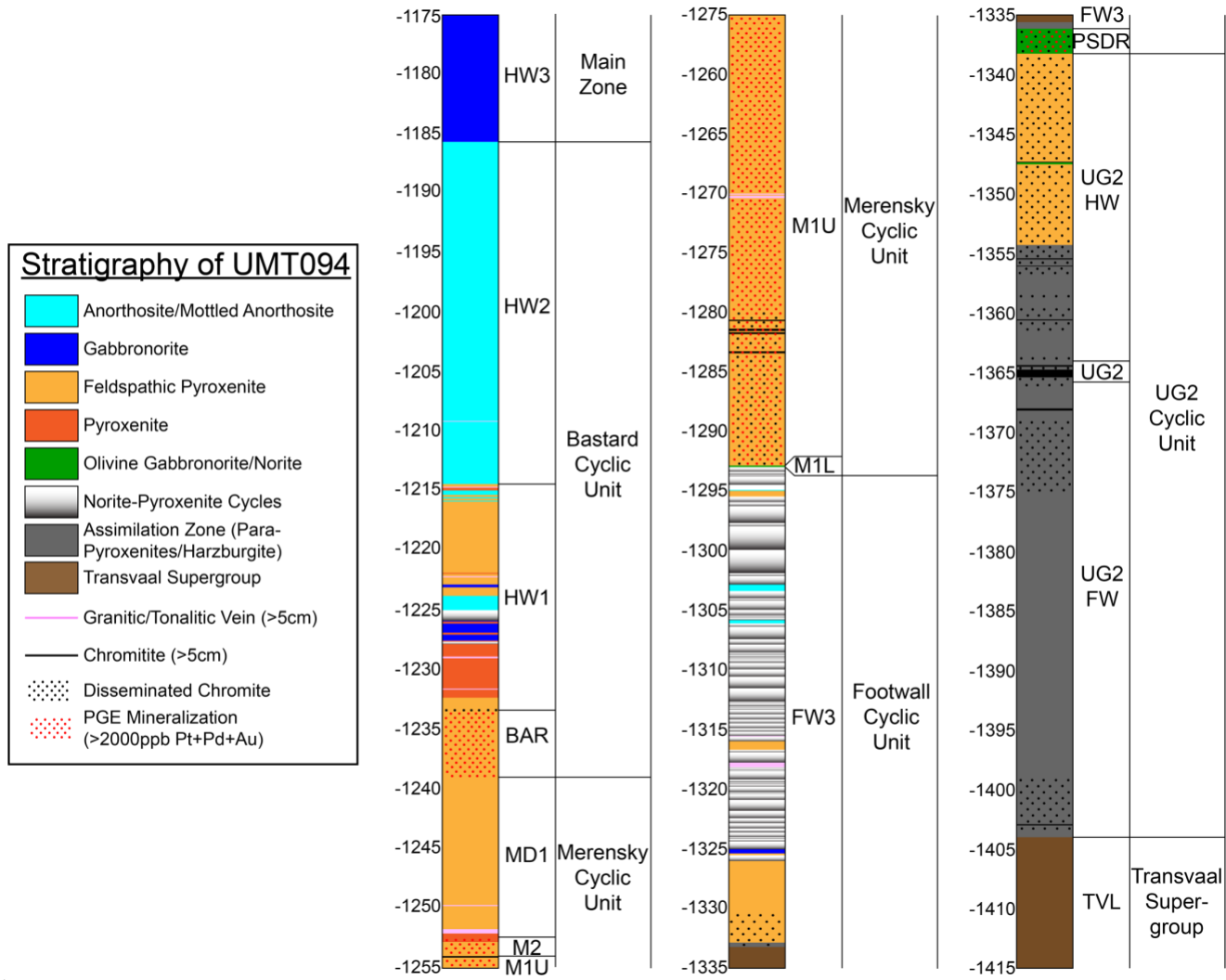


Figure 6

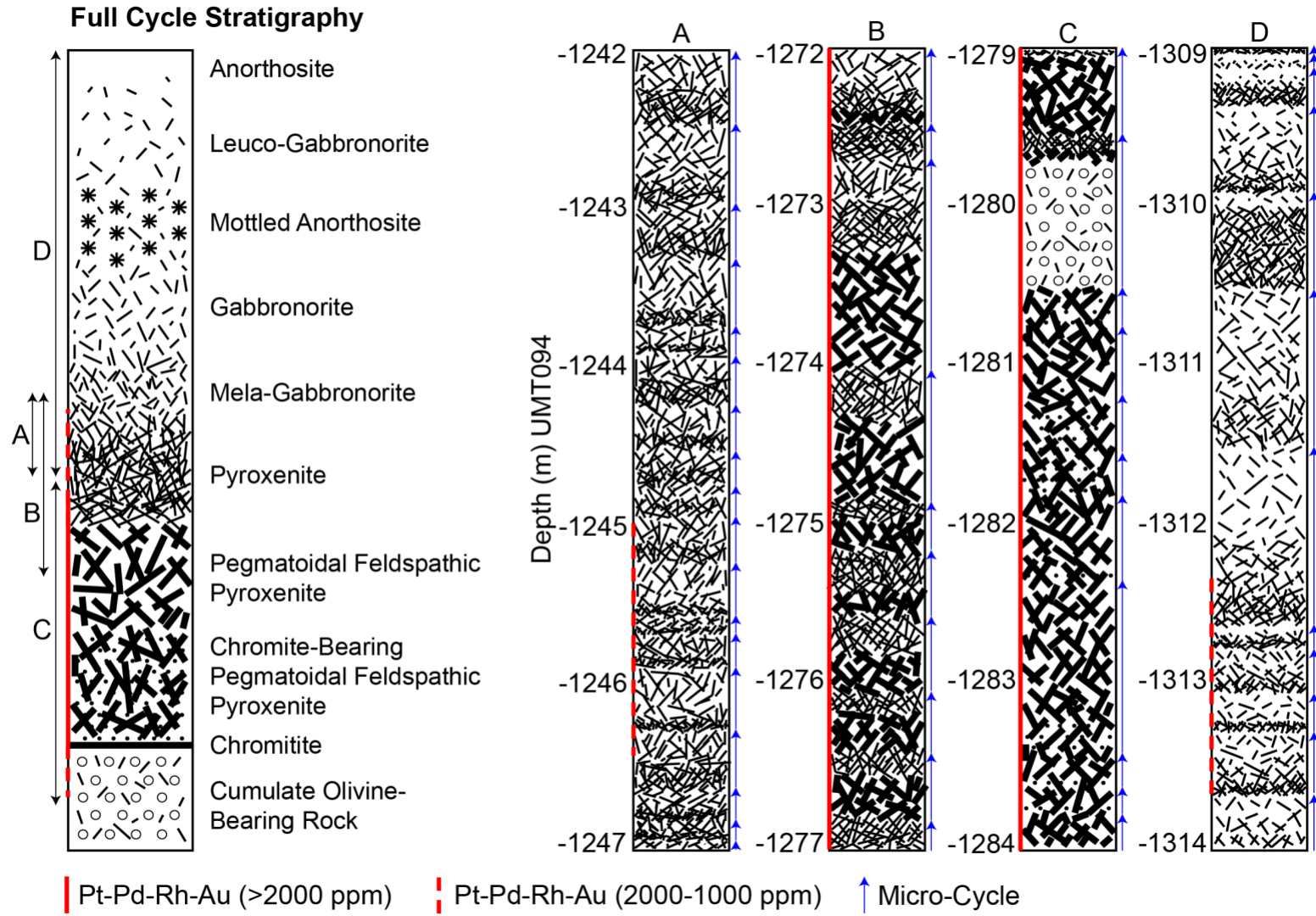


Figure 7



Figure 8

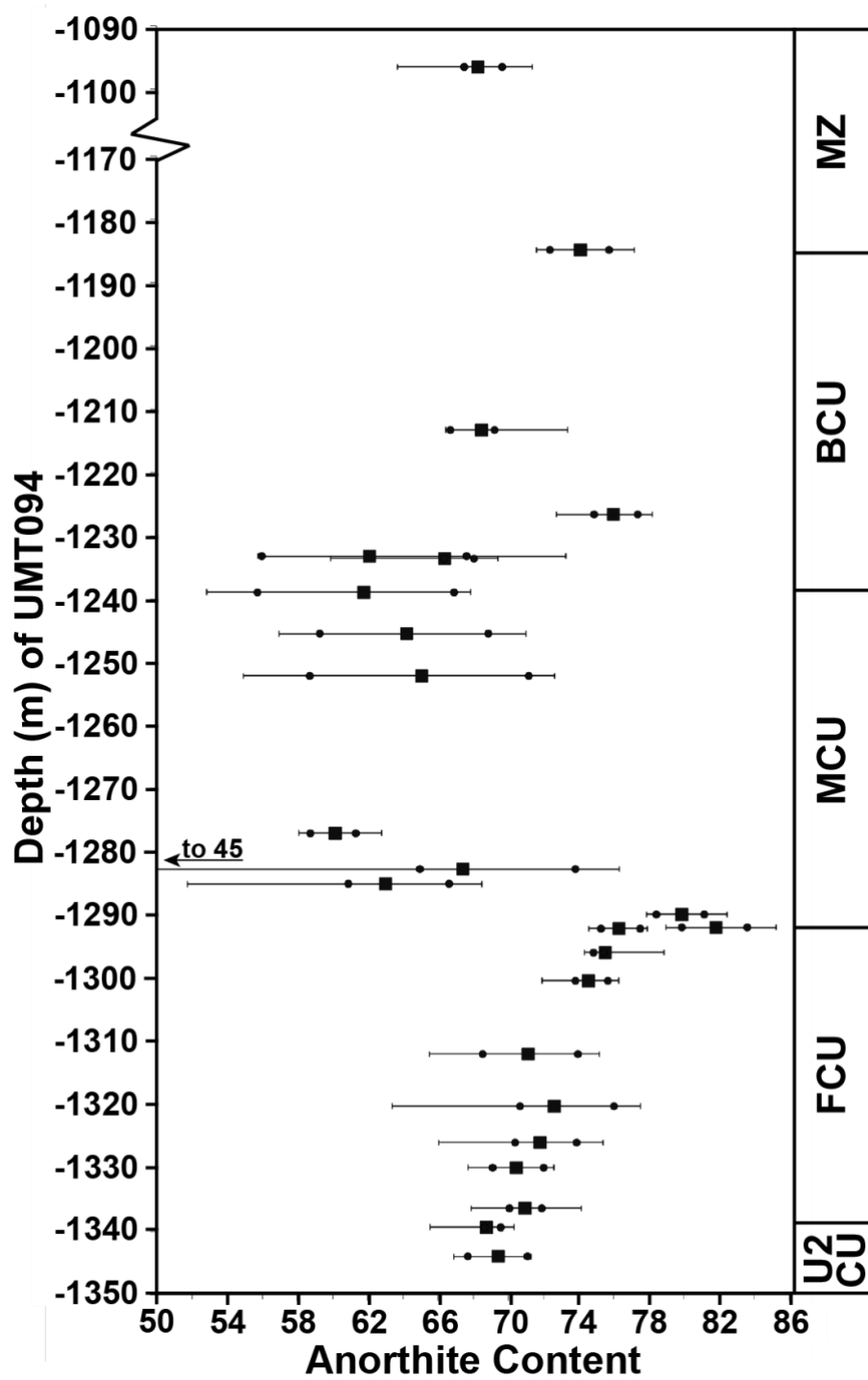


Figure 9

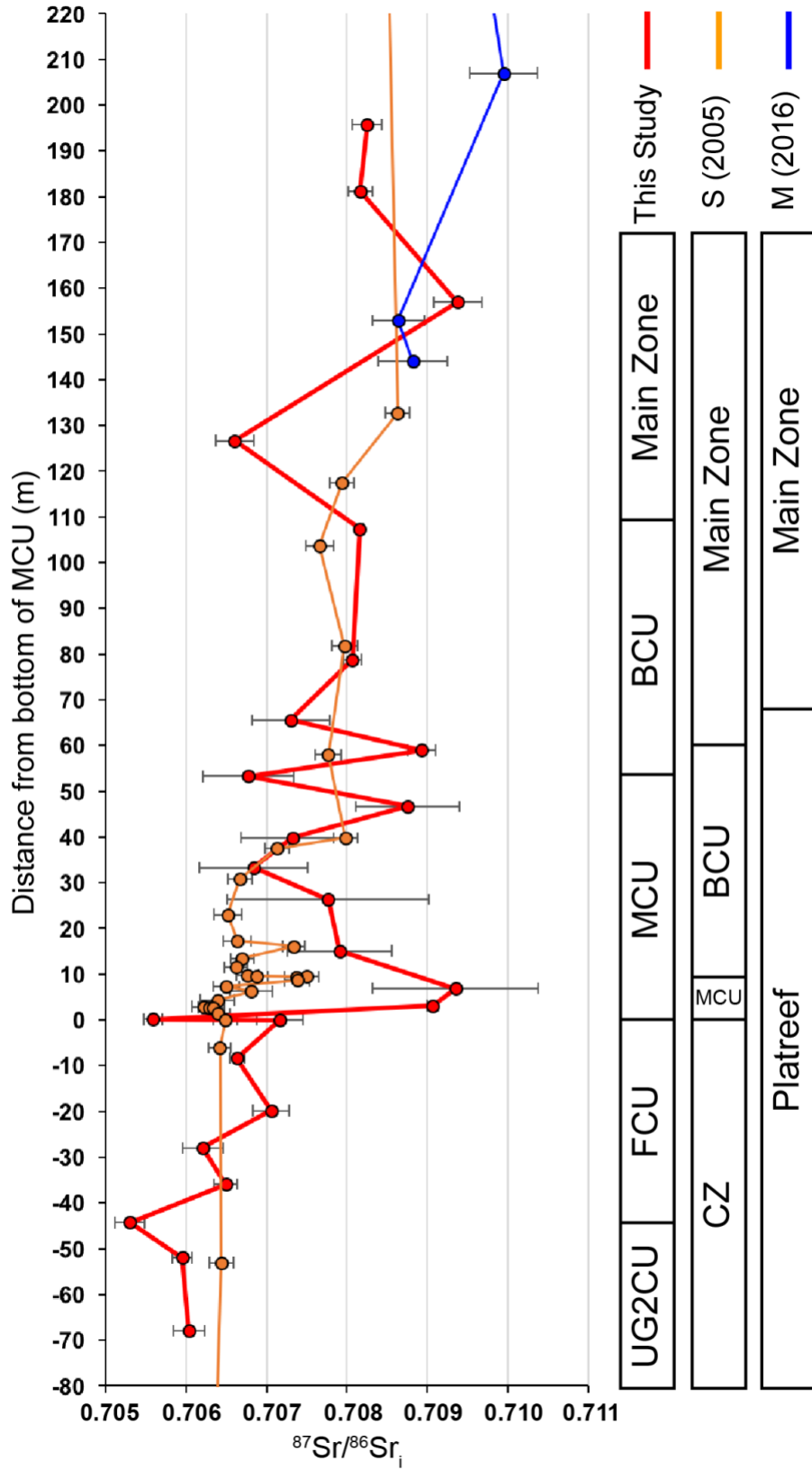


Figure 10

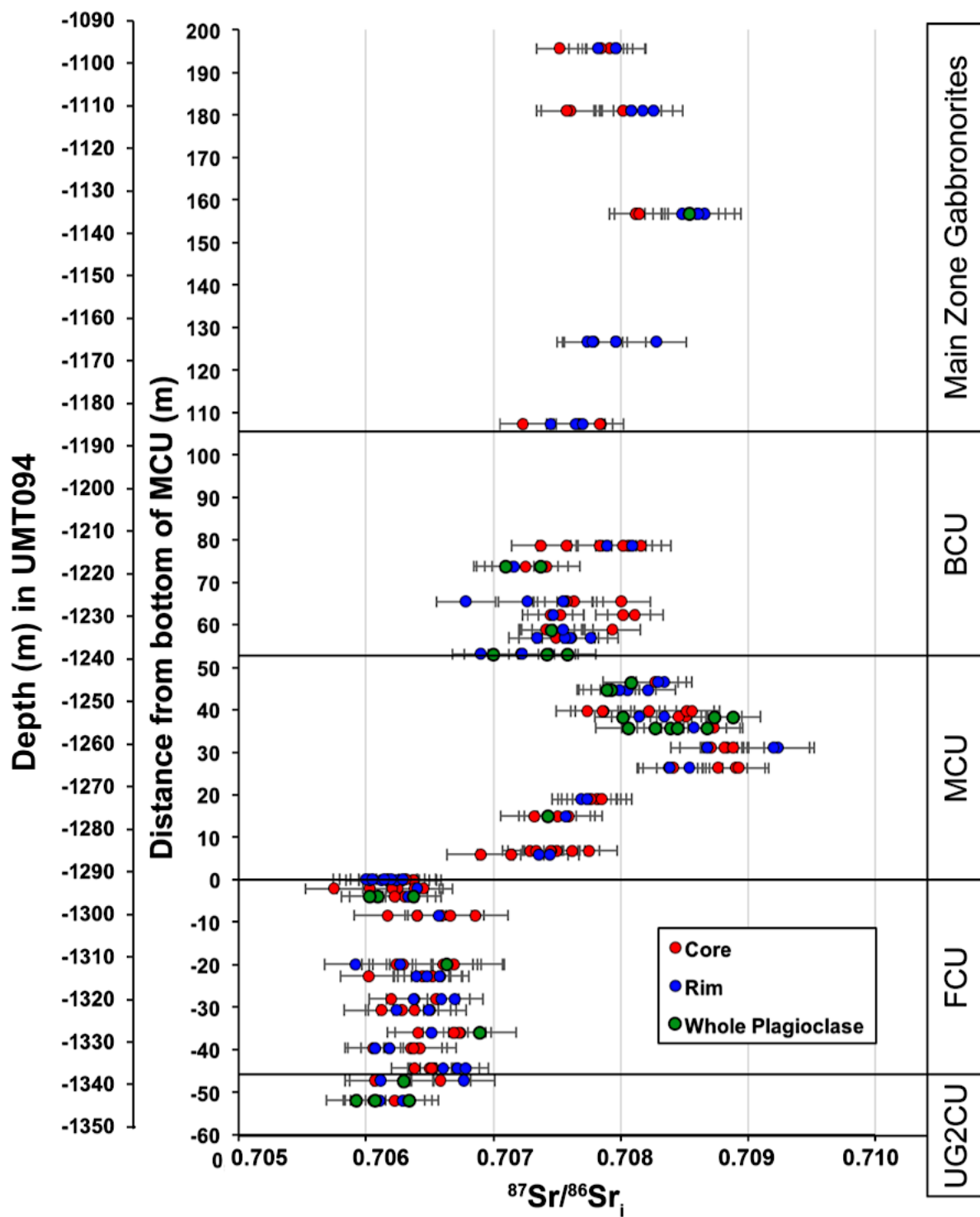


Figure 11

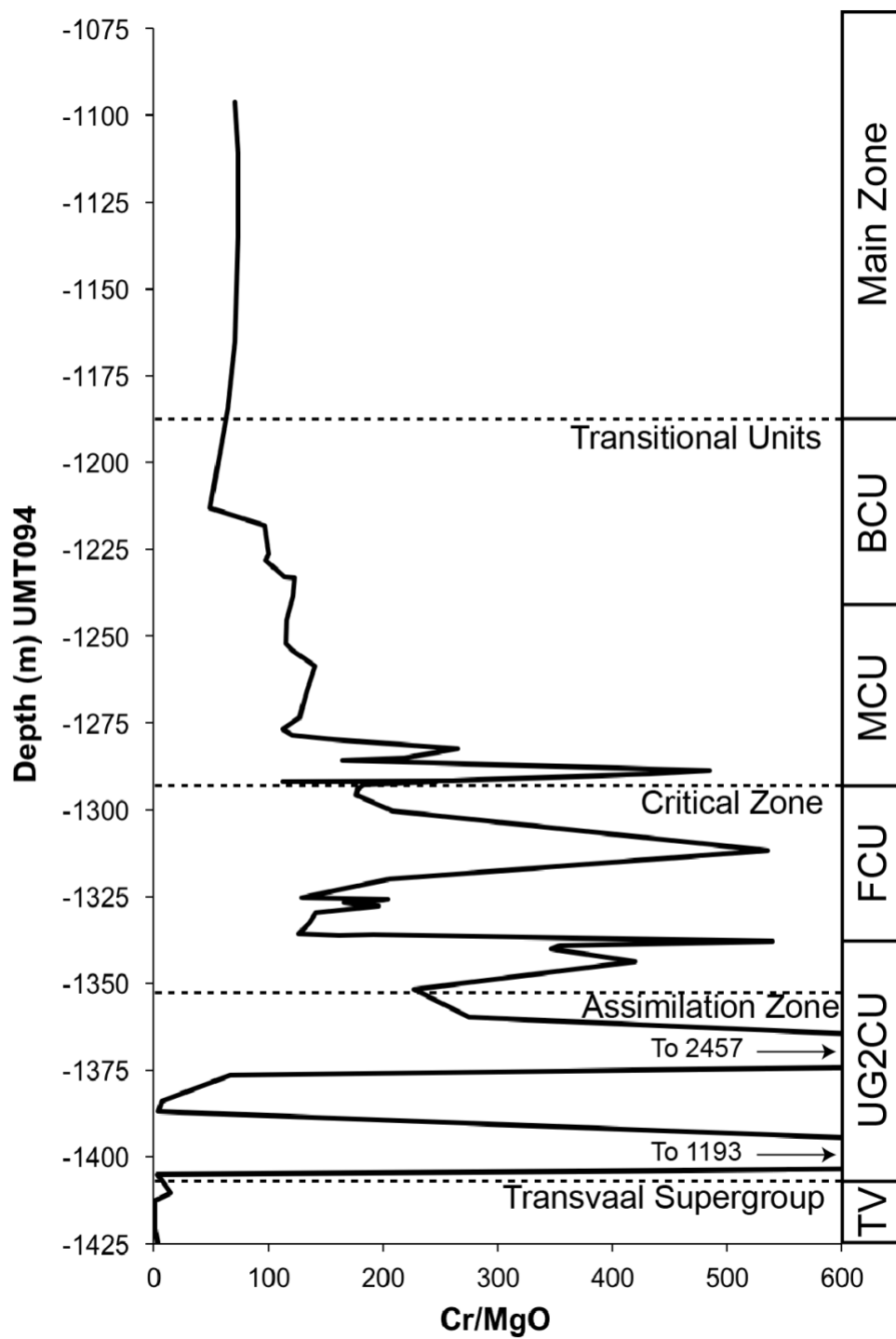


Figure 12

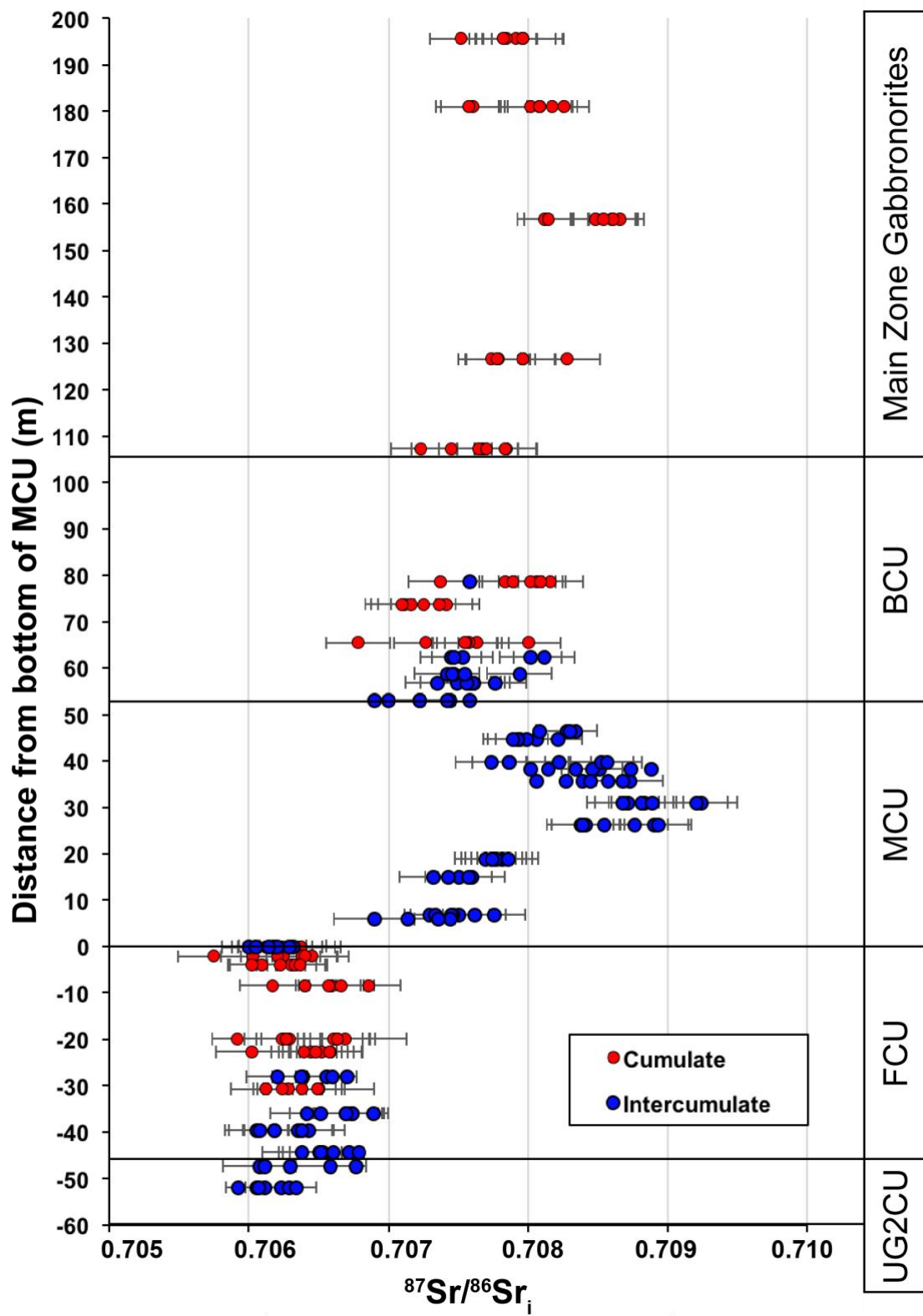


Figure 13

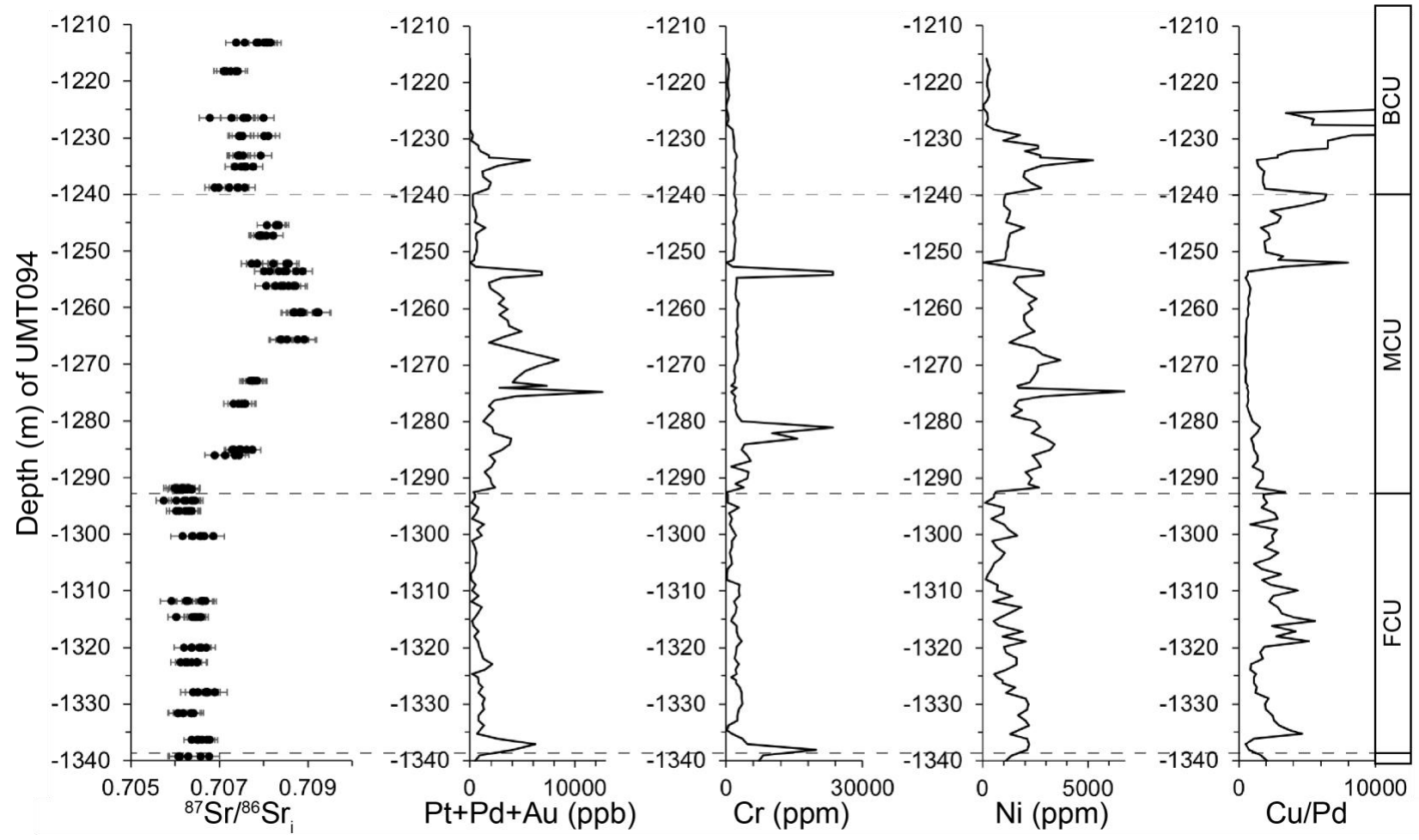


Figure 14

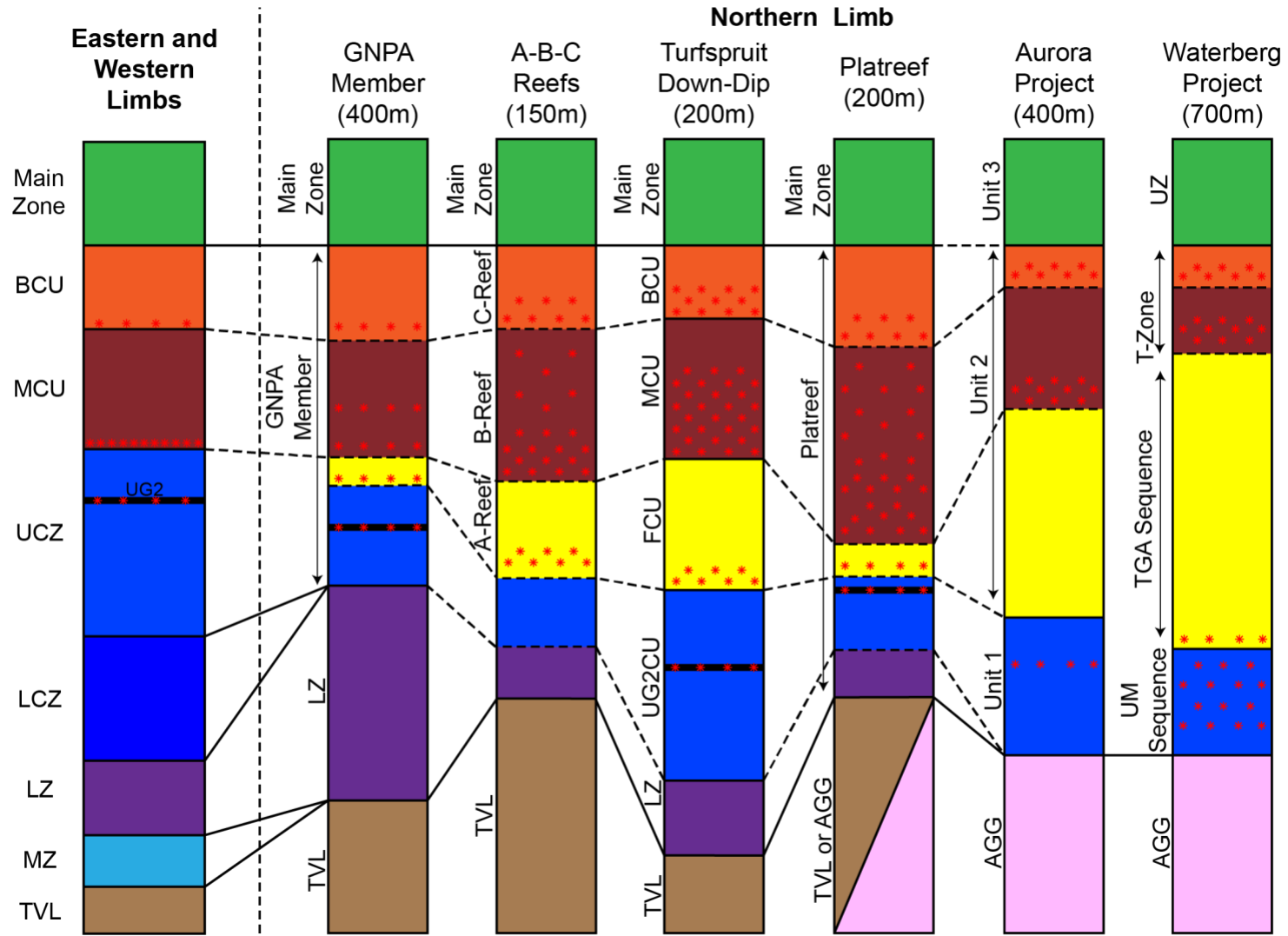


Figure 15

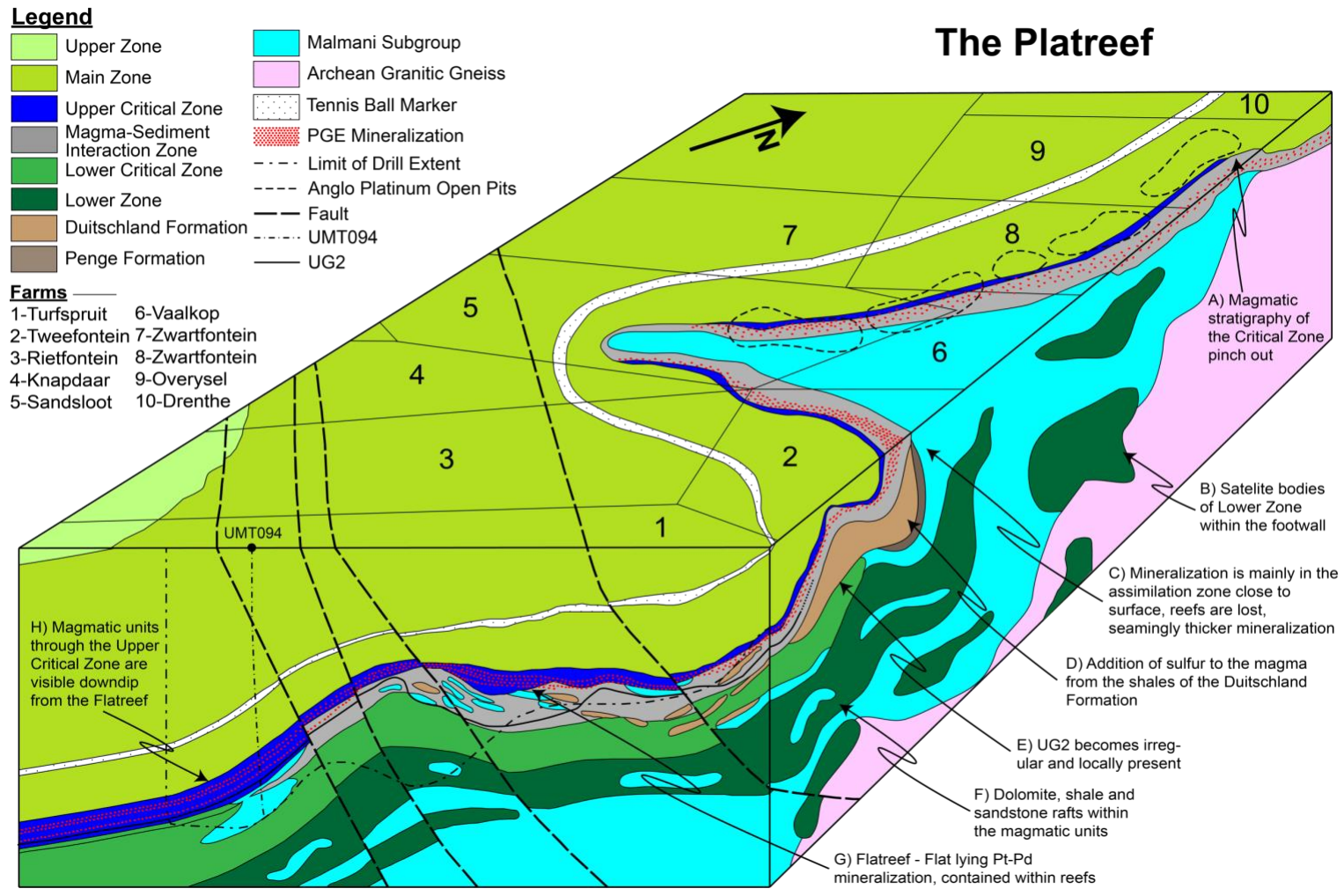


Figure 16

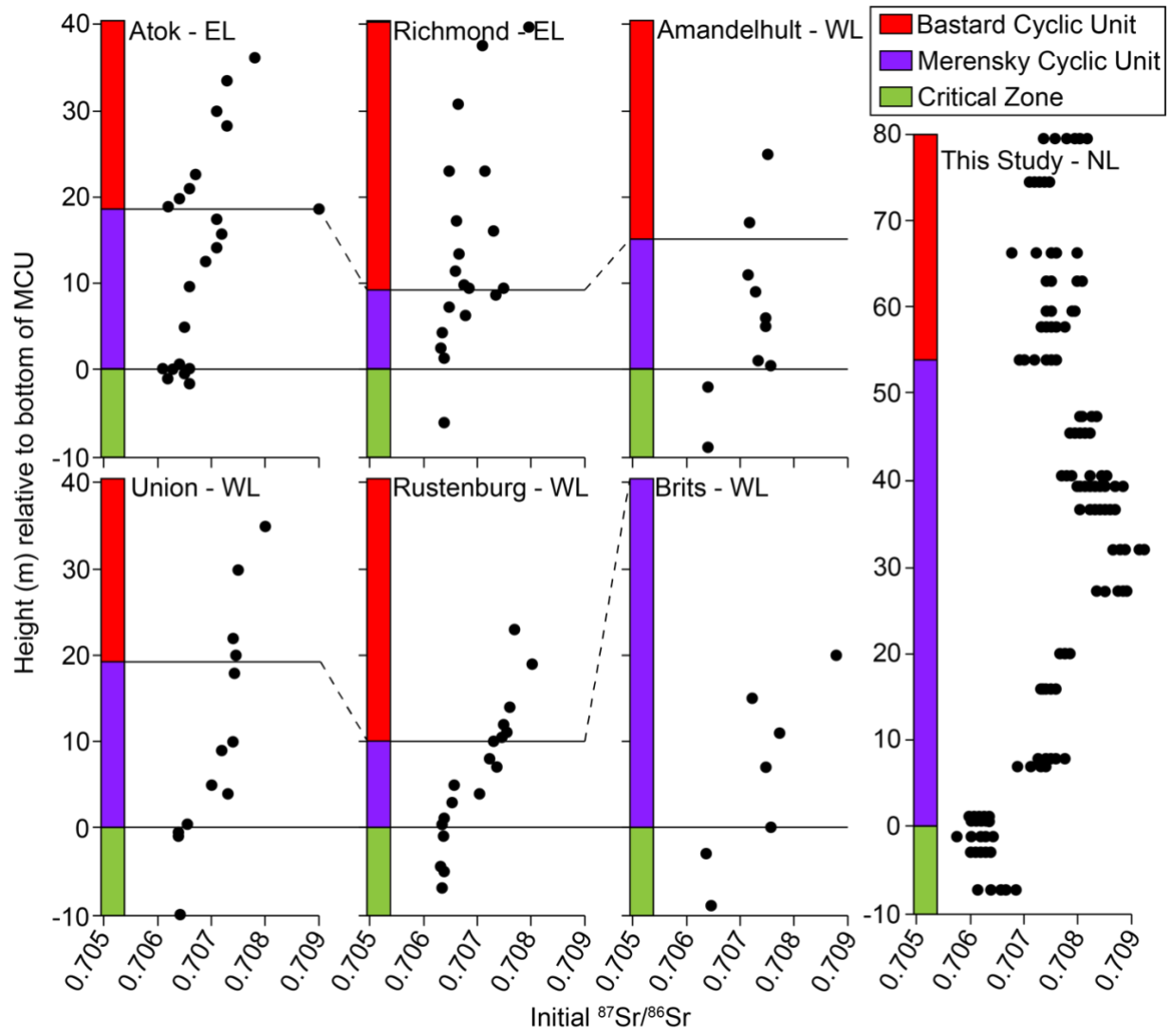


Figure 17

11. Tables

Table 1. Summary of strontium isotope studies throughout the Bushveld Igneous Complex.

Limb	Limb/Location	Analytical Details	⁸⁷Sr/⁸⁶Sr_i per Stratigraphic Zone	Age*	Model	Conclusion	Reference
EL, WL	N/S	WR and MS (cpx, plag, biotite)	Upper: 0.70769-0.70735 Main: 0.70592-0.70863 Critical: 0.70639-0.70603 Transition**: 0.70563	2100 Ma	Contamination at level of emplacement, contamination at depth or nature of melting event	Magmatic influxes caused isotopic shifts	(Hamilton 1977)
WL	Rustenburg Platinum Mines	WR and MS (plag)	Transitional Units***: 0.7064-0.7075	2100 Ma	Relation between PGE mineralization related and magma influxes	Magma influxes	(Kruger and Marsh 1982)
EL	Galgstroom	WR	Upper: 0.7073 Main: 0.7085 Critical: 0.7065	2050 Ma	Density stratification, double diffusive convection and magma mixing	Main Zone magma intruded between cumulate pile and Upper Zone crystals+liquid	(Sharpe 1985)
EL	Burgersfort to Stoffberg	WR	Marginal B1: 0.7032-0.7057 Marginal B2: 0.7064-0.7077 Marginal B3: 0.7059-0.7072	2050 Ma	Marginal rocks are derived from mixing of two mantle domains	Multistage subcratonic history for the evolution of the Bushveld	(Harmer and Sharpe 1985)
WL	Union Section	WR	Main: 0.70731-0.70890	2050 Ma	Main Zone can be separated into sub-units based on rock type and geochemistry	Main Zone is from the Pyroxenite Marker to the top of the Bastard Cyclic Unit based on Sr isotopes	(Mitchell 1986)

Table 1. Summary of strontium isotope studies throughout the Bushveld Igneous Complex (continued).

Limb	Limb/Location	Analytical Details	$^{87}\text{Sr}/^{86}\text{Sr}_i$ per Stratigraphic Zone	Age*	Model	Conclusion	Reference
WL	Union Section	WR	Main: 0.7087 Transitional Units: 0.7064-0.7087 Critical Zone: 0.7063	N/S	Wedge Main Zone liquid above crystalline floor with hybrid layer in between, multiple magma influxes	Magma influx associated with each cyclic unit	(Eales et al. 1986)
WL	Bierkraal	N/S	Upper: 0.7073	2050 Ma	Upper Zone is a single magmatic series due to an influx of magma at the Pyroxenite Marker	Upper-Main Zone boundary should be at the Pyroxenite Marker	(Kruger et al. 1987)
EL	Atok Section	WR	Transitional Units: 0.7062-0.708	2050 Ma	Sharp contacts and bifurcation along strike indicate intrusive nature, Sr isotopes gradually change upwards of intrusion	The Merensky and Bastard Reef are intrusive (sills) in nature	(Butcher 1990)
WL	Union Section	WR and MS (plag, opx)	Transitional Units: 0.7064-0.7078 Upper Critical: 0.7049-0.7070	2050 Ma	New magma pulse injected near crystalline floor, hybridizes by partial reabsorption of cumulate pile	Jetting (LCZ) followed by pluming (UCZ-LMZ) for new magma pulses into the chamber	(Eales et al. 1990)
WL	Nooitgedagt and Union Section	WR and MS (plag, px)	Lower Critical: 0.7047-0.7055 Lower: 0.7046-0.7071	N/S	Interaction between magma batches and fractionation rather than fractionation alone	Magma influxes	(Eales et al. 1990)

Table 1. Summary of strontium isotope studies throughout the Bushveld Igneous Complex (continued).

Limb	Limb/Location	Analytical Details	$^{87}\text{Sr}/^{86}\text{Sr}_i$ per Stratigraphic Zone	Age*	Model	Conclusion	Reference
WL, EL	Union Section, Amandelbult Section, Rustenburg Sections and Atok Mine	N/S	Transitional Units: 0.7064-0.7080 (Amandelbult)	2060 Ma (Amandelbult)	Cool Magma Fountain Model	New magma was compositionally denser, sank to the bottom of the chamber and scavenged the metals from the resident magma creating the Merensky and Bastard Reefs	(Kruger 1992)
WL	Northam to Rustenburg	WR and MS (plag)	Upper: 0.7072-0.7077 Upper Main: 0.7080-0.7085 Lower Main: 0.7072-0.7090 Upper Critical: 0.7060-0.7073 Lower Critical: 0.7048-0.7056 Lower: 0.7047-0.7071	2060 Ma	Integration Stage (multiple pulses of new magma) and Differentiation Stage (dominantly fractionation)	Lower Zone to Lower Main Zone is part of the Integration Stage, Upper Main Zone and Upper Zone is part of Differentiation Stage	(Kruger 1994)
WL	Western Platinum Mine	WR and MS (plag)	Transitional Units: 0.7065-0.7068	2060 Ma	Footwall Extension Model	Extension of the magmatic chamber during the formation of the Merensky Reef	(Carr et al. 1999)

Table 1. Summary of strontium isotope studies throughout the Bushveld Igneous Complex (continued).

Limb	Limb/Location	Analytical Details	$^{87}\text{Sr}/^{86}\text{Sr}_i$ per Stratigraphic Zone	Age*	Model	Conclusion	Reference
WL, EL	Brakspruit and Steelport	WR and MS (plag)	Upper Critical: 0.7057-0.7080 (AM38 - South of the Steelport Lineament - EL) Lower Critical: 0.7057-0.7077 (AM38 - South of the Steelport Lineament - EL) Upper Critical: 0.7059-0.7086 (KF17 - North of the Steelport Lineament - EL) Upper Critical: 0.7062-0.7099 (BK - WL) Upper Critical: 0.7062-0.7083 (SK9 - Union Section - WL)	2057 Ma	New magma entering the chamber triggers chromite to be formed	Each chromitite layer represents a new replenishment of magma into the chamber	(Kinnaird et al. 2002)
EL	Richmond	MS (plag)	Main: 0.7077-0.7087 Transitional Units: 0.7062-0.7080 Critical: 0.7061-0.7071	2059 Ma	Co-accumulation of minerals in the Bastard and Merensky Reef due to stratified magmas	Bastard and Merensky Cyclic Units should be classified as transitional units because they contain minerals from both the Main and Critical Zone	(Seabrook et al. 2005)
NL, SL	Turfspruit (NL), Bethal (SL)	MS (plag, opx)	Assimilation Zone: 0.70723-0.71459 (NL) Upper: 0.70514-0.70581 (SL)	2055 Ma (NL) 2060 Ma (SL)	Four different magmas contributed to forming the Rustenburg Layered Suite (BvLz, BvCz, BvMz and BvUz)	Magmatic unconformities are ideal for stratabound mineralization	(Kruger 2005)

Table 1. Summary of strontium isotope studies throughout the Bushveld Igneous Complex (continued).

Limb	Limb/Location	Analytical Details	$^{87}\text{Sr}/^{86}\text{Sr}_i$ per Stratigraphic Zone	Age*	Model	Conclusion	Reference
EL	Jagdlust Section	MS (plag, opx)	Critical: 0.7032-0.7063 Lower: 0.7029-0.7063	2060 Ma	Isotopic disequilibrium between minerals in the Critical and Lower Zone	Bulk rock nor mineral separates can be used to infer primary magmatic isotopic ratios, processes or sources	(Chutas et al. 2012)
WL	Union Section	WR and MS (plag rim and core)	Transitional Unit: 0.7062-0.7088 Upper Critical: 0.7050-0.7073	2055 Ma	Plagioclase from the Main and Critical Zone are incorporated in the Merensky and Bastard Cyclic Units because of mineral sorting due to slumping crystal mushes	Disequilibrium between core and rim of plagioclase is due to overgrowth of plagioclase from silicate melts with a different composition	(Yang et al. 2013)
NL	Moordkopje and Bellevue	<i>In-situ</i> plag	Upper: 0.7063-0.70786 Main: 0.70694-0.71061	2054.4 Ma	Strontium isotope analyses record similar processes as the Western Limb (Kruger 1994)	Variations within samples and grains is likely due to the intrusion of crystal mushes	(Mangwegape et al. 2016)

Compilation of strontium isotope work completed through the Rustenburg Layered Suite of the Bushveld Complex. Each row describes the location, methods, $^{87}\text{Sr}/^{86}\text{Sr}_i$ values, age used in calculation for the initial ratio and the main model and conclusions of each publication.

*Age used to calculate $^{87}\text{Sr}/^{86}\text{Sr}_i$

**Zone between the Critical and Lower Zone (now likely the LCZ)

***Transitional Units include the Bastard Cyclic Unit and Merensky Cyclic Unit

N/S = Not specified WR = Whole rock, MS = Mineral separates, WL = Western Limb, EL = Eastern Limb, NL = Northern Limb

Table 2. Mineralogical abundances throughout magmatic units within UMT094.

Stratigraphy	Cycle	Rock Type	Grain Size	Major (>10%)	Minor (<10%;>1%)	Trace (<1%)
HW3	MZ	Norite to Gabbronorite	MG-CG	Pl (65-55), Opx (30), Cpx (15-5)		Bt, Mag, Po, Ccp, Py, -
HW2	BCU	Norite	CG	Pl (70), Opx (25)	Cpx (3), WM (2)	Bt, Mag, Po, Ccp, Py
HW1	BCU	Gabbronorite	MG	Pl (57), Cpx (20), Opx (20)	WM (3)	Po, Ccp, Py
BAR	BCU	Gabbronorite to Olivine Gabbronorite	MG-CG	Opx (64-52), Pl (25-15), Cpx (18-5)	Ol (5-0), WM (4-3), Ccp (2-1), Po (1), Bt (1-tr), Cr (1-0)	Mag, Pn, Chl
MD1	MCU	Norite to Gabbronorite	MG	Opx (72-71), Pl (20-15)	Cpx (10-3), WM (4-2), Bt (1), Po (1-tr)	Mag, Ccp, Pn, Chl
M1U	MCU	Orthopyroxenite/ Pyroxenite to Gabbro/ Gabbronorite	CG	Opx (73-1), Cpx (67-8), Pl (25-10), WM (15-3)	Cr (3-0), Chl (3-tr), Bt (2-tr), Po (2-0), Ccp (2-tr), Pn (2-tr), Cal (2-tr)	Mag, Ged
M1L	MCU	Olivine Gabbronorite to Olivine Norite	MG-CG	Srp (44), Ol (20), Cpx (15)	Pl (8), Opx (3), Mag (3), WM (3), Cr (1), Po (1), Ccp (1), Pn (1)	Bt
FW2	FCU	Anorthosite to Gabbronorite	MG-CG	Pl (91-15), Opx (63-2), Cpx (40-1)	WM (3-1), Cr (2-0), Bt (1-0), Po (1-tr), Ccp (1-tr), Pn (1-0), Chl (1-0)	Mag, Py, Ged
PSDR	FCU	Olivine Gabbronorite to Olivine Norite	MG	Pl (38-20), Ol (25-20), Opx (31-30)	Cr (8-tr), WM (5-2), Cpx (7-4), Srp (2), Po (2-1), Mag (1-tr), Ccp (1-tr), Pn (1-tr)	Bt
UG2HW	UG2CU	Gabbronorite	MG-CG	Opx (61-60), Pl (20-18), Cpx (16-15)	Cr (5-2), WM (2-tr), Po (1-tr)	Bt, Ccp

Table 3. Plagioclase composition and anorthite (An) content (by EPMA-WDS).

Sample	SiO ₂	Al ₂ O ₃	MgO	CaO	FeO _t	Na ₂ O	K ₂ O	Total	An Cont.
1096-1	52.12	29.74	0.03	13.21	0.33	3.99	0.26	99.72	63.7
1096-2	51.15	30.41	0.03	13.91	0.40	3.49	0.22	99.65	67.9
1096-3	51.18	30.66	0.02	14.14	0.39	3.41	0.24	100.08	68.7
1096-4	50.78	30.92	0.01	14.20	0.34	3.37	0.19	99.84	69.2
1096-5	50.38	30.96	0.03	14.39	0.39	3.22	0.24	99.61	70.2
1096-6	50.10	31.22	0.03	14.67	0.38	3.13	0.18	99.74	71.4
1096-7	51.19	30.37	0.03	13.89	0.35	3.58	0.27	99.71	67.1
1184-1	48.77	32.00	0.03	15.70	0.28	2.44	0.19	99.40	77.2
1184-2	49.50	31.67	0.04	15.19	0.35	2.69	0.18	99.66	74.9
1184-3	49.74	31.75	0.02	15.10	0.31	2.82	0.23	100.00	73.7
1184-4	48.87	32.01	0.04	15.54	0.33	2.51	0.18	99.51	76.6
1184-5	50.36	31.19	0.04	14.71	0.33	3.06	0.25	99.97	71.6
1184-6	49.96	31.25	0.03	14.68	0.34	3.04	0.25	99.58	71.7
1184-7	49.55	31.49	0.04	14.80	0.34	2.85	0.26	99.37	73.0
1213-1	51.07	30.19	0.04	13.74	0.42	3.62	0.29	99.41	66.6
1213-2	50.88	30.52	0.02	13.92	0.37	3.51	0.25	99.52	67.7
1213-3	51.43	30.26	0.03	13.72	0.38	3.67	0.24	99.77	66.5
1213-4	49.52	31.44	0.03	15.06	0.32	2.90	0.18	99.44	73.4
1213-5	50.56	30.84	0.03	14.30	0.41	3.21	0.28	99.64	70.0
1213-6	50.89	30.71	0.02	14.18	0.39	3.41	0.29	99.92	68.5
1213-7	51.25	30.30	0.03	13.86	0.46	3.62	0.27	99.81	66.9
1226-1	48.82	31.95	0.05	15.78	0.38	2.57	0.15	99.78	76.6
1226-2	49.83	31.28	0.03	15.05	0.32	2.90	0.21	99.66	73.2
1226-3	48.38	32.20	0.03	16.08	0.44	2.38	0.15	99.67	78.2
1226-4	48.61	32.35	0.02	15.85	0.31	2.50	0.14	99.78	77.2
1226-5	49.01	31.80	0.04	15.63	0.36	2.55	0.15	99.56	76.5
1226-6	48.53	32.11	0.04	15.95	0.34	2.46	0.14	99.59	77.5
1226-7	49.83	31.33	0.05	14.90	0.35	2.96	0.19	99.62	72.7
1232-1	54.12	28.72	0.03	11.62	0.19	4.81	0.38	99.90	55.9
1232-2	54.23	28.84	0.03	11.69	0.20	4.82	0.39	100.33	56.0
1232-3	52.60	29.73	0.03	12.80	0.22	4.08	0.34	99.84	62.2
1232-4	54.09	28.67	0.03	11.56	0.17	4.87	0.31	99.75	55.7
1232-5	49.88	31.50	0.03	14.93	0.20	2.90	0.22	99.68	73.0
1232-6	53.66	29.06	0.03	12.12	0.21	4.48	0.38	100.10	58.6
1232-7	49.68	31.70	0.02	14.95	0.20	2.94	0.11	99.64	73.3
1233-1	51.33	30.43	0.03	13.61	0.25	3.59	0.32	99.69	66.4
1233-2	51.19	30.86	0.04	14.12	0.21	3.44	0.29	100.25	68.2
1233-3	53.21	29.50	0.03	12.47	0.20	4.42	0.30	100.19	59.9
1233-4	51.40	30.54	0.04	13.79	0.22	3.56	0.38	100.03	66.7
1233-5	51.31	30.52	0.03	13.60	0.24	3.62	0.31	99.65	66.3
1233-6	50.71	30.73	0.03	14.29	0.24	3.29	0.29	99.62	69.4
1233-7	51.39	30.69	0.03	13.85	0.26	3.40	0.34	99.98	67.9
1238-1	53.41	28.63	0.02	11.76	0.19	4.64	0.51	99.22	56.6
1238-2	51.26	30.48	0.03	13.81	0.23	3.56	0.26	99.67	67.2
1238-3	51.44	30.58	0.03	13.54	0.23	3.60	0.29	99.72	66.4
1238-4	54.51	28.58	0.03	11.33	0.18	4.91	0.39	99.97	54.8
1238-5	51.17	30.52	0.02	13.71	0.19	3.61	0.27	99.59	66.7
1238-6	55.10	28.41	0.02	11.00	0.15	5.17	0.39	100.29	52.8
1238-7	51.03	30.56	0.03	13.77	0.19	3.55	0.24	99.40	67.2
1245-1	53.75	28.93	0.03	11.87	0.21	4.79	0.26	99.87	56.9

Table 3. Plagioclase composition and anorthite (An) content (by EPMA-WDS; continued).

Sample	SiO ₂	Al ₂ O ₃	MgO	CaO	FeO _t	Na ₂ O	K ₂ O	Total	An Cont.
1245-2	52.68	29.38	0.03	12.61	0.23	4.46	0.24	99.66	60.1
1245-3	53.18	29.00	0.03	12.16	0.24	4.63	0.25	99.55	58.4
1245-4	51.34	30.45	0.03	13.69	0.23	3.78	0.31	99.96	65.5
1245-5	50.94	30.65	0.09	14.06	0.28	3.36	0.42	99.84	68.1
1245-6	50.16	31.13	0.03	14.63	0.22	3.15	0.23	99.57	71.0
1245-7	50.51	30.75	0.04	14.39	0.20	3.31	0.25	99.47	69.6
1252-1	51.09	31.05	0.03	14.13	0.24	3.46	0.30	100.29	68.1
1252-2	52.55	29.87	0.03	12.99	0.20	4.12	0.36	100.26	62.2
1252-3	50.35	31.28	0.03	14.67	0.19	3.26	0.23	100.02	70.4
1252-4	54.16	28.77	0.03	11.41	0.17	4.87	0.38	99.85	55.2
1252-5	54.35	28.77	0.02	11.45	0.14	4.97	0.34	100.09	54.9
1252-6	49.95	31.68	0.02	14.92	0.24	2.98	0.19	100.00	72.6
1252-7	49.77	31.41	0.02	14.79	0.23	3.07	0.18	99.61	71.9
1277-1	52.34	29.78	0.02	13.05	0.27	4.10	0.26	99.86	62.8
1277-2	52.13	29.88	0.02	12.98	0.24	4.13	0.27	99.79	62.5
1277-3	53.13	29.31	0.02	12.30	0.23	4.53	0.31	99.97	58.9
1277-4	52.99	29.53	0.02	12.51	0.23	4.35	0.34	100.01	60.2
1277-5	52.93	29.32	0.03	12.42	0.19	4.39	0.30	99.61	59.9
1277-6	53.25	29.19	0.02	12.13	0.20	4.57	0.28	99.75	58.5
1277-7	53.70	29.16	0.03	11.99	0.27	4.56	0.34	100.08	58.1
1282-1	53.85	29.04	0.02	11.99	0.17	4.57	0.38	100.08	57.9
1282-2	48.95	31.96	0.02	15.63	0.32	2.52	0.24	99.74	76.3
1282-3	49.40	31.72	0.05	15.26	0.32	2.76	0.24	99.78	74.3
1282-4	49.71	31.60	0.03	15.20	0.30	2.88	0.27	100.00	73.3
1282-5	49.84	31.70	0.03	15.19	0.32	2.94	0.17	100.31	73.3
1282-6	49.78	31.45	0.03	14.84	0.29	3.03	0.23	99.75	72.0
1282-7	56.55	26.82	0.02	9.45	0.25	6.30	0.22	99.68	44.8
1285-1	51.30	30.44	0.03	13.62	0.30	3.64	0.39	99.76	65.9
1285-2	53.23	28.98	0.02	11.90	0.25	4.59	0.50	99.49	57.2
1285-3	51.65	30.23	0.03	13.39	0.27	3.78	0.42	99.81	64.6
1285-4	50.61	30.77	0.06	14.11	0.26	3.31	0.42	99.65	68.5
1285-5	51.16	30.54	0.03	13.91	0.34	3.51	0.44	99.95	66.9
1285-6	51.14	30.58	0.04	13.75	0.36	3.66	0.30	99.85	66.3
1285-7	54.81	28.19	0.02	10.88	0.27	5.32	0.44	99.97	51.7
1289-1	47.81	32.80	0.03	16.31	0.43	2.09	0.15	99.62	80.5
1289-2	47.26	33.09	0.02	16.58	0.38	1.95	0.13	99.52	81.8
1289-3	47.37	33.16	0.01	16.83	0.32	1.92	0.09	99.70	82.5
1289-4	48.41	32.20	0.02	15.80	0.44	2.34	0.21	99.42	77.9
1289-5	47.77	32.57	0.02	16.24	0.45	2.17	0.17	99.48	79.7
1289-6	47.83	32.47	0.03	16.05	0.40	2.29	0.12	99.20	78.9
1289-7	48.04	32.18	0.03	15.80	0.47	2.32	0.23	99.13	77.9
1291B-1	47.69	32.83	0.06	16.45	0.39	2.09	0.15	99.67	80.6
1291B-2	46.53	33.68	0.03	17.37	0.33	1.60	0.09	99.62	85.3
1291B-3	48.34	32.66	0.03	16.13	0.33	2.27	0.11	99.86	79.2
1291B-4	46.41	33.55	0.02	17.49	0.30	1.62	0.08	99.47	85.2
1291B-5	47.91	32.62	0.03	16.12	0.35	2.26	0.17	99.49	79.0
1291B-6	47.43	33.13	0.03	16.67	0.35	2.02	0.10	99.72	81.5
1291B-7	47.44	33.19	0.02	16.98	0.34	2.02	0.07	100.19	82.0
1292A-2-1	49.62	31.89	0.03	15.38	0.41	2.76	0.21	100.32	74.6
1292A-2-2	48.85	31.89	0.03	15.64	0.46	2.63	0.18	99.70	75.9
1292A-2-3	48.98	31.71	0.03	15.59	0.48	2.60	0.17	99.68	76.1

Table 3. Plagioclase composition and anorthite (An) content (by EPMA-WDS; continued).

Sample	SiO ₂	Al ₂ O ₃	MgO	CaO	FeO _T	Na ₂ O	K ₂ O	Total	An Cont.
1292A-2-4	49.11	31.75	0.04	15.45	0.47	2.77	0.19	99.88	74.7
1292A-2-5	48.35	31.99	0.05	16.04	0.54	2.39	0.19	99.58	77.9
1292A-2-6	48.62	32.01	0.05	15.98	0.54	2.42	0.16	99.81	77.8
1292A-2-7	48.36	32.22	0.04	15.95	0.51	2.48	0.17	99.88	77.3
1296-1	49.30	31.80	0.04	15.31	0.37	2.73	0.17	99.72	74.9
1296-2	49.38	31.77	0.04	15.34	0.31	2.73	0.18	99.76	74.8
1296-3	49.27	31.70	0.04	15.53	0.38	2.69	0.19	99.84	75.3
1296-4	49.28	31.76	0.04	15.52	0.36	2.66	0.18	99.80	75.5
1296-5	48.35	32.12	0.04	16.13	0.37	2.29	0.15	99.48	78.9
1296-6	49.23	31.74	0.04	15.37	0.33	2.80	0.20	99.74	74.3
1296-7	49.32	31.67	0.04	15.34	0.35	2.73	0.18	99.65	74.8
1300-1	49.82	31.46	0.05	15.05	0.35	2.83	0.23	99.80	73.6
1300-2	49.00	31.87	0.05	15.68	0.35	2.58	0.17	99.71	76.3
1300-3	49.06	31.73	0.03	15.67	0.26	2.66	0.19	99.71	75.7
1300-4	49.07	31.81	0.05	15.51	0.34	2.64	0.18	99.63	75.7
1300-5	49.69	31.66	0.04	15.19	0.32	2.81	0.21	99.93	74.0
1300-6	50.04	31.17	0.04	14.84	0.37	3.05	0.23	99.84	71.9
1300-7	49.16	31.69	0.04	15.33	0.34	2.70	0.21	99.50	74.9
1311-1	49.25	31.52	0.04	15.24	0.30	2.77	0.21	99.32	74.3
1311-2	49.39	31.42	0.04	15.09	0.31	2.83	0.24	99.34	73.6
1311-3	51.40	30.03	0.03	13.40	0.29	3.66	0.36	99.20	65.5
1311-4	49.20	31.71	0.02	15.34	0.25	2.69	0.16	99.39	75.2
1311-5	50.44	30.84	0.03	14.39	0.31	3.20	0.27	99.58	70.2
1311-6	51.31	30.50	0.04	13.84	0.32	3.63	0.24	99.92	66.9
1311-7	50.06	31.39	0.02	14.90	0.31	3.00	0.25	99.92	72.2
1319-1	51.30	30.50	0.03	13.91	0.27	3.44	0.36	99.91	67.6
1319-2	49.63	31.52	0.03	15.40	0.26	2.82	0.26	99.92	74.0
1319-3	49.23	32.28	0.02	15.69	0.30	2.49	0.18	100.22	76.9
1319-4	49.14	31.78	0.04	15.29	0.29	2.65	0.22	99.55	75.1
1319-5	52.10	30.03	0.03	13.14	0.23	3.93	0.40	100.00	63.4
1319-6	48.28	32.43	0.02	15.86	0.29	2.45	0.14	99.48	77.5
1319-7	49.60	31.26	0.01	15.12	0.23	2.17	1.24	99.70	73.7
1325B-1	49.71	31.44	0.03	14.97	0.32	2.82	0.26	99.57	73.4
1325B-2	49.52	31.68	0.03	15.34	0.38	2.77	0.23	99.97	74.4
1325B-3	49.88	31.37	0.04	14.77	0.31	2.89	0.29	99.69	72.6
1325B-4	51.57	30.30	0.04	13.45	0.37	3.54	0.43	99.73	66.0
1325B-5	50.09	31.06	0.03	14.56	0.33	3.05	0.28	99.52	71.3
1325B-6	50.87	30.76	0.03	14.40	0.25	3.31	0.29	99.93	69.4
1325B-7	49.27	31.83	0.02	15.43	0.31	2.63	0.23	99.75	75.4
1329-1	50.85	30.89	0.03	13.89	0.20	3.48	0.27	99.65	67.7
1329-2	50.00	31.55	0.02	14.84	0.23	2.99	0.26	99.90	72.2
1329-3	50.81	30.98	0.03	14.10	0.21	3.43	0.32	99.91	68.2
1329-4	49.90	31.58	0.02	14.88	0.25	2.97	0.20	99.81	72.6
1329-5	49.94	31.44	0.02	14.73	0.26	2.99	0.31	99.68	71.8
1329-6	50.42	31.26	0.04	14.55	0.28	3.19	0.26	100.14	70.5
1329-7	50.50	31.47	0.01	14.49	0.23	3.33	0.13	100.16	70.1
1336-1	49.93	31.18	0.02	14.64	0.27	3.13	0.36	99.67	70.6
1336-2	50.93	30.78	0.04	14.09	0.29	3.43	0.38	99.96	67.9
1336-3	49.46	31.63	0.03	15.26	0.31	2.95	0.24	100.00	73.1
1336-4	50.17	31.15	0.03	14.74	0.30	3.19	0.27	99.90	70.7
1336-5	49.49	31.74	0.03	15.34	0.27	2.82	0.20	99.99	74.2
1336-6	50.32	31.10	0.03	14.27	0.31	3.25	0.28	99.62	69.7

Table 3. Plagioclase composition and anorthite (An) content (by EPMA-WDS; continued).

Sample	SiO ₂	Al ₂ O ₃	MgO	CaO	FeO _t	Na ₂ O	K ₂ O	Total	An Cont.
1336-7	50.48	31.16	0.03	14.67	0.28	3.21	0.28	100.25	70.5
1339-1	50.81	31.14	0.03	14.36	0.25	3.30	0.34	100.33	69.3
1339-2	50.73	30.95	0.02	14.26	0.19	3.31	0.36	99.82	69.0
1339-3	51.50	30.19	0.03	13.51	0.20	3.53	0.60	99.65	65.5
1339-4	50.17	31.16	0.03	14.43	0.28	3.12	0.37	99.64	70.3
1339-5	50.39	31.10	0.02	14.32	0.27	3.19	0.33	99.65	69.9
1339-6	50.88	31.14	0.02	14.13	0.24	3.34	0.36	100.12	68.6
1339-7	50.87	31.00	0.03	14.17	0.24	3.29	0.42	100.02	68.7
1343-1	50.86	30.73	0.03	14.00	0.21	3.43	0.35	99.68	67.9
1343-2	50.41	31.09	0.03	14.57	0.22	3.22	0.27	99.84	70.3
1343-3	50.29	31.34	0.02	14.65	0.21	3.13	0.26	99.98	71.0
1343-4	49.96	31.47	0.03	14.65	0.22	3.08	0.27	99.80	71.3
1343-5	50.92	30.66	0.02	13.80	0.24	3.45	0.34	99.55	67.5
1343-6	50.02	31.16	0.02	14.55	0.22	3.10	0.25	99.31	71.1
1343-7	50.99	30.53	0.02	13.84	0.21	3.52	0.40	99.63	66.9

* Detection limits (wt.%): SiO₂: 0.024, Al₂O₃: 0.019, MgO: 0.009, CaO: 0.018, FeO_t: 0.026, Na₂O: 0.012 and K₂O: 0.014.

Table 4. Whole-rock strontium isotope data.

Sample	Depth (m)	Sr (ppm)	Rb (ppm)	$^{87}\text{Sr}/^{86}\text{Sr}$	2σ	$^{87}\text{Rb}/^{86}\text{Sr}$	2σ	$^{87}\text{Sr}/^{86}\text{Sr}_i$	2σ
1096	195.73	279.0	10.9	0.71154	0.00003	0.1130	0.0063	0.70825	0.00018
1111	181.17	247.0	7.8	0.71082	0.00003	0.0914	0.0051	0.70817	0.00015
1135	156.91	279.0	18.1	0.71483	0.00003	0.1878	0.0104	0.70938	0.00030
1135	156.91	279.0	18.1	0.71489	0.00003	0.1878	0.0104	0.70944	0.00030
1165	126.65	243.0	12.2	0.71082	0.00003	0.1453	0.0080	0.70661	0.00024
1184	107.38	302.0	2.4	0.70883	0.00003	0.0230	0.0013	0.70816	0.00005
1213	78.81	307.0	6.9	0.70996	0.00003	0.0650	0.0036	0.70807	0.00011
1226	65.57	337.0	34.7	0.71596	0.00003	0.2981	0.0165	0.70730	0.00048
1232	58.96	53.8	2.0	0.71205	0.00003	0.1076	0.0060	0.70893	0.00018
1238	53.29	61.9	7.5	0.71696	0.00003	0.3508	0.0194	0.70678	0.00056
1245	46.67	78.4	10.9	0.72045	0.00003	0.4027	0.0223	0.70876	0.00065
1252	39.87	44.4	6.1	0.71888	0.00003	0.3978	0.0220	0.70732	0.00064
1258	33.30	30.5	4.4	0.71897	0.00003	0.4177	0.0231	0.70684	0.00067
1265	26.36	33.8	9.1	0.73043	0.00003	0.7805	0.0432	0.70777	0.00125
1277	15.10	25.9	3.6	0.71937	0.00003	0.4025	0.0223	0.70768	0.00065
1277	15.10	25.9	3.6	0.71960	0.00003	0.4025	0.0223	0.70791	0.00065
1285	6.91	30.6	6.8	0.72805	0.00003	0.6441	0.0356	0.70935	0.00104
1288	3.13	109.5	1.5	0.71022	0.00003	0.0396	0.0022	0.70907	0.00007
1291B	0.15	67.4	1.6	0.70759	0.00003	0.0687	0.0038	0.70559	0.00011
1291B	0.15	67.4	1.6	0.70766	0.00003	0.0687	0.0038	0.70567	0.00011
1292A	0	513.0	31.7	0.71236	0.00003	0.1788	0.0099	0.70716	0.00029
1300	-8.31	328.0	6.4	0.70828	0.00003	0.0564	0.0031	0.70664	0.00010
1311	-19.78	280.0	13.2	0.71102	0.00003	0.1364	0.0075	0.70706	0.00022
1319	-27.95	114.0	6.1	0.71071	0.00003	0.1548	0.0086	0.70621	0.00025
1327	-35.89	103.5	3.1	0.70901	0.00003	0.0866	0.0048	0.70650	0.00014
1336	-44.27	122.5	4.9	0.70866	0.00003	0.1157	0.0064	0.70530	0.00019
1343	-52.01	78.7	2.0	0.70809	0.00003	0.0735	0.0041	0.70595	0.00012
1359	-67.89	90.8	3.8	0.70955	0.00003	0.1211	0.0067	0.70604	0.00020
1365	-73.80	34.4	0.8	0.70882	0.00003	0.0673	0.0037	0.70686	0.00011
1376	-84.72	107.5	14.0	0.71954	0.00003	0.3771	0.0209	0.70859	0.00061
1410	-118.7	30.3	0.2	0.70761	0.00003	0.0191	0.0011	-	-
1436	-144.44	5.4	0.1	0.71079	0.00003	0.0536	0.0030	-	-
1461	-169.66	30.0	0.8	0.74345	0.00003	0.0774	0.0043	-	-
1537	-245.28	64.6	0.2	0.70656	0.00003	0.0090	0.0005	-	-
1601	-309.51	100.5	0.2	0.70698	0.00003	0.0058	0.0003	-	-
LUD006	o/c	32.9	1.5	0.72238	0.00003	0.1321	0.0073	-	-
LUD007-2	o/c	47.9	124.0	0.94578	0.00004	7.6682	0.4255	-	-
LUD007-2	o/c	47.9	124.0	0.94583	0.00004	7.6679	0.4254	-	-
LUD008	o/c	10.3	0.6	0.71872	0.00003	0.1687	0.0094	-	-
LUD002	o/c	108.5	177.5	0.86381	0.00004	4.8093	0.2668	-	-

* Uncertainties for Sr and Rb concentrations are 5% based on ALS quality standards.
Depth is relative to the contact between the Footwall and Merensky Cyclic Units located at 1291.93 meters depth.

Table 5. Strontium isotope data from *in-situ* analyses of plagioclase.

Sample	Depth (m)	$^{87}\text{Sr}/^{86}\text{Sr}$	1 σ	$^{87}\text{Rb}/^{86}\text{Sr}$	1 σ	$^{87}\text{Sr}/^{86}\text{Sr}_i$	1 σ
1096_R	-1096.33	0.70789	0.00023	0.00245	0.00009	0.70782	0.00023
1096_C	-1096.33	0.70806	0.00023	0.00505	0.00018	0.70791	0.00023
1096_R	-1096.33	0.70804	0.00023	0.00275	0.00010	0.70796	0.00023
1096_C	-1096.33	0.70756	0.00023	0.00157	0.00006	0.70752	0.00023
1096_C	-1096.33	0.70790	0.00023	0.00205	0.00007	0.70784	0.00023
1096_R	-1096.33	0.70808	0.00023	0.00411	0.00015	0.70796	0.00023
1111_R	-1110.89	0.70829	0.00023	0.00119	0.00011	0.70825	0.00023
1111_C	-1110.89	0.70807	0.00023	0.00164	0.00016	0.70802	0.00023
1111_R	-1110.89	0.70822	0.00023	0.00170	0.00016	0.70817	0.00023
1111_C	-1110.89	0.70814	0.00023	0.00203	0.00019	0.70808	0.00023
1111_R	-1110.89	0.70815	0.00023	0.00250	0.00024	0.70808	0.00023
1111_C	-1110.89	0.70766	0.00023	0.00183	0.00017	0.70760	0.00023
1111_C	-1110.89	0.70775	0.00023	0.00618	0.00059	0.70757	0.00023
1135_W	-1135.16	0.70865	0.00029	0.00393	0.00027	0.70854	0.00029
1135_C	-1135.16	0.70827	0.00029	0.00504	0.00035	0.70812	0.00029
1135_R	-1135.16	0.70888	0.00029	0.00762	0.00053	0.70866	0.00029
1135_R	-1135.16	0.70891	0.00029	0.01056	0.00073	0.70860	0.00029
1135_C	-1135.16	0.70830	0.00029	0.00539	0.00037	0.70815	0.00029
1135_R	-1135.16	0.70877	0.00029	0.01010	0.00070	0.70848	0.00029
1135_R	-1135.16	0.70868	0.00029	0.00250	0.00017	0.70861	0.00029
1165_C	-1165.42	0.70811	0.00023	0.01123	0.00106	0.70779	0.00023
1165_R	-1165.42	0.70786	0.00023	0.00421	0.00040	0.70773	0.00023
1165_C	-1165.42	0.70812	0.00023	0.00520	0.00049	0.70796	0.00023
1165_R	-1165.42	0.70839	0.00023	0.00371	0.00035	0.70828	0.00023
1165_R	-1165.42	0.70816	0.00023	0.01319	0.00125	0.70778	0.00023
1165_R	-1165.42	0.70819	0.00023	0.00800	0.00076	0.70796	0.00023
1184_C	-1184.68	0.70802	0.00023	0.00596	0.00021	0.70784	0.00023
1184_C	-1184.68	0.70805	0.00023	0.00747	0.00027	0.70784	0.00023
1184_R	-1184.68	0.70795	0.00023	0.01037	0.00037	0.70765	0.00023
1184_R	-1184.68	0.70775	0.00023	0.01020	0.00037	0.70745	0.00023
1184_C	-1184.68	0.70739	0.00023	0.00522	0.00019	0.70723	0.00023
1184_C	-1184.68	0.70776	0.00023	0.00300	0.00011	0.70767	0.00023
1184_R	-1184.68	0.70789	0.00023	0.00629	0.00023	0.70770	0.00023
1213_R	-1213.25	0.70799	0.00023	0.00356	0.00013	0.70789	0.00023
1213_C	-1213.25	0.70813	0.00023	0.00224	0.00008	0.70806	0.00023
1213_C	-1213.25	0.70812	0.00023	0.00355	0.00013	0.70802	0.00023
1213_R	-1213.25	0.70826	0.00023	0.00589	0.00021	0.70809	0.00023
1213_C	-1213.25	0.70792	0.00023	0.00306	0.00011	0.70783	0.00023
1213_C	-1213.25	0.70751	0.00023	0.00456	0.00016	0.70738	0.00023
1213_C	-1213.25	0.70824	0.00023	0.00272	0.00010	0.70816	0.00023
1218_W	-1218.19	0.70745	0.00022	0.00292	0.00019	0.70737	0.00022
1218_C	-1218.19	0.70740	0.00022	0.00496	0.00032	0.70725	0.00022
1218_C	-1218.19	0.70747	0.00022	0.00169	0.00011	0.70742	0.00022
1218_R	-1218.19	0.70726	0.00022	0.00335	0.00022	0.70716	0.00022
1218_C	-1218.19	0.70720	0.00022	0.00310	0.00020	0.70711	0.00022
1218_W	-1218.19	0.70713	0.00022	0.00102	0.00007	0.70710	0.00022
1226_R	-1226.5	0.70733	0.00023	0.00205	0.00019	0.70727	0.00023
1226_C	-1226.5	0.70768	0.00023	0.00175	0.00017	0.70763	0.00023
1226_R	-1226.5	0.70760	0.00023	0.00162	0.00015	0.70755	0.00023
1226_C	-1226.5	0.70805	0.00023	0.00148	0.00014	0.70800	0.00023
1226_C	-1226.5	0.70766	0.00023	0.00290	0.00028	0.70758	0.00023
1226_R	-1226.5	0.70682	0.00023	0.00129	0.00012	0.70678	0.00023

Table 5. Strontium isotope data from *in-situ* analyses of plagioclase (continued).

Sample	Depth (m)	$^{87}\text{Sr}/^{86}\text{Sr}$	1σ	$^{87}\text{Rb}/^{86}\text{Sr}$	1σ	$^{87}\text{Sr}/^{86}\text{Sr}_i$	1σ
1226_R	-1226.5	0.70757	0.00023	0.00068	0.00006	0.70755	0.00023
1229_R	-1229.65	0.70759	0.00024	0.00422	0.00044	0.70747	0.00024
1229_C	-1229.65	0.70814	0.00024	0.02378	0.00249	0.70745	0.00025
1229_C	-1229.65	0.70755	0.00024	0.00083	0.00009	0.70753	0.00024
1229_C	-1229.65	0.70821	0.00024	0.00331	0.00035	0.70811	0.00024
1229_C	-1229.65	0.70822	0.00024	0.00702	0.00074	0.70802	0.00024
1232_C	-1233.12	0.70799	0.00024	0.00190	0.00020	0.70794	0.00024
1232_C	-1233.12	0.70744	0.00024	0.00067	0.00007	0.70742	0.00024
1232_R	-1233.12	0.70748	0.00024	0.00049	0.00005	0.70746	0.00024
1232_W	-1233.12	0.70758	0.00024	0.00450	0.00047	0.70745	0.00024
1232_R	-1233.12	0.70758	0.00024	0.00120	0.00013	0.70754	0.00024
1235_R	-1235.09	0.70767	0.00022	0.00320	0.00015	0.70758	0.00022
1235_R	-1235.09	0.70738	0.00022	0.00134	0.00006	0.70734	0.00022
1235_R	-1235.09	0.70782	0.00022	0.00211	0.00010	0.70776	0.00022
1235_R	-1235.09	0.70767	0.00022	0.00220	0.00010	0.70760	0.00022
1235_R	-1235.09	0.70759	0.00022	0.00119	0.00006	0.70756	0.00022
1235_C	-1235.09	0.70758	0.00022	0.00319	0.00015	0.70749	0.00022
1235_C	-1235.09	0.70771	0.00022	0.00350	0.00016	0.70761	0.00022
1238_R	-1238.78	0.70756	0.00022	0.00418	0.00027	0.70744	0.00022
1238_R	-1238.78	0.70727	0.00022	0.00140	0.00009	0.70722	0.00022
1238_R	-1238.78	0.70694	0.00022	0.00129	0.00008	0.70690	0.00022
1238_W	-1238.78	0.70702	0.00022	0.00103	0.00007	0.70699	0.00022
1238_W	-1238.78	0.70764	0.00022	0.00202	0.00013	0.70758	0.00022
1238_C	-1238.78	0.70727	0.00022	0.00175	0.00011	0.70722	0.00022
1238_W	-1238.78	0.70746	0.00022	0.00155	0.00010	0.70742	0.00022
1245_R	-1245.39	0.70837	0.00022	0.00095	0.00005	0.70834	0.00022
1245_R	-1245.39	0.70832	0.00022	0.00076	0.00004	0.70830	0.00022
1245_W	-1245.39	0.70828	0.00022	0.00703	0.00039	0.70808	0.00022
1245_C	-1245.39	0.70838	0.00022	0.00351	0.00020	0.70827	0.00022
1247_R	-1247.23	0.70814	0.00022	0.00277	0.00013	0.70806	0.00022
1247_R	-1247.23	0.70841	0.00022	0.00673	0.00031	0.70821	0.00022
1247_R	-1247.23	0.70810	0.00022	0.00594	0.00028	0.70793	0.00022
1247_R	-1247.23	0.70803	0.00022	0.00157	0.00007	0.70799	0.00022
1247_W	-1247.23	0.70795	0.00022	0.00089	0.00004	0.70792	0.00022
1247_C	-1247.23	0.70803	0.00022	0.00308	0.00014	0.70794	0.00022
1247_W	-1247.23	0.70793	0.00022	0.00130	0.00006	0.70789	0.00022
1252_C	-1252.22	0.70832	0.00024	0.00346	0.00036	0.70822	0.00024
1252_C	-1252.22	0.70858	0.00024	0.00203	0.00021	0.70852	0.00024
1252_C	-1252.22	0.70790	0.00024	0.00114	0.00012	0.70786	0.00024
1252_C	-1252.22	0.70859	0.00024	0.00093	0.00010	0.70856	0.00024
1252_C	-1252.22	0.70789	0.00024	0.00106	0.00011	0.70786	0.00024
1252_C	-1252.22	0.70778	0.00024	0.00146	0.00015	0.70774	0.00024
1253_W	-1253.56	0.70918	0.00022	0.01012	0.00057	0.70888	0.00022
1253_W	-1253.56	0.70881	0.00022	0.00250	0.00014	0.70873	0.00022
1253_C	-1253.56	0.70856	0.00022	0.00192	0.00011	0.70851	0.00022
1253_W	-1253.56	0.70803	0.00022	0.00045	0.00003	0.70802	0.00022
1253_R	-1253.56	0.70817	0.00022	0.00105	0.00006	0.70814	0.00022
1253_C	-1253.56	0.70850	0.00022	0.00135	0.00008	0.70846	0.00022
1253_R	-1253.56	0.70837	0.00022	0.00099	0.00006	0.70834	0.00022
1256_R	-1256.18	0.70867	0.00026	0.00344	0.00021	0.70857	0.00026
1256_W	-1256.18	0.70818	0.00026	0.00400	0.00025	0.70806	0.00026

Table 5. Strontium isotope data from *in-situ* analyses of plagioclase (continued).

Sample	Depth (m)	$^{87}\text{Sr}/^{86}\text{Sr}$	1 σ	$^{87}\text{Rb}/^{86}\text{Sr}$	1 σ	$^{87}\text{Sr}/^{86}\text{Sr}_i$	1 σ
1256_W	-1256.18	0.70880	0.00026	0.00433	0.00027	0.70867	0.00026
1256_W	-1256.18	0.70839	0.00026	0.00404	0.00025	0.70827	0.00026
1256_W	-1256.18	0.70854	0.00026	0.00514	0.00032	0.70839	0.00026
1256_C	-1256.18	0.70888	0.00026	0.00517	0.00032	0.70873	0.00026
1256_W	-1256.18	0.70865	0.00026	0.00689	0.00042	0.70845	0.00026
1260_R	-1260.88	0.70938	0.00029	0.00500	0.00035	0.70924	0.00029
1260_R	-1260.88	0.70885	0.00029	0.00579	0.00040	0.70868	0.00029
1260_C	-1260.88	0.70924	0.00029	0.00139	0.00010	0.70920	0.00029
1260_C	-1260.88	0.70893	0.00029	0.00335	0.00023	0.70883	0.00029
1260_C	-1260.88	0.70900	0.00029	0.00668	0.00046	0.70881	0.00029
1260_C	-1260.88	0.70916	0.00029	0.00938	0.00065	0.70888	0.00029
1260_R	-1260.88	0.70896	0.00029	0.00869	0.00060	0.70871	0.00029
1265_C	-1265.68	0.70859	0.00026	0.00189	0.00012	0.70854	0.00026
1265_C	-1265.68	0.70863	0.00026	0.00771	0.00047	0.70841	0.00026
1265_C	-1265.68	0.70947	0.00026	0.01945	0.00120	0.70890	0.00026
1265_C	-1265.68	0.70890	0.00026	0.00478	0.00029	0.70876	0.00026
1265_C	-1265.68	0.70844	0.00026	0.00230	0.00014	0.70837	0.00026
1265_R	-1265.68	0.70903	0.00026	0.00354	0.00022	0.70893	0.00026
1265_R	-1265.68	0.70848	0.00026	0.00315	0.00019	0.70839	0.00026
1273_C	-1213.25	0.70774	0.00023	0.00568	0.00020	0.70758	0.00023
1273_C	-1272.95	0.70784	0.00023	0.00083	0.00003	0.70781	0.00023
1273_R	-1272.95	0.70772	0.00023	0.00099	0.00004	0.70769	0.00023
1273_C	-1272.95	0.70776	0.00023	0.00065	0.00002	0.70774	0.00023
1273_C	-1272.95	0.70779	0.00023	0.00086	0.00003	0.70777	0.00023
1273_R	-1272.95	0.70776	0.00023	0.00070	0.00003	0.70774	0.00023
1273_C	-1272.95	0.70789	0.00023	0.00138	0.00005	0.70785	0.00023
1277_C	-1276.94	0.70741	0.00022	0.00305	0.00020	0.70732	0.00022
1277_C	-1276.94	0.70754	0.00022	0.00124	0.00008	0.70750	0.00022
1277_C	-1276.94	0.70789	0.00022	0.01034	0.00066	0.70759	0.00023
1277_W	-1276.94	0.70758	0.00022	0.00538	0.00035	0.70742	0.00022
1277_R	-1276.94	0.70767	0.00022	0.00340	0.00022	0.70757	0.00022
1285_C	-1285.12	0.70799	0.00018	0.01300	0.00075	0.70762	0.00018
1285_C	-1285.12	0.70784	0.00018	0.01157	0.00067	0.70750	0.00018
1285_C	-1285.12	0.70800	0.00018	0.00868	0.00050	0.70775	0.00018
1285_C	-1285.12	0.70775	0.00018	0.01002	0.00058	0.70746	0.00018
1285_C	-1285.12	0.70769	0.00018	0.01381	0.00079	0.70729	0.00018
1285_C	-1285.12	0.70791	0.00018	0.01993	0.00115	0.70734	0.00018
1285_C	-1285.12	0.70782	0.00018	0.01273	0.00073	0.70745	0.00018
1286_C	-1286.03	0.70737	0.00022	0.00815	0.00052	0.70714	0.00022
1286_C	-1286.03	0.70748	0.00022	0.01994	0.00128	0.70690	0.00023
1286_R	-1286.03	0.70788	0.00022	0.01512	0.00097	0.70744	0.00023
1286_R	-1286.03	0.70795	0.00022	0.02027	0.00130	0.70736	0.00023
1291_C	-1291.87	0.70624	0.00026	0.00217	0.00013	0.70617	0.00026
1291_R	-1291.87	0.70630	0.00026	0.00058	0.00004	0.70629	0.00026
1291_R	-1291.87	0.70625	0.00026	0.00181	0.00011	0.70620	0.00026
1291_C	-1291.87	0.70633	0.00026	0.00061	0.00004	0.70631	0.00026
1291_R	-1291.87	0.70603	0.00026	0.00104	0.00006	0.70600	0.00026
1291_R	-1291.87	0.70619	0.00026	0.00184	0.00011	0.70614	0.00026
1291_R	-1291.87	0.70615	0.00026	0.00340	0.00021	0.70605	0.00026
1292_C	-1292.1	0.70656	0.00018	0.00659	0.00038	0.70637	0.00018
1292_C	-1292.1	0.70653	0.00018	0.00874	0.00050	0.70628	0.00018

Table 5. Strontium isotope data from *in-situ* analyses of plagioclase (continued).

Sample	Depth (m)	$^{87}\text{Sr}/^{86}\text{Sr}$	1 σ	$^{87}\text{Rb}/^{86}\text{Sr}$	1 σ	$^{87}\text{Sr}/^{86}\text{Sr}_i$	1 σ
1292_C	-1292.1	0.70641	0.00018	0.00843	0.00048	0.70617	0.00018
1292_R	-1292.1	0.70649	0.00018	0.00862	0.00050	0.70624	0.00018
1292_C	-1292.1	0.70661	0.00018	0.00830	0.00048	0.70637	0.00018
1292_R	-1292.1	0.70627	0.00018	0.00842	0.00048	0.70603	0.00018
1292_R	-1292.1	0.70634	0.00018	0.00752	0.00043	0.70612	0.00018
1294_C	-1294.07	0.70614	0.00017	0.00381	0.00030	0.70603	0.00017
1294_C	-1294.07	0.70657	0.00017	0.00396	0.00031	0.70645	0.00017
1294_C	-1294.07	0.70633	0.00017	0.00278	0.00022	0.70625	0.00017
1294_C	-1294.07	0.70647	0.00017	0.00305	0.00024	0.70638	0.00017
1294_R	-1294.07	0.70653	0.00017	0.00447	0.00035	0.70640	0.00017
1294_C	-1294.07	0.70586	0.00017	0.00389	0.00030	0.70575	0.00017
1294_C	-1294.07	0.70631	0.00017	0.00356	0.00028	0.70620	0.00017
1296_R	-1295.92	0.70639	0.00022	0.00193	0.00011	0.70633	0.00022
1296_C	-1295.92	0.70634	0.00022	0.00136	0.00008	0.70631	0.00022
1296_C	-1295.92	0.70632	0.00022	0.00326	0.00018	0.70623	0.00022
1296_W	-1295.92	0.70615	0.00022	0.00202	0.00011	0.70609	0.00022
1296_W	-1295.92	0.70640	0.00022	0.00090	0.00005	0.70637	0.00022
1296_W	-1295.92	0.70606	0.00022	0.00111	0.00006	0.70603	0.00022
1300_C	-1300.38	0.70669	0.00026	0.00995	0.00061	0.70640	0.00026
1300_R	-1300.38	0.70680	0.00026	0.00784	0.00048	0.70657	0.00026
1300_C	-1300.38	0.70667	0.00026	0.00939	0.00058	0.70640	0.00026
1300_C	-1300.38	0.70677	0.00026	0.00622	0.00038	0.70659	0.00026
1300_C	-1300.38	0.70709	0.00026	0.00792	0.00049	0.70686	0.00026
1300_C	-1300.38	0.70692	0.00026	0.00886	0.00055	0.70666	0.00026
1300_C	-1300.38	0.70642	0.00026	0.00883	0.00054	0.70617	0.00026
1311_C	-1311.83	0.70680	0.00024	0.00378	0.00033	0.70669	0.00024
1311_C	-1311.83	0.70675	0.00024	0.00418	0.00037	0.70663	0.00024
1311_C	-1311.83	0.70653	0.00024	0.00985	0.00087	0.70624	0.00024
1311_C	-1311.83	0.70687	0.00024	0.00811	0.00072	0.70663	0.00024
1311_W	-1311.83	0.70679	0.00024	0.00525	0.00046	0.70663	0.00024
1311_C	-1311.83	0.70652	0.00024	0.00770	0.00068	0.70629	0.00024
1311_C	-1311.83	0.70688	0.00024	0.00964	0.00085	0.70660	0.00024
1311_R	-1311.83	0.70611	0.00024	0.00670	0.00059	0.70592	0.00024
1311_R	-1311.83	0.70639	0.00024	0.00422	0.00037	0.70627	0.00024
1314_C	-1314.61	0.70609	0.00017	0.00242	0.00019	0.70602	0.00017
1314_R	-1314.61	0.70657	0.00017	0.00330	0.00026	0.70648	0.00017
1314_C	-1314.61	0.70662	0.00017	0.00346	0.00027	0.70652	0.00017
1314_R	-1314.61	0.70652	0.00017	0.00426	0.00033	0.70640	0.00017
1314_R	-1314.61	0.70673	0.00017	0.00525	0.00041	0.70658	0.00017
1314_C	-1314.61	0.70677	0.00017	0.00627	0.00049	0.70658	0.00018
1314_C	-1314.61	0.70661	0.00017	0.00577	0.00045	0.70644	0.00017
1319_R	-1320.02	0.70676	0.00022	0.00215	0.00012	0.70670	0.00022
1319_R	-1320.02	0.70647	0.00022	0.00338	0.00019	0.70637	0.00022
1319_R	-1320.02	0.70673	0.00022	0.00479	0.00027	0.70659	0.00022
1319_C	-1320.02	0.70653	0.00022	0.00500	0.00028	0.70638	0.00022
1319_C	-1320.02	0.70671	0.00022	0.00541	0.00030	0.70655	0.00022
1319_C	-1320.02	0.70634	0.00022	0.00474	0.00027	0.70620	0.00022
1322_C	-1322.65	0.70664	0.00022	0.00467	0.00022	0.70650	0.00022
1322_C	-1322.65	0.70662	0.00022	0.00428	0.00020	0.70650	0.00022
1322_R	-1322.65	0.70676	0.00022	0.00910	0.00042	0.70649	0.00022
1322_C	-1322.65	0.70640	0.00022	0.00429	0.00020	0.70628	0.00022

Table 5. Strontium isotope data from *in-situ* analyses of plagioclase (continued).

Sample	Depth (m)	$^{87}\text{Sr}/^{86}\text{Sr}$	1 σ	$^{87}\text{Rb}/^{86}\text{Sr}$	1 σ	$^{87}\text{Sr}/^{86}\text{Sr}_i$	1 σ
1322_C	-1322.65	0.70663	0.00022	0.00842	0.00039	0.70638	0.00022
1322_R	-1322.65	0.70637	0.00022	0.00461	0.00021	0.70624	0.00022
1322_C	-1322.65	0.70629	0.00022	0.00590	0.00027	0.70612	0.00022
1327_C	-1327.94	0.70683	0.00028	0.00321	0.00022	0.70674	0.00028
1327_W	-1327.94	0.70705	0.00028	0.00531	0.00037	0.70689	0.00028
1327_C	-1327.94	0.70682	0.00028	0.00439	0.00030	0.70669	0.00028
1327_C	-1327.94	0.70660	0.00028	0.00645	0.00045	0.70641	0.00028
1327_C	-1327.94	0.70680	0.00028	0.00206	0.00014	0.70674	0.00028
1327_R	-1327.94	0.70655	0.00028	0.00137	0.00010	0.70651	0.00028
1327_C	-1327.94	0.70678	0.00028	0.00312	0.00022	0.70669	0.00028
1331_R	-1331.59	0.70627	0.00022	0.00308	0.00014	0.70618	0.00022
1331_C	-1331.59	0.70653	0.00022	0.00346	0.00016	0.70643	0.00022
1331_C	-1331.59	0.70644	0.00022	0.00285	0.00013	0.70635	0.00022
1331_R	-1331.59	0.70624	0.00022	0.00582	0.00027	0.70607	0.00022
1331_C	-1331.59	0.70658	0.00022	0.00692	0.00032	0.70637	0.00022
1331_C	-1331.59	0.70645	0.00022	0.00909	0.00042	0.70618	0.00022
1331_C	-1331.59	0.70618	0.00022	0.00424	0.00020	0.70606	0.00022
1336_C	-1336.34	0.70684	0.00017	0.01165	0.00091	0.70650	0.00018
1336_R	-1336.34	0.70677	0.00017	0.00557	0.00043	0.70660	0.00017
1336_C	-1336.34	0.70661	0.00017	0.00298	0.00023	0.70653	0.00017
1336_R	-1336.34	0.70692	0.00017	0.00694	0.00054	0.70672	0.00018
1336_C	-1336.34	0.70650	0.00017	0.00429	0.00033	0.70638	0.00017
1336_C	-1336.34	0.70684	0.00017	0.01117	0.00087	0.70651	0.00018
1336_R	-1336.34	0.70703	0.00017	0.00831	0.00065	0.70678	0.00018
1339_R	-1339.2	0.70638	0.00024	0.00920	0.00097	0.70611	0.00024
1339_R	-1339.2	0.70718	0.00024	0.01418	0.00149	0.70677	0.00024
1339_C	-1339.2	0.70670	0.00024	0.00403	0.00042	0.70658	0.00024
1339_W	-1339.2	0.70641	0.00024	0.00409	0.00043	0.70629	0.00024
1339_C	-1339.2	0.70624	0.00024	0.00563	0.00059	0.70608	0.00024
1343_W	-1343.84	0.70611	0.00023	0.00655	0.00062	0.70592	0.00023
1343_R	-1343.84	0.70639	0.00023	0.00354	0.00034	0.70629	0.00023
1343_W	-1343.84	0.70626	0.00023	0.00665	0.00063	0.70607	0.00023
1343_W	-1343.84	0.70649	0.00023	0.00539	0.00051	0.70633	0.00023
1343_C	-1343.84	0.70614	0.00023	0.00281	0.00027	0.70606	0.00023
1343_C	-1343.84	0.70638	0.00023	0.00510	0.00048	0.70623	0.00023
1343_R	-1343.84	0.70626	0.00023	0.00503	0.00048	0.70611	0.00023

* C = core, R = rim, W = whole plagioclase (grain too small for core or rim analysis)

Table 6. Cr/Mgo values with depth in UMT094.

Sample	Depth	Cr (ppm)	MgO (%)	Cr/MgO
UMT094-1096	-1096.21	480	6.8	70.6
UMT094-1111	-1110.77	670	9.1	74.0
UMT094-1135	-1135.03	570	7.7	73.6
UMT094-1165	-1165.29	580	8.2	70.5
UMT094-1184	-1184.56	390	6.0	64.6
UMT094-1213	-1213.13	250	5.1	48.7
UMT094-1218	-1218.07	1200	12.4	97.2
UMT094-1226	-1226.37	380	3.8	100.3
UMT094-1228	-1228.04	2330	23.9	97.5
UMT094-1232	-1232.98	2850	25.0	114.0
UMT094-1233	-1233.26	2840	23.1	122.9
UMT094-1238	-1238.65	2830	23.3	121.5
UMT094-1245	-1245.27	2720	23.5	115.7
UMT094-1252	-1252.07	2910	25.3	115.0
UMT094-1254	-1254.10	3230	26.8	120.5
UMT094-1258	-1258.64	3770	26.9	140.1
UMT094-1265	-1265.58	3400	25.5	133.3
UMT094-1273	-1273.51	1860	14.6	127.4
UMT094-1277	-1276.84	2970	26.4	112.5
94-1278	-1278.56	3110	25.7	121.0
94-1279	-1279.71	4900	31.4	156.1
UMT094-1282	-1282.51	6280	23.7	265.0
UMT094-1285	-1285.03	5660	25.9	218.5
UMT094-1286	-1285.91	3730	22.7	164.3
UMT094-1288	-1288.81	7310	15.1	484.1
UMT094-1289	-1289.62	6020	13.9	433.1
UMT094-1291A	-1291.54	3690	14.2	260.8
UMT094-1291B	-1291.79	3230	28.7	112.5
UMT094-1292A	-1291.94	390	1.6	246.8
UMT094-1292B	-1292.74	920	5.0	182.5
UMT094-1294	-1293.98	480	2.7	177.8
UMT094-1296	-1295.78	1430	8.1	176.1
UMT094-1300	-1300.25	1960	9.4	207.6
UMT094-1311	-1311.72	6630	12.4	534.7
UMT094-1319	-1319.89	4070	19.9	205.0
UMT094-1325A	-1325.31	2880	22.3	129.1
UMT094-1325B	-1325.75	3120	15.3	203.9
UMT094-1326A	-1325.97	4460	22.3	200.0
UMT094-1326B	-1326.67	4030	24.3	165.8
UMT094-1327	-1327.83	4130	21.1	195.7
UMT094-1329	-1329.78	3500	24.8	141.1
UMT094-1332	-1332.55	2950	21.8	135.3
UMT094-1335	-1335.80	2190	17.4	126.2
UMT094-1336	-1336.21	3790	23.5	161.3
94-1336	-1336.10	4090	21.3	192.0
UMT094-1337	-1337.88	12453	23.1	539.1
UMT094-1339	-1339.09	8700	24.6	353.7
UMT094-1340	-1340.10	8010	23.1	346.8
UMT094-1343	-1343.72	9700	23.1	419.9
UMT094-1351	-1351.71	5810	25.6	227.0
94-1359	-1359.67	7260	26.4	275.0
UMT094-1365	-1365.74	19637	28.4	691.4
94-1366	-1366.64	45089	18.4	2457.2

Table 6. Cr/Mgo values with depth in UMT094 continued.

Sample	Depth	Cr (ppm)	MgO (%)	Cr/MgO
94-1376	-1376.52	1020	15.3	66.7
UMT094-1384	-1384.07	170	25.3	6.7
94-1386	-1386.83	100	24.0	4.2
UMT094-1402	-1402.00	26000	21.8	1192.7
94-1405	-1405.08	110	32.5	3.4
94-1410	-1410.50	170	11.7	14.5
94-1412	-1412.56	20	23.4	0.9
94-1421	-1420.77	30	27.8	1.1
94-1424	-1424.64	80	26.5	3.0

12. Appendices

Appendix A: Element distribution maps

In-situ laser ablation inductively coupled plasma mass spectrometry (LA-ICP-MS) element distribution maps were completed to: first, assess trace element zonation in plagioclase; second, compare element distribution in altered versus fresh plagioclase and pyroxene; and third, assess compositional differences between cumulate and intercumulate plagioclase among the samples analyzed. Four samples were chosen: (1) sample UMT094-1311, containing cumulate plagioclase with weak alteration (Fig. A1); (2) sample UMT094-1238, containing intercumulate plagioclase with no alteration (Fig. A2); (3) sample UMT094-1285, having intercumulate plagioclase with moderate alteration (Fig. A3); and (4) sample UMT094-1282, containing intercumulate plagioclase with pervasive alteration (Fig. A4).

A.1 Alteration

The elemental distribution maps show 3 prominent types of alteration: (1) alteration within plagioclase, (2) semi-massive fine-grained alteration within the sample, and (3) alteration within fractures dominantly in pyroxene. The alteration within plagioclase is characterized by high K and Rb. Semi-massive alteration is represented by high K, Rb, Sr and Eu. Alteration within fractures is high in Cs and rarely Pb. Other elements commonly associated with alteration are Al, Ga and some LREE (La, Ce, Pr and Nd).

A.2 Cumulate vs. intercumulate

Geochemical comparison between cumulate and intercumulate plagioclase is essential because they represent two types of formation and could have signatures representing these different processes. Cumulate plagioclase could have been formed in a previous holding chamber before being brought into the BIC magma chamber and deposited or could represent geochemical signatures of the magma chamber at the time of formation (Roelofse et al. 2015). Intercumulate plagioclase can be the last phase to form during the crystallization of a cumulate rock and can represent the crystallization of the last intercumulate liquid, which could result in plagioclase having a different chemical composition than cumulate plagioclase (Prevec et al. 2005; Chutas et al. 2012; Yang et al. 2013). Although chemical changes should be present between the cumulate and intercumulate plagioclase due to forming from different processes, their chemical signatures are relatively the same. Only one minor difference can be observed, which is the presence of zoned Ba in the cumulate plagioclase where intercumulate plagioclase has no zonation in Ba. Although there are only minor differences in major and trace element geochemistry between cumulate and intercumulate plagioclase, isotopic differences can occur between the two have been documented in the Bushveld (Chutas et al. 2012; Yang et al. 2013).

A.3 Plagioclase zonation

Zonation in plagioclase is not prominent in both the cumulate and intercumulate plagioclase. As mentioned above, the cumulate plagioclase shows zonation in Ba from high at the core to low at the rim. Both cumulate and intercumulate plagioclase show very minor zonation in La and Ce, also higher at the core and lower at the rims. All other elements show no zonation within plagioclase.

A.4 Pyroxene

Both opx and cpx were present during the analysis of plagioclase. Although the maps were focused on the plagioclase, one can see geochemical trends within the pyroxenes. Both opx and cpx have minor zonation in elements such as Zr, Ti, Y, REE and Cr. The most prominent zonation is Zr with typically the pyroxene having a Zr-depleted core and Zr-rich rim. This has been interpreted as interaction with fluids during post-cumulate processes as seen in gabbroic intrusions (Gao et al. 2007). Cr also show a moderate zonation from core (high) to rim (low) but is the only element that has a higher concentration at the core than at the rim. Both Y and Ti show lower concentrations at the core and higher at the rims, similar to Zr but with less of a contrast between core and rim but possibly related to similar processes as Zr. The REE show a zonation from high in the rim to low at the core within cpx but not opx. Within sample UMT094-1282, an altered sample occurring within the MCU, a Na-Al-rich amphibole (lower left corner) is present adjacent to opx (lower right corner) and plagioclase altering to white mica.

A.5 Interpretation

The goal of the elemental distribution maps was to identify if there was zonation within the cumulate or intercumulate plagioclase, which would affect the EMPA of plagioclase to measure anorthite content. Other than minor zonation for Ba in cumulate plagioclase and La and Ce in intercumulate plagioclase, no other zonation was present within plagioclase. Therefore, EPMA data from core to rim for anorthite content of plagioclase will not be affected. The lack of chemical difference between the cumulate and intercumulate plagioclase is likely due to both forming from similar melts with possibly different isotopic signatures (Chutas et al. 2012; Yang et al. 2013). The zonation within both cpx and opx of Ti, Zr and REE from high in the rim and lower at the core indicates that there might have been interaction with pyroxene crystals and post-cumulate fluids (Gao et al. 2007). The faint zonation of high-Cr at the core to low-Cr at the rims

indicate that this might be primary zonation in pyroxene or replacement of Cr with Ti, Zr and REE in the rim. Three types of alteration are seen through the samples: (1) alteration within plagioclase, (2) black semi-massive alteration, and (3) alteration with fraction of pyroxene.

Alteration within plagioclase is recognized dominantly by high K-Rb-Ba and likely represents the formation of white mica. This alteration usually occurs at the core of plagioclase or pockets throughout. Black semi-massive fine-grain alteration can be identified by high Na-Sr-Eu-Ca and is usually pervasive throughout the samples, almost completely replacing intercumulate plagioclase in between cumulate pyroxene. This alteration is commonly found in pegmatoidal feldspathic pyroxenites and can be associated with the presence amphiboles. The last alteration is strongly correlated with pyroxene and occurs only within or at grain edges of pyroxene. This alteration can be identified with very high Cs.

A.6 References

- Chutas NI, Bates E, Prevec SA, Coleman DS and Boudreau AE. (2012) *Sr and Pb Isotopic Disequilibrium between Coexisting Plagioclase and Orthopyroxene in the Bushveld Complex, South Africa: Microdrilling and Progressive Leaching Evidence for Sub-Liquidus Contamination within a Crystal Mush*. Contributions to Mineralogy and Petrology 163 (4): 653–68.
- Gao Y, Hoefs J, Hellebrand E, von der Handt A and Snow JE. (2007) *Trace Element Zoning in Pyroxenes from ODP Hole 735B Gabbros: Diffusive Exchange or Synkinematic Crystal Fractionation?* Contributions to Mineralogy and Petrology 153: 429–42.
- Prevec SA, Ashwal LD and Mkaza MS. (2005) *Mineral Disequilibrium in the Merensky Reef, Western Bushveld Complex, South Africa: New Sm-Nd Isotopic Evidence*. Contributions to Mineralogy and Petrology 149 (3): 306–15.
- Roelofse F, Ashwal LD and Romer RL. (2015) *Multiple, Isotopically Heterogeneous Plagioclase Populations in the Bushveld Complex Suggest Mush Intrusion*. Chemie Der Erde - Geochemistry 75 (3): 357–64.
- Yang S-H, Maier WD, Lahaye Y and O'Brien H. (2013) *Strontium Isotope Disequilibrium of Plagioclase in the Upper Critical Zone of the Bushveld Complex: Evidence for Mixing of Crystal Slurries*." Contributions to Mineralogy and Petrology 166 (4): 959–74.

A.7 Figures

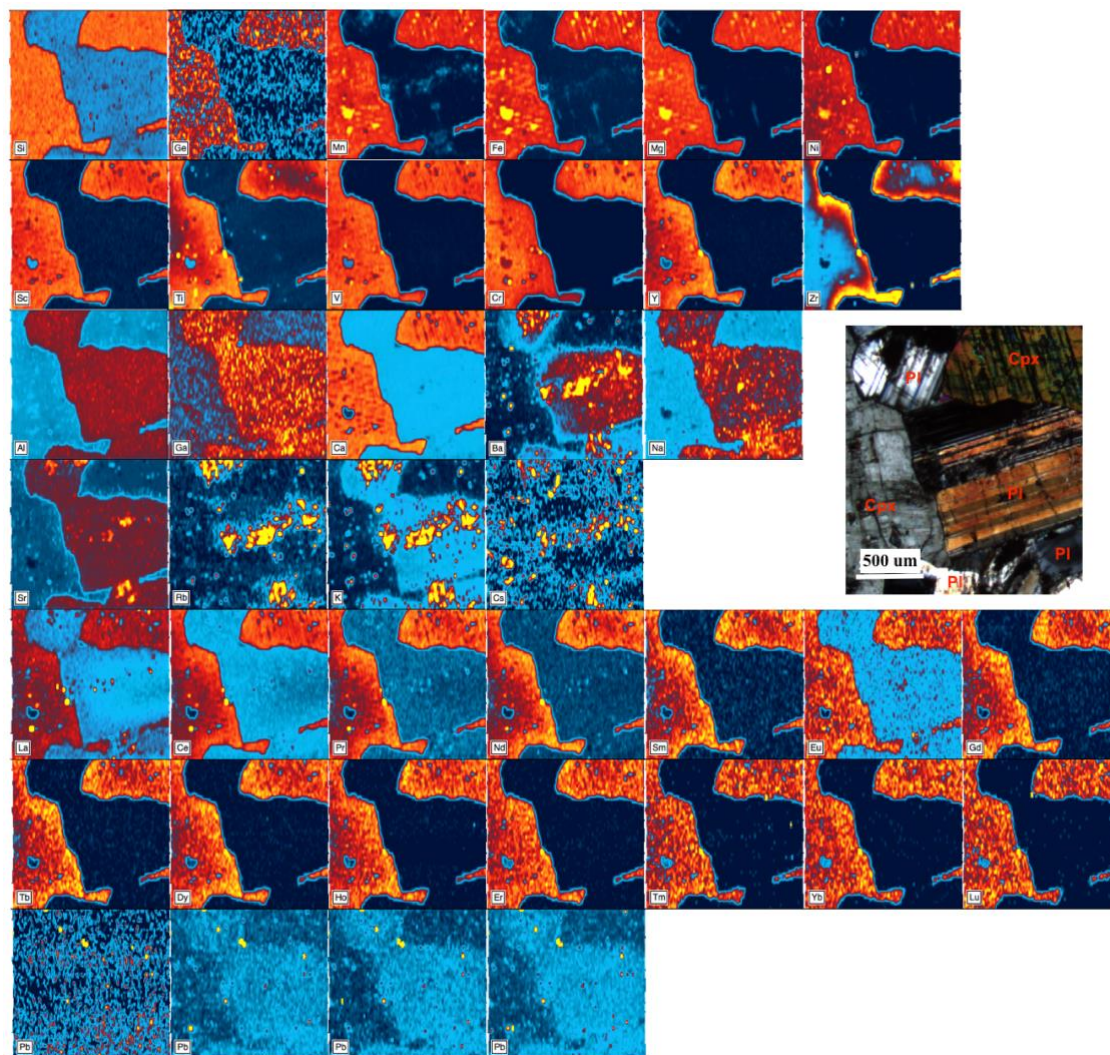


Figure A 1. LA-ICP-MS elemental distribution maps of sample UMT094-1311. Elements have been separated into rows based on mineral association. The first two rows are elements strongly associated with clinopyroxene (augite), the third row is elements associated with plagioclase and the fourth row are elements associated with alteration. Both fifth and sixth row are the REE and the last row is Pb isotopes; ^{204}Pb , ^{206}Pb , ^{207}Pb and ^{208}Pb respectively. Small inset in cross-polarized light was added of the thin section mapped.

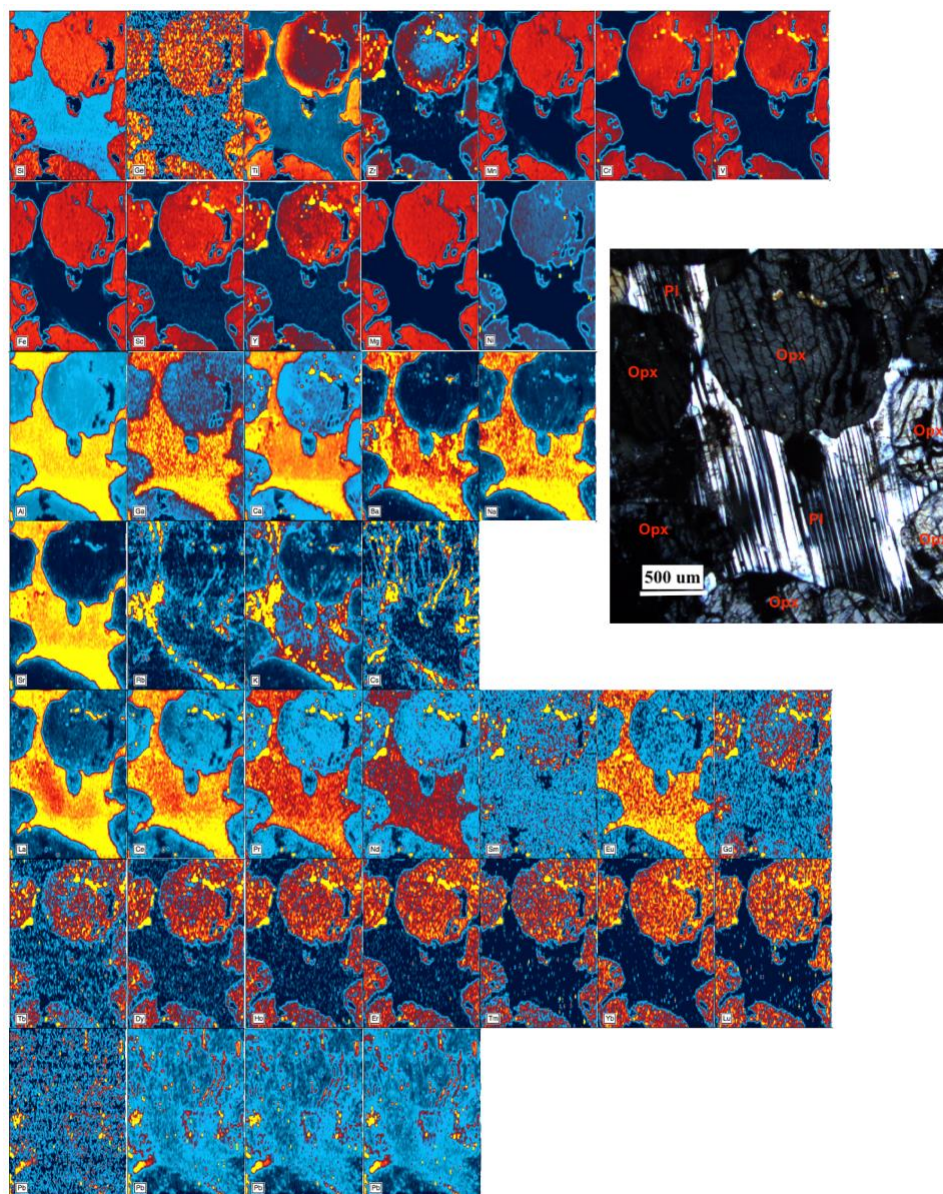


Figure A 2. LA-ICP-MS elemental distribution maps of sample 094-1238. Elements have been separated into rows based on mineral association. The first 2 rows are elements strongly associated with orthopyroxene, the third row is elements associated with plagioclase and the fourth row are elements associated with alteration. Both fifth and sixth row are the REE and the last row is Pb isotopes; ^{204}Pb , ^{206}Pb , ^{207}Pb and ^{208}Pb respectively. Small inset in crossed-polarized light was added of the thin section mapped.

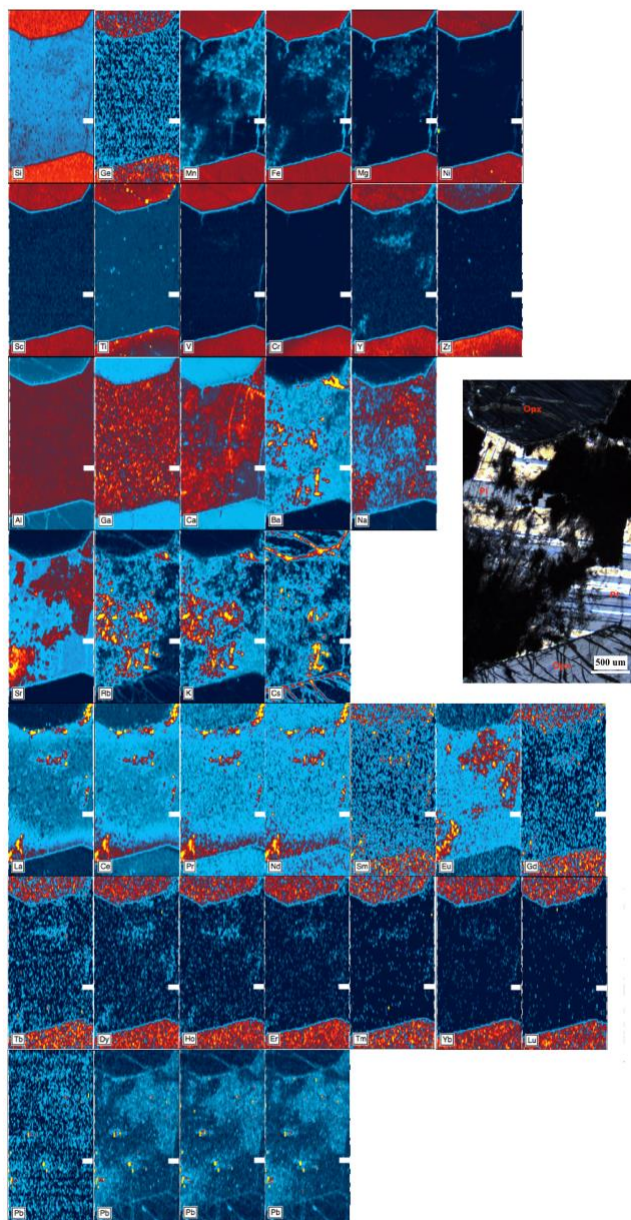


Figure A 3. LA-ICP-MS elemental distribution maps of sample 094-1285. Elements have been separated into rows based on mineral association. The first 2 rows are elements strongly associated with clinopyroxene, the third row is elements associated with plagioclase and the fourth row are elements associated with alteration. Both fifth and sixth row are the REE and the last row is Pb isotopes; ^{204}Pb , ^{206}Pb , ^{207}Pb and ^{208}Pb respectively. Small inset in crossed-polarized light was added of the thin section mapped.

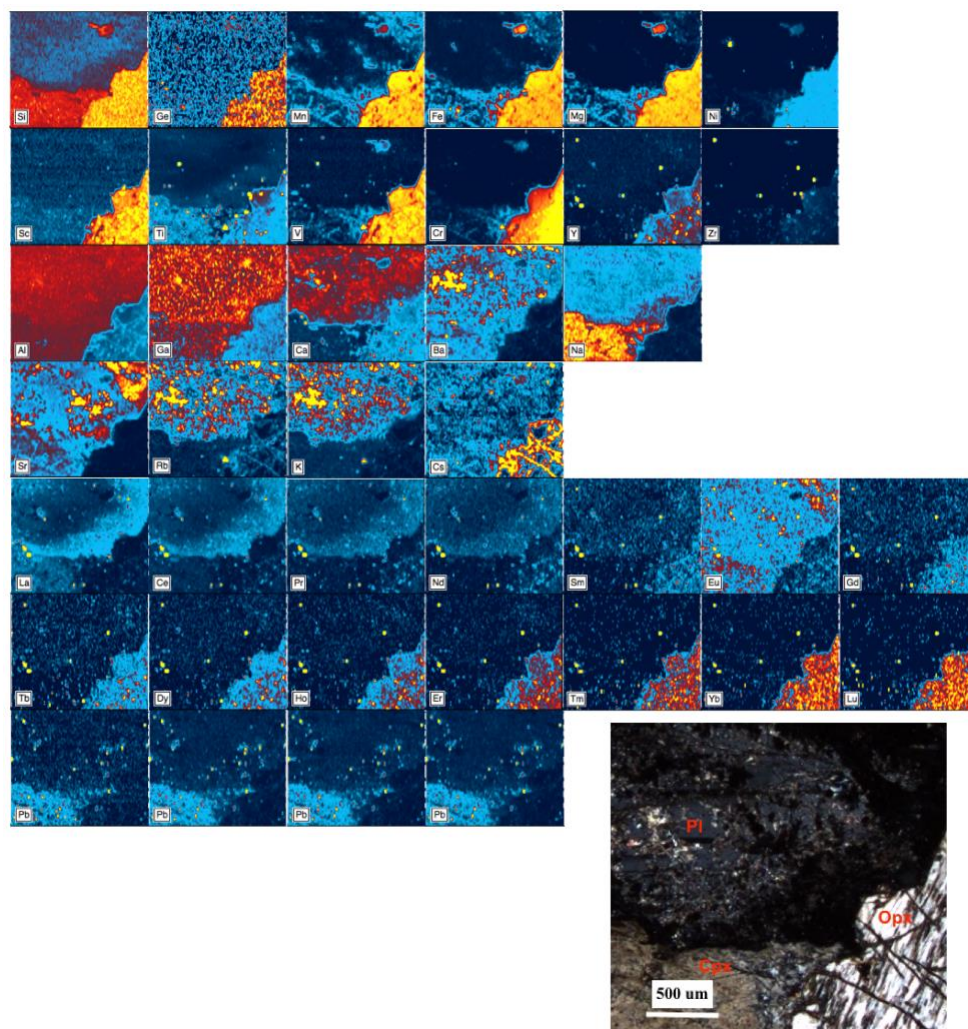


Figure A 4. Figure B4. LA-ICP-MS elemental distribution maps of sample 094-1282. Elements have been separated into rows based on mineral association. The first 2 rows are elements strongly associated with orthopyroxene, the third row is elements associated with plagioclase and clinopyroxene, and the fourth row are elements associated with alteration. Both fifth and sixth row are the REE and the last row is Pb isotopes; ^{204}Pb , ^{206}Pb , ^{207}Pb and ^{208}Pb respectively. Small inset in crossed-polarized light was added of the thin section mapped.

Appendix B: Whole-rock geochemistry

Sample	Sampler	Lithology	Stratigraphy	From Bottom of MCU (m)	From (m)	To (m)
UMT094-1096	CM	GN	MZ	195.73	1096.21	1096.45
UMT094-1111	CM	GN	MZ	181.17	1110.77	1111.01
UMT094-1135	CM	GN	MZ	156.91	1135.03	1135.28
UMT094-1165	CM	GN	MZ	126.65	1165.29	1165.54
UMT094-1184	CM	GN	MZ	107.38	1184.56	1184.8
UMT094-1213	CM	MAN	BCU	78.81	1213.13	1213.36
UMT094-1218	CM	NC	BCU	73.87	1218.07	1218.31
UMT094-1226	CM	NC	BCU	65.57	1226.37	1226.62
UMT094-1228	CM	FPX	BCU	63.9	1228.04	1228.3
UMT094-1232	CM	FPX	BCU	58.96	1232.98	1233.26
UMT094-1233	CM	FPX	MCU	58.68	1233.26	1233.59
UMT094-1238	CM	FPX	MCU	53.29	1238.65	1238.91
UMT094-1245	CM	FPX	MCU	46.67	1245.27	1245.5
UMT094-1252	CM	FPX	MCU	39.87	1252.07	1252.36
UMT094-1254	CM	FPX	MCU	37.84	1254.1	1254.95
UMT094-1258	CM	FPX	MCU	33.3	1258.64	1259.64
UMT094-1265	CM	FPX	MCU	26.36	1265.58	1266.58
UMT094-1273	CM	FPX	MCU	18.43	1273.51	1273.89
UMT094-1277	CM	PGFPX	MCU	15.1	1276.84	1277.04
UMT094-1282	CM	PGFPX	MCU	9.43	1282.51	1282.72
UMT094-1285	CM	PGFPX	MCU	6.91	1285.03	1285.21
UMT094-1286	CM	PGFPX	MCU	6.03	1285.91	1286.14
UMT094-1288	CM	PGFPX	MCU	3.13	1288.81	1289.09
UMT094-1289	CM	FPX	MCU	2.32	1289.62	1289.85
UMT094-1291A	CM	FPX	MCU	0.4	1291.54	1291.79
UMT094-1291B	CM	OLPX	MCU	0.15	1291.79	1291.94
UMT094-1292A	CM	NC	FCU	0	1291.94	1292.25
UMT094-1292B	CM	NC	FCU	-0.8	1292.74	1292.92
UMT094-1294	CM	AN	FCU	-2.04	1293.98	1294.16
UMT094-1296	CM	NC	FCU	-3.84	1295.78	1296.05
UMT094-1300	CM	NC	FCU	-8.31	1300.25	1300.5
UMT094-1311	CM	GN	FCU	-19.78	1311.72	1311.93
UMT094-1319	CM	FPX	FCU	-27.95	1319.89	1320.15
UMT094-1325A	CM	PX	FCU	-33.37	1325.31	1325.52
UMT094-1325B	CM	NC	FCU	-33.81	1325.75	1325.93
UMT094-1326A	CM	FPX	FCU	-34.03	1325.97	1326.28
UMT094-1326B	CM	PX	FCU	-34.73	1326.67	1326.91
UMT094-1327	CM	FPX	FCU	-35.89	1327.83	1328.05
UMT094-1329	CM	PX	FCU	-37.84	1329.78	1330
UMT094-1332	CM	FPX	FCU	-40.61	1332.55	1332.79
UMT094-1335	CM	FPX	PSDR	-43.86	1335.8	1335.98
UMT094-1336	CM	OLFPX	PSDR	-44.27	1336.21	1336.47
UMT094-1337	CM	FPX	PSDR	-45.94	1337.88	1338.1
UMT094-1339	CM	FPX	UG2HW	-47.15	1339.09	1339.31
UMT094-1340	CM	FPX	UG2HW	-48.16	1340.1	1340.26
UMT094-1343	CM	FPX	UG2HW	-51.78	1343.72	1343.95
UMT094-1351	CM	PAPX	UG2HW	-59.77	1351.71	1351.94
UMT094-1365	CM	PAPX	UG2FW	-73.8	1365.74	1365.93
UMT094-1384	CM	PAPX	UG2FW	-92.13	1384.07	1384.31
UMT094-1402	CM	PAPX	UG2FW	-110.06	1402	1402.24

CM = Cedric Mayer, GN = Gabbronorite, MAN = Mottled Anorthosite, NC = Noritic Cycles, FPX = Feldspathic Pyroxenite, PGFPX = Pegmatoidal Feldspathic Pyroxenite, OLPX = Olivine-Bearing Pyroxenite, AN = Anorthosite, PX = Pyroxenite, OLFPX = Olivine-Bearing Feldspathic Pyroxenite, PAPX = Para-Pyroxenite, MZ = Main Zone, BCU = Bastard Cyclic Unit, MCU = Merensky Cyclic Unit, FCU = Footwall Cyclic Unit, PSDR = Pseudoreef, UG2HW = UG2 Hanging Wall, UG2FW = UG2 Footwall

Table 1B. Major Elements (ME-ICP06, OA-GRA05, TOT-ICP06).

D.L. %	SiO2	Al2O3	Fe2O3	CaO	MgO	Na2O	K2O	Cr2O3	TiO2	MnO	P2O5	SrO	BaO	LOI	Total
	0.01	0.01	0.01	0.01	0.01	0.01	0.01	0.01	0.01	0.01	0.01	0.01	0.01	0.01	0.01
UMT094-1096	51.4	20.8	6.16	10.85	6.8	2.28	0.43	0.07	0.22	0.1	0.02	0.03	0.01	0.22	99.39
UMT094-1111	52	18.55	7.38	10.6	9.06	2.08	0.34	0.09	0.23	0.12	0.01	0.03	0.01	0.15	100.65
UMT094-1135	52.3	19.65	6.86	10.35	7.74	2.36	0.42	0.07	0.29	0.11	0.01	0.03	0.01	0.65	100.85
UMT094-1165	50	18.55	7.24	9.99	8.23	1.96	0.36	0.08	0.2	0.13	0.02	0.03	0.01	1.62	98.42
UMT094-1184	49.7	23.2	5.27	12.65	6.04	2.07	0.21	0.05	0.12	0.09	0.01	0.03	0.01	0.21	99.66
UMT094-1213	50.3	23.5	5.34	12.15	5.13	2.41	0.3	0.04	0.14	0.09	0.03	0.03	0.01	0.32	99.79
UMT094-1218	51	17.15	7.49	9.18	12.35	1.6	0.18	0.16	0.15	0.13	0.01	0.03	0.01	0.33	99.77
UMT094-1226	47.9	26.9	2.69	13.3	3.79	2.18	0.77	0.05	0.08	0.05	0.01	0.04	0.02	1.26	99.04
UMT094-1228	52.4	5.09	12.2	3.92	23.9	0.61	0.07	0.32	0.2	0.22	0.02	0.01	<0.01	-0.02	98.94
UMT094-1232	53.3	4.66	12.8	4.14	25	0.46	0.07	0.4	0.21	0.23	<0.01	<0.01	<0.01	0.53	101.8
UMT094-1233	52.8	6.79	11.95	5.11	23.1	0.7	0.15	0.41	0.15	0.2	<0.01	0.01	0.01	0.61	101.99
UMT094-1238	52.1	5.42	11.5	4.56	23.3	0.62	0.19	0.4	0.18	0.2	0.02	0.01	<0.01	0.4	98.9
UMT094-1245	52.5	6.56	10.9	4.42	23.5	0.6	0.24	0.38	0.13	0.21	0.01	0.01	0.01	0.36	99.83
UMT094-1252	53.3	4.3	12.2	3.71	25.3	0.5	0.16	0.4	0.19	0.22	0.01	0.01	<0.01	0.31	100.61
UMT094-1254	53.8	2.95	13.05	3.07	26.8	0.35	0.13	0.45	0.17	0.23	0.01	<0.01	<0.01	0.72	101.73
UMT094-1258	52.7	3.19	12.35	2.96	26.9	0.27	0.09	0.52	0.15	0.22	<0.01	<0.01	<0.01	0.77	100.12
UMT094-1265	52.6	3.84	11.75	3.93	25.5	0.36	0.19	0.46	0.18	0.21	0.01	<0.01	0.01	1.03	100.07
UMT094-1273	52.2	13.25	8.18	8.27	14.6	1.79	0.59	0.25	0.15	0.15	0.1	0.02	0.02	1.23	100.8
UMT094-1277	53	2.92	13.85	3.16	26.4	0.29	0.09	0.41	0.17	0.23	0.01	<0.01	<0.01	0.53	101.06
UMT094-1282	50.3	5.1	12.35	3.83	23.7	0.56	0.07	0.86	0.17	0.21	0.01	0.01	<0.01	1.54	98.71
UMT094-1285	51.8	3.24	14.8	2.89	25.9	0.36	0.12	0.79	0.23	0.22	0.03	<0.01	<0.01	0.44	100.82
UMT094-1286	47.7	3.34	12.1	10.45	22.7	0.33	0.1	0.52	0.27	0.19	0.01	<0.01	<0.01	1.02	98.73
UMT094-1288	47	5.35	8.67	20.1	15.1	0.42	0.04	1.03	0.36	0.17	0.03	0.01	<0.01	1.25	99.53
UMT094-1289	47.6	8.09	8.05	19.95	13.9	0.62	0.19	0.86	0.36	0.15	0.02	0.02	0.01	1.61	101.43
UMT094-1291A	47.9	6.55	7.29	19.55	14.15	0.72	0.08	0.51	0.26	0.13	<0.01	0.01	<0.01	1.28	98.43
UMT094-1291B	38	4.85	15.1	6.24	28.7	0.26	0.04	0.45	0.09	0.15	0.01	0.01	<0.01	5.66	99.56
UMT094-1292A	44.5	28.1	4.04	15.25	1.58	2.17	0.62	0.05	0.04	0.03	0.01	0.06	0.02	2.12	98.59
UMT094-1292B	49.3	26.8	2.91	13.35	5.04	2.21	0.5	0.13	0.05	0.05	0.02	0.05	0.01	0.97	101.39
UMT094-1294	48.7	29.1	1.97	14.45	2.7	2.39	0.44	0.07	0.04	0.03	<0.01	0.05	0.01	0.98	100.93
UMT094-1296	48.2	22	5	11.6	8.12	1.89	0.25	0.19	0.07	0.08	<0.01	0.04	0.01	0.85	98.3
UMT094-1300	50	21.4	5.05	11.55	9.44	1.84	0.19	0.27	0.09	0.09	<0.01	0.04	0.01	0.65	100.62
UMT094-1311	48.7	15.75	8.62	9.04	12.4	1.64	0.28	0.9	0.17	0.13	0.01	0.03	0.01	0.82	98.5
UMT094-1319	51	8.3	11.25	5.86	19.85	0.78	0.15	0.56	0.16	0.2	0.01	0.01	0.01	0.6	98.74
UMT094-1325A	51.1	5.46	13	4.86	22.3	0.55	0.1	0.4	0.17	0.22	0.02	0.01	0.01	0.67	98.87
UMT094-1325B	51	13.8	8.66	8.37	15.3	1.29	0.16	0.43	0.15	0.16	0.01	0.02	0.01	0.21	99.57
UMT094-1326A	52.2	5.87	12.65	5.2	22.3	0.54	0.1	0.63	0.2	0.22	0.02	0.01	<0.01	1	100.94
UMT094-1326B	51.9	4.43	12.45	3.84	24.3	0.32	0.03	0.56	0.12	0.22	0.01	<0.01	<0.01	0.36	98.54
UMT094-1327	51	7.26	11.45	5.22	21.1	0.72	0.13	0.62	0.18	0.21	0.01	0.01	0.01	0.42	98.34
UMT094-1329	52.2	4.36	12.45	4.22	24.8	0.41	0.05	0.47	0.14	0.22	<0.01	0.01	<0.01	0.22	99.55

Table 1B. Major Elements (ME-ICP06, OA-GRA05, TOT-ICP06) continued.

D.L. %	SiO2	Al2O3	Fe2O3	CaO	MgO	Na2O	K2O	Cr2O3	TiO2	MnO	P2O5	SrO	BaO	LOI	Total
	0.01	0.01	0.01	0.01	0.01	0.01	0.01	0.01	0.01	0.01	0.01	0.01	0.01	0.01	0.01
UMT094-1332	51.3	6.39	11.95	5.13	21.8	0.67	0.11	0.4	0.15	0.21	0.01	0.01	0.01	0.43	98.57
UMT094-1335	44.6	6.97	9.9	18.15	17.35	0.34	0.09	0.31	0.33	0.14	0.01	0.01	0.01	1.79	100
UMT094-1336	46.5	8.1	12.9	5.72	23.5	0.71	0.17	0.54	0.11	0.19	<0.01	0.01	<0.01	0.95	99.4
UMT094-1337	48.9	5.02	15.15	3.83	23.1	0.46	0.06	1.82	0.21	0.22	0.01	0.01	<0.01	0.14	98.93
UMT094-1339	50.7	3.72	13.55	3.82	24.6	0.34	0.07	1.19	0.2	0.23	0.01	0.01	<0.01	0.39	98.83
UMT094-1340	51.3	5.49	12.65	5.24	23.1	0.54	0.1	1.14	0.18	0.22	<0.01	0.01	<0.01	0.61	100.58
UMT094-1343	50.4	6.05	12.4	4.7	23.1	0.53	0.08	1.35	0.18	0.22	0.01	0.01	<0.01	0.26	99.29
UMT094-1351	46.9	5.81	13.45	5.3	25.6	0.57	0.08	0.81	0.13	0.22	0.01	0.01	<0.01	1.11	100
UMT094-1365	34.2	5.68	15.1	7.62	28.4	0.16	0.01	2.87	0.19	0.19	0.01	<0.01	<0.01	5.39	99.82
UMT094-1384	36.2	10.25	10.6	7.87	25.3	0.5	0.13	0.02	0.22	0.15	0.02	0.01	0.01	6.79	98.07
UMT094-1402	32.4	9.5	15.55	10.15	21.8	0.25	0.17	3.8	0.36	0.17	0.01	<0.01	<0.01	3.85	98.01

Table 2B-1. Trace Elements (ME-MS81).

D.L. ppm	Ba	Ce	Cr	Cs	Dy	Er	Eu	Ga	Gd	Hf	Ho	La	Lu	Nb	Nd
	0.5	0.5	10	0.01	0.05	0.03	0.03	0.1	0.05	0.2	0.01	0.5	0.01	0.2	0.1
UMT094-1096	134.5	13.6	480	0.39	1.14	0.74	0.64	16.3	1.09	1	0.25	7.2	0.1	1.6	5.7
UMT094-1111	123	14	670	0.38	1.38	0.87	0.71	15.1	1.43	0.6	0.3	7.3	0.12	1.1	6.2
UMT094-1135	113.5	13.5	570	0.8	1.2	0.84	0.58	16.4	1.16	1	0.27	7	0.13	2.2	5.8
UMT094-1165	120.5	10	580	0.92	0.97	0.64	0.53	14.3	0.93	0.6	0.2	5.3	0.1	1	4.4
UMT094-1184	81	5.7	390	0.12	0.64	0.4	0.51	16.7	0.52	0.3	0.14	3	0.07	0.3	2.5
UMT094-1213	93	8.1	250	0.36	0.65	0.46	0.53	16.7	0.77	0.4	0.16	4.3	0.07	0.7	3.6
UMT094-1218	69.9	6.7	1200	0.47	0.64	0.49	0.39	13.5	0.46	0.3	0.16	3.6	0.1	0.4	2.7
UMT094-1226	196	6.3	380	1.26	0.4	0.23	0.43	18.4	0.43	0.2	0.09	3.6	0.03	0.3	2.5
UMT094-1228	28	4.7	2330	0.45	0.96	0.7	0.19	6.2	0.66	0.4	0.2	2.3	0.13	0.6	2.4
UMT094-1232	26.5	3.2	2850	0.97	0.83	0.58	0.16	5.5	0.67	0.3	0.2	1.5	0.09	0.2	2
UMT094-1233	57.8	4	2840	0.58	0.62	0.48	0.18	6.6	0.59	0.3	0.14	2	0.08	<0.2	1.9
UMT094-1238	45	6	2830	0.74	0.88	0.56	0.23	6.3	0.73	0.3	0.18	2.9	0.1	1.2	3
UMT094-1245	69.5	2.9	2720	0.95	0.53	0.35	0.19	6.2	0.4	0.2	0.12	1.5	0.07	<0.2	1.3
UMT094-1252	39.1	5	2910	0.55	0.86	0.59	0.16	5.7	0.72	0.4	0.19	2.4	0.1	0.6	2.6
UMT094-1254	29.2	4.1	3230	0.98	0.76	0.54	0.15	4.6	0.63	0.3	0.18	1.9	0.1	0.5	2.1
UMT094-1258	30.9	3.5	3770	0.76	0.65	0.53	0.13	5	0.48	0.3	0.15	1.7	0.09	0.2	1.8
UMT094-1265	47.5	5.6	3400	1.14	0.89	0.56	0.21	5.4	0.75	0.4	0.19	2.6	0.1	0.6	3
UMT094-1273	210	14.1	1860	1.27	0.89	0.61	0.35	11	0.93	0.7	0.19	7.5	0.09	1.3	5.6
UMT094-1277	29.5	2.9	2970	1.04	0.81	0.53	0.12	4.8	0.54	0.3	0.19	1.3	0.11	0.2	1.6
UMT094-1282	19.8	3.6	6280	2.15	0.48	0.43	0.13	6.4	0.41	0.3	0.14	1.9	0.09	0.3	1.8
UMT094-1285	35.9	5.6	5660	1.08	0.75	0.53	0.15	5.8	0.6	0.5	0.17	2.9	0.1	0.9	2.4
UMT094-1286	39.3	9.7	3730	0.69	1.87	1.07	0.47	5.3	1.92	0.8	0.39	3.3	0.15	0.2	7.1
UMT094-1288	15.7	16.2	7310	0.37	2.42	1.34	0.65	7.8	2.42	1.5	0.5	6.5	0.17	0.4	9.7
UMT094-1289	69.4	17.9	6020	0.7	2.34	1.37	0.66	8.6	2.52	1.6	0.51	7.3	0.16	0.7	10.7
UMT094-1291A	33.8	8.5	3690	0.52	1.6	0.96	0.42	7.1	1.49	0.7	0.37	3.3	0.13	0.3	5.6
UMT094-1291B	12.2	2.1	3230	0.75	0.48	0.3	0.12	4.4	0.49	0.3	0.11	0.9	0.05	<0.2	1.4
UMT094-1292A	148	2.7	390	0.92	0.19	0.11	0.28	16.9	0.17	<0.2	0.03	1.5	0.01	<0.2	1.2
UMT094-1292B	123	2.9	920	1.04	0.18	0.14	0.25	16.4	0.2	<0.2	0.05	1.6	0.02	0.2	1.2
UMT094-1294	97.5	2.7	480	0.88	0.2	0.13	0.27	17.8	0.15	<0.2	0.04	1.6	0.01	0.2	1.1
UMT094-1296	74.5	3.5	1430	0.76	0.27	0.2	0.28	15.1	0.26	0.2	0.07	1.9	0.03	0.2	1.4
UMT094-1300	62.9	3.4	1960	0.52	0.33	0.26	0.26	14.3	0.26	0.2	0.08	1.9	0.03	0.2	1.5
UMT094-1311	89.2	6.8	6630	0.61	0.57	0.33	0.36	13.3	0.55	0.3	0.13	3.7	0.06	0.6	2.9
UMT094-1319	49.4	4.5	4070	0.62	0.58	0.46	0.26	8.2	0.54	0.3	0.13	2.4	0.08	0.4	2.3
UMT094-1325A	50	4.1	2880	0.65	0.71	0.48	0.17	6.1	0.57	0.3	0.15	1.9	0.1	0.6	2
UMT094-1325B	60.1	4.1	3120	0.24	0.49	0.4	0.3	10.8	0.5	0.3	0.12	2.2	0.08	0.2	2.1
UMT094-1326A	34	4.9	4460	1.07	0.76	0.58	0.19	6.9	0.61	0.4	0.18	2.3	0.09	0.7	2.4
UMT094-1326B	13.9	3.5	4030	0.15	0.37	0.28	0.12	5	0.31	<0.2	0.08	1.5	0.07	1.7	1.8
UMT094-1327	53.4	4.7	4130	0.24	0.65	0.45	0.23	7.5	0.52	0.3	0.16	2.5	0.09	0.4	2.4
UMT094-1329	21	2	3500	0.12	0.56	0.41	0.12	5.2	0.34	0.2	0.11	1	0.06	0.2	1.2

Table 2B-1. Trace Elements (ME-MS81) continued.

D.L. ppm	Ba	Ce	Cr	Cs	Dy	Er	Eu	Ga	Gd	Hf	Ho	La	Lu	Nb	Nd
	0.5	0.5	10	0.01	0.05	0.03	0.03	0.1	0.05	0.2	0.01	0.5	0.01	0.2	0.1
UMT094-1332	50.8	4.1	2950	0.2	0.64	0.41	0.17	6.8	0.43	0.3	0.14	2.1	0.08	0.5	2
UMT094-1335	49.1	12.3	2190	0.52	1.91	1.11	0.59	8.1	2.05	1.7	0.41	4.4	0.16	0.4	8.2
UMT094-1336	34	2.2	3790	0.85	0.38	0.29	0.15	7.2	0.27	0.2	0.08	1.2	0.05	<0.2	1.1
UMT094-1337	30.9	4.5	>10000	0.27	0.57	0.43	0.17	8.1	0.46	0.2	0.13	2.2	0.09	0.4	2.2
UMT094-1339	26.1	2.9	8700	0.36	0.6	0.53	0.13	6.9	0.49	0.3	0.15	1.3	0.11	0.3	1.7
UMT094-1340	30.7	3	8010	0.45	0.65	0.47	0.15	7.1	0.5	0.3	0.14	1.3	0.09	0.2	1.8
UMT094-1343	30	2.5	9700	0.24	0.54	0.34	0.13	7.9	0.39	0.2	0.12	1.2	0.08	0.2	1.3
UMT094-1351	32.4	3	5810	0.08	0.55	0.35	0.17	6.3	0.45	0.2	0.11	1.4	0.06	0.2	1.6
UMT094-1365	9.3	6.9	>10000	0.14	0.76	0.42	0.22	8.4	0.82	0.6	0.17	3	0.06	0.5	3.6
UMT094-1384	65.9	7.3	170	0.77	1.12	0.67	0.28	12.8	1.08	1	0.24	3.3	0.12	0.4	4.4
UMT094-1402	32.4	9.3	>10000	1.05	1.57	0.9	0.37	23.9	1.58	1.2	0.31	3.4	0.12	0.4	6.4

Table 2B-2. Trace Elements (ME-MS81).

D.L. ppm	Pr	Rb	Sm	Sn	Sr	Ta	Tb	Th	Tm	U	V	W	Y	Yb	Zr
	0.03	0.2	0.03	1	0.1	0.1	0.01	0.05	0.01	0.05	5	1	0.5	0.03	2
UMT094-1096	1.55	10.9	1.12	<1	279	0.1	0.18	1.71	0.11	0.35	99	<1	6.4	0.8	31
UMT094-1111	1.63	7.8	1.41	<1	247	0.1	0.22	1.34	0.13	0.12	124	<1	7.7	0.83	19
UMT094-1135	1.51	18.1	1.23	<1	279	0.1	0.19	1.46	0.12	0.37	124	<1	7.2	0.87	38
UMT094-1165	1.11	12.2	0.85	<1	243	<0.1	0.16	0.86	0.11	0.19	111	1	5.6	0.62	21
UMT094-1184	0.67	2.4	0.54	<1	302	<0.1	0.11	0.3	0.06	<0.05	91	<1	3.5	0.42	9
UMT094-1213	0.92	6.9	0.78	<1	307	<0.1	0.12	0.58	0.07	0.15	80	<1	4.3	0.4	15
UMT094-1218	0.72	4.4	0.63	<1	246	<0.1	0.1	0.35	0.09	0.1	87	<1	4	0.55	10
UMT094-1226	0.72	34.7	0.48	<1	337	<0.1	0.08	0.18	0.03	<0.05	38	<1	2.2	0.19	6
UMT094-1228	0.58	2.1	0.62	<1	56.4	<0.1	0.12	0.5	0.09	0.19	139	<1	5.6	0.75	11
UMT094-1232	0.41	2	0.55	<1	53.8	<0.1	0.12	0.1	0.09	<0.05	129	<1	5.2	0.63	6
UMT094-1233	0.49	5.2	0.43	<1	111	<0.1	0.1	0.15	0.08	<0.05	113	<1	4.1	0.45	7
UMT094-1238	0.72	7.5	0.57	<1	61.9	0.1	0.14	0.41	0.09	<0.05	123	<1	5.1	0.62	10
UMT094-1245	0.33	10.9	0.38	<1	78.4	<0.1	0.08	0.13	0.08	<0.05	104	<1	3.2	0.49	5
UMT094-1252	0.56	6.1	0.6	<1	44.4	<0.1	0.14	0.7	0.09	<0.05	121	<1	5.1	0.64	11
UMT094-1254	0.52	6	0.49	1	22.4	<0.1	0.11	0.43	0.08	0.07	126	<1	4.8	0.61	8
UMT094-1258	0.44	4.4	0.42	<1	30.5	<0.1	0.09	0.24	0.08	<0.05	121	<1	3.9	0.47	8
UMT094-1265	0.69	9.1	0.7	<1	33.8	<0.1	0.13	0.66	0.08	0.33	118	<1	5.1	0.65	16
UMT094-1273	1.54	25.6	1.06	<1	194	<0.1	0.15	1.38	0.08	0.32	82	<1	5.3	0.45	26
UMT094-1277	0.39	3.6	0.45	<1	25.9	<0.1	0.1	0.23	0.1	<0.05	123	1	5.1	0.7	8
UMT094-1282	0.46	4.2	0.37	<1	64.3	<0.1	0.08	0.29	0.07	0.09	140	<1	3.6	0.48	12
UMT094-1285	0.63	6.8	0.65	<1	30.6	<0.1	0.11	0.8	0.1	0.22	141	1	4.7	0.58	16
UMT094-1286	1.48	3.3	1.81	1	42.4	<0.1	0.29	0.24	0.15	<0.05	146	3	10.1	0.95	21
UMT094-1288	2.36	1.5	2.36	1	109.5	0.1	0.43	0.72	0.2	0.37	215	<1	12.8	1.18	48
UMT094-1289	2.48	7.9	2.35	1	178	0.1	0.41	0.62	0.2	0.12	178	<1	12.9	1.13	43
UMT094-1291A	1.18	2.5	1.35	<1	108.5	<0.1	0.26	0.19	0.12	<0.05	163	<1	8.6	0.76	17
UMT094-1291B	0.35	1.6	0.35	<1	67.4	<0.1	0.08	0.17	0.05	<0.05	63	<1	2.7	0.27	7
UMT094-1292A	0.31	31.7	0.2	1	513	<0.1	0.03	0.11	0.02	<0.05	19	<1	0.9	0.09	3
UMT094-1292B	0.31	23.5	0.25	<1	423	<0.1	0.03	0.12	0.02	<0.05	29	<1	1	0.1	4
UMT094-1294	0.29	19	0.17	<1	440	<0.1	0.03	0.14	0.01	<0.05	22	<1	0.9	0.11	3
UMT094-1296	0.4	10.2	0.27	<1	374	<0.1	0.04	0.19	0.03	<0.05	47	<1	1.6	0.22	5
UMT094-1300	0.43	6.4	0.26	<1	328	<0.1	0.06	0.18	0.04	<0.05	58	<1	2	0.22	6
UMT094-1311	0.79	13.2	0.57	<1	280	<0.1	0.1	0.41	0.04	0.08	142	<1	3.1	0.35	11
UMT094-1319	0.54	6.1	0.47	<1	114	<0.1	0.1	0.23	0.08	0.07	131	<1	3.8	0.43	10
UMT094-1325A	0.5	5.3	0.52	<1	74.8	<0.1	0.1	0.52	0.09	0.07	124	<1	4.2	0.56	11
UMT094-1325B	0.48	2.7	0.36	<1	206	<0.1	0.08	0.16	0.06	0.05	105	<1	3.3	0.38	8
UMT094-1326A	0.6	5.2	0.56	<1	63.3	<0.1	0.13	0.55	0.09	0.12	153	<1	4.8	0.61	15
UMT094-1326B	0.42	0.5	0.32	<1	49.7	<0.1	0.06	0.17	0.04	<0.05	112	<1	2.2	0.33	3
UMT094-1327	0.55	3.1	0.53	<1	103.5	<0.1	0.09	0.34	0.08	0.1	126	<1	3.9	0.48	11
UMT094-1329	0.29	1.2	0.29	<1	50.6	<0.1	0.06	0.11	0.05	<0.05	107	<1	2.9	0.44	6

Table 2B-2. Trace Elements (ME-MS81) continued.

D.L. ppm	Pr	Rb	Sm	Sn	Sr	Ta	Tb	Th	Tm	U	V	W	Y	Yb	Zr
	0.03	0.2	0.03	1	0.1	0.1	0.01	0.05	0.01	0.05	5	1	0.5	0.03	2
UMT094-1332	0.5	2.8	0.54	<1	93.6	<0.1	0.1	0.24	0.07	0.06	105	<1	3.7	0.46	8
UMT094-1335	1.84	3.9	2.07	1	74.5	<0.1	0.33	0.38	0.17	0.05	96	<1	10.8	0.93	43
UMT094-1336	0.26	4.9	0.24	<1	122.5	<0.1	0.05	0.11	0.04	<0.05	90	<1	2.3	0.25	5
UMT094-1337	0.5	1.8	0.48	<1	59.3	<0.1	0.09	0.61	0.08	0.06	198	<1	3.6	0.54	6
UMT094-1339	0.38	2.7	0.5	<1	40.2	<0.1	0.1	0.27	0.08	0.07	164	<1	4.1	0.56	9
UMT094-1340	0.37	3.3	0.43	<1	71.6	<0.1	0.08	0.14	0.07	<0.05	150	<1	3.9	0.48	7
UMT094-1343	0.33	2	0.36	<1	78.7	<0.1	0.08	0.14	0.05	<0.05	160	<1	3.2	0.47	5
UMT094-1351	0.37	1.7	0.41	<1	91.9	<0.1	0.09	0.24	0.05	<0.05	110	<1	3.1	0.38	7
UMT094-1365	0.89	0.8	0.82	1	34.4	<0.1	0.13	0.51	0.08	0.07	121	<1	3.9	0.42	23
UMT094-1384	0.98	4.9	0.93	<1	121.5	<0.1	0.17	0.34	0.11	0.05	89	<1	6.3	0.62	25
UMT094-1402	1.37	12.7	1.43	1	36.7	<0.1	0.26	0.31	0.13	<0.05	220	<1	8.5	0.9	29

Table 3B-1. Trace Elements (ME-MS61L)

D.L. %	Al 0.01	Ca 0.01	Fe 0.002	K 0.01	Mg 0.01	Na 0.001	P 0.001	S 0.01	Ti 0.001
UMT094-1096	8.35	7.29	3.79	0.28	3.24	1.59	0.008	<0.01	0.126
UMT094-1111	9.08	6.81	4.55	0.27	4.94	1.43	0.007	<0.01	0.146
UMT094-1135	8.37	6.96	4.25	0.31	3.79	1.69	0.004	<0.01	0.173
UMT094-1165	8.9	6.94	4.77	0.27	4.71	1.445	0.007	<0.01	0.122
UMT094-1184	9.77	8.29	3.22	0.11	2.99	1.405	0.004	<0.01	0.074
UMT094-1213	8.92	8.26	3.37	0.12	2.34	1.675	0.009	<0.01	0.089
UMT094-1218	7.49	6	4.38	0.14	6.23	1.12	0.005	0.02	0.081
UMT094-1226	10.2	8.83	1.69	0.43	1.79	1.51	0.004	<0.01	0.051
UMT094-1228	2.88	2.82	8.21	0.07	14.55	0.447	0.005	<0.01	0.138
UMT094-1232	2.5	2.88	8.55	0.05	15.05	0.326	0.002	0.41	0.13
UMT094-1233	3.46	3.33	7.61	0.12	13.25	0.475	0.002	0.62	0.096
UMT094-1238	2.92	3.15	7.58	0.17	13.85	0.442	0.005	0.33	0.12
UMT094-1245	3.3	2.98	7.14	0.2	13.75	0.43	0.002	0.05	0.08
UMT094-1252	2.28	2.48	7.85	0.14	14.6	0.352	0.003	0.22	0.122
UMT094-1254	1.58	2.07	8.52	0.11	15.8	0.245	0.003	0.33	0.112
UMT094-1258	1.75	2.1	8.14	0.08	15.55	0.213	0.002	0.44	0.096
UMT094-1265	2	2.58	7.47	0.15	14.7	0.254	0.004	0.17	0.111
UMT094-1273	6.57	5.38	5.14	0.45	8.4	1.23	0.041	0.41	0.097
UMT094-1277	1.5	2.11	9.05	0.08	15.55	0.194	0.002	0.33	0.11
UMT094-1282	2.73	2.63	8.31	0.05	14.45	0.4	0.004	0.16	0.108
UMT094-1285	1.67	1.92	9.52	0.1	15.1	0.256	0.012	0.94	0.136
UMT094-1286	1.79	6.98	7.92	0.08	13.4	0.219	0.004	0.62	0.166
UMT094-1288	2.9	12.9	5.68	0.03	8.73	0.304	0.01	0.6	0.217
UMT094-1289	4.15	12.6	5.22	0.14	8.11	0.422	0.009	0.39	0.215
UMT094-1291A	3.58	13.05	4.86	0.07	8.57	0.514	0.002	0.5	0.168
UMT094-1291B	2.65	4.21	9.67	0.03	17.05	0.167	0.003	0.57	0.057
UMT094-1292A	11.8	10	2.56	0.41	0.7	1.515	0.002	1.09	0.025
UMT094-1292B	10.85	8.84	1.77	0.25	2.37	1.505	0.002	0.01	0.034
UMT094-1294	11.35	9.35	1.18	0.23	1.17	1.64	0.002	<0.01	0.028
UMT094-1296	10.4	7.84	3.31	0.17	4.59	1.325	0.002	0.24	0.047
UMT094-1300	9.99	7.61	3.16	0.13	5.16	1.275	0.003	0.03	0.053
UMT094-1311	8.17	6.07	5.37	0.23	7.01	1.17	0.005	0.56	0.101
UMT094-1319	4.44	4.01	7.36	0.12	12	0.561	0.003	0.2	0.097
UMT094-1325A	3	3.35	8.6	0.09	13.15	0.384	0.007	0.34	0.105
UMT094-1325B	6.39	5.34	5.39	0.11	8.42	0.912	0.005	0.02	0.086
UMT094-1326A	3.03	3.42	7.92	0.07	12.65	0.37	0.009	0.08	0.114
UMT094-1326B	2.5	2.78	8.67	0.02	14.6	0.246	<0.001	0.49	0.076
UMT094-1327	3.81	3.63	7.6	0.09	12.65	0.529	0.004	0.07	0.102
UMT094-1329	2.46	3.03	8.6	0.04	15.35	0.287	0.002	0.18	0.091
UMT094-1332	3.31	3.47	7.5	0.09	12.65	0.479	0.003	0.28	0.094
UMT094-1335	3.55	11.45	6.3	0.07	9.84	0.228	0.005	1.21	0.208
UMT094-1336	4.07	3.73	8.28	0.12	13.35	0.512	0.003	0.45	0.066
UMT094-1337	2.65	2.61	9.81	0.05	13.75	0.328	0.002	0.9	0.116
UMT094-1339	1.92	2.55	8.93	0.06	14.75	0.235	0.006	0.09	0.123
UMT094-1340	2.89	3.46	7.84	0.08	13.2	0.378	0.001	0.15	0.1
UMT094-1343	3.14	3.15	8.01	0.06	13.75	0.368	0.002	0.03	0.104
UMT094-1351	3.1	3.64	8.69	0.06	15	0.4	0.003	0.07	0.081
UMT094-1365	1.59	5.18	8.14	0.01	16.5	0.09	0.004	0.54	0.099
UMT094-1384	4.01	5.04	6.73	0.1	14.75	0.343	0.005	0.42	0.132
UMT094-1402	2.44	6.67	6.84	0.14	11.75	0.154	0.003	0.46	0.191

Table 3B-2 Trace Elements (ME-MS61L).

D.L. ppm	Ag	As	Ba	Be	Bi	Cd	Ce	Co	Cr	Cs	Cu	Ga	Ge	Hf	In
	0.002	0.05	1	0.02	0.005	0.005	0.01	0.005	0.3	0.01	0.02	0.05	0.05	0.004	0.005
UMT094-1096	0.021	0.45	126	0.37	0.009	0.032	9.17	32.4	323	0.22	26.5	16.35	<0.05	0.705	0.022
UMT094-1111	0.034	0.46	117	0.42	0.006	0.042	11.05	39.6	447	0.26	32.9	15.15	0.08	0.661	0.021
UMT094-1135	0.028	0.53	98	0.46	0.011	0.042	10.05	40.7	352	0.53	30.7	15.15	0.05	0.728	0.018
UMT094-1165	0.064	1.34	111	0.38	0.083	0.117	9.16	42.8	402	0.67	22.2	14.8	0.05	0.574	0.028
UMT094-1184	0.018	0.2	78	0.26	<0.005	0.028	3.85	29.8	241	0.05	12	16.85	0.06	0.233	0.017
UMT094-1213	0.029	0.5	79	0.29	0.006	0.043	4.74	28.9	188.5	0.13	26.7	16.55	<0.05	0.335	0.009
UMT094-1218	0.025	0.19	58	0.29	0.011	0.035	4.99	44.9	747	0.3	30	12.9	<0.05	0.198	0.018
UMT094-1226	0.014	0.34	177	0.25	0.012	0.026	2.76	15.95	211	0.42	28.1	19.1	<0.05	0.158	0.011
UMT094-1228	0.021	0.35	29	0.2	0.014	0.061	5.03	89.4	1630	0.43	39.9	6.85	0.08	0.378	0.027
UMT094-1232	0.455	0.1	24	0.11	0.201	0.125	2.93	115	2060	0.84	1010	6.07	0.1	0.202	0.028
UMT094-1233	0.603	0.2	59	0.16	0.885	0.169	4.02	123	1960	0.57	1350	6.71	0.12	0.226	0.033
UMT094-1238	0.34	0.36	46	0.22	0.235	0.116	6.25	101	2030	0.74	812	6.58	0.1	0.327	0.03
UMT094-1245	0.111	0.24	66	0.13	0.039	0.069	2.72	84.7	1880	0.88	351	6.41	0.07	0.156	0.02
UMT094-1252	0.155	0.24	39	0.16	0.092	0.087	5.01	96.7	1910	0.55	456	5.56	0.08	0.335	0.026
UMT094-1254	0.185	0.88	30	0.14	0.199	0.126	4.12	112	2370	1.05	675	5.12	0.1	0.33	0.028
UMT094-1258	0.261	0.43	28	0.09	0.179	0.132	3	114	2640	0.81	928	4.86	0.1	0.246	0.025
UMT094-1265	0.139	0.44	42	0.14	0.089	0.106	4.96	96	2300	1.02	392	5.02	0.08	0.363	0.028
UMT094-1273	0.277	2.1	189	0.29	0.455	0.113	13.15	74.9	1110	1.15	931	10.2	0.07	0.357	0.025
UMT094-1277	0.255	0.33	29	0.12	0.214	0.165	2.82	107.5	2150	1.07	565	4.87	0.11	0.255	0.031
UMT094-1282	0.2	0.23	17	0.15	0.079	0.117	3.5	101	4840	1.88	592	6.4	0.08	0.186	0.029
UMT094-1285	0.716	0.56	34	0.12	0.738	0.244	5.44	146	3840	1.04	1880	5.39	0.12	0.445	0.037
UMT094-1286	0.479	0.32	41	0.13	0.346	0.172	9.91	123.5	2450	0.72	1140	5.18	0.1	0.799	0.038
UMT094-1288	0.492	0.62	16	0.25	0.313	0.29	15.3	80.9	5440	0.36	1220	8.26	0.09	1.33	0.033
UMT094-1289	0.512	0.67	57	0.33	0.351	0.265	17.15	69.9	4140	0.66	1150	8.89	0.1	1.505	0.038
UMT094-1291A	0.525	0.51	35	0.15	0.323	0.229	8.72	66.9	2580	0.55	1430	7.38	0.09	0.72	0.038
UMT094-1291B	0.456	0.31	12	0.04	0.371	0.122	2.16	173.5	2090	0.75	1360	4.23	0.12	0.276	0.02
UMT094-1292A	1.33	0.28	144	0.15	1.015	0.296	1.64	79.7	261	0.42	2680	17.55	0.12	0.095	0.022
UMT094-1292B	0.031	0.2	114	0.13	0.015	0.037	1.49	19.35	488	0.31	40.9	17.75	<0.05	0.102	<0.005
UMT094-1294	0.03	0.48	94	0.16	0.008	0.029	1.43	11.2	271	0.31	26.6	18.7	<0.05	0.092	0.005
UMT094-1296	0.318	0.3	73	0.17	0.154	0.09	2.69	50.2	881	0.41	710	15.7	0.05	0.147	0.014
UMT094-1300	0.035	0.21	61	0.17	0.02	0.039	2.68	35.2	1155	0.27	79.8	14.85	0.07	0.156	0.01
UMT094-1311	0.691	0.56	86	0.27	0.552	0.198	6.97	83.6	4140	0.53	1150	13.4	0.09	0.314	0.028
UMT094-1319	0.209	0.39	44	0.15	0.218	0.115	4.42	89	2750	0.6	516	8.15	0.06	0.293	0.022
UMT094-1325A	0.337	0.38	50	0.13	0.413	0.178	3.87	105	2070	0.65	706	6.32	0.08	0.342	0.031
UMT094-1325B	0.03	0.18	56	0.19	0.04	0.051	3.85	63.2	1955	0.16	88.1	10.5	0.05	0.175	0.017
UMT094-1326A	0.129	0.4	32	0.15	0.227	0.103	4.86	102.5	3040	1.04	281	6.98	0.07	0.405	0.03
UMT094-1326B	0.504	0.15	13	0.04	0.402	0.165	0.97	117	2880	0.15	1180	5.32	0.08	0.1	0.023
UMT094-1327	0.133	0.15	48	0.18	0.074	0.079	4.64	87.9	3050	0.2	238	7.39	0.06	0.289	0.026
UMT094-1329	0.19	0.18	21	0.07	0.225	0.116	2.09	103.5	2440	0.12	439	5.51	0.08	0.2	0.029

Table 3B-2 Trace Elements (ME-MS61L) continued.

D.L. ppm	Ag	As	Ba	Be	Bi	Cd	Ce	Co	Cr	Cs	Cu	Ga	Ge	Hf	In
	0.002	0.05	1	0.02	0.005	0.005	0.01	0.005	0.3	0.01	0.02	0.05	0.05	0.004	0.005
UMT094-1332	0.257	0.47	47	0.15	0.296	0.116	3.76	96.6	1930	0.19	572	6.38	0.07	0.234	0.02
UMT094-1335	0.598	0.59	48	0.11	0.582	0.287	11.85	90.5	1440	0.53	1680	8.07	0.11	1.735	0.052
UMT094-1336	1.325	0.26	31	0.11	0.625	0.181	1.95	126	2360	0.71	957	7.9	0.09	0.147	0.024
UMT094-1337	0.776	0.27	24	0.09	0.73	0.287	2.1	145	8770	0.25	1680	7.56	0.1	0.194	0.037
UMT094-1339	0.171	0.19	24	0.1	0.166	0.132	2.76	105	6010	0.37	277	6.15	0.07	0.256	0.03
UMT094-1340	0.149	0.14	30	0.11	0.144	0.123	2.64	89.4	5140	0.46	354	6.82	0.07	0.211	0.024
UMT094-1343	0.083	0.14	27	0.09	0.058	0.071	2.34	91.1	6320	0.27	143.5	7.35	0.08	0.179	0.025
UMT094-1351	0.115	0.33	33	0.11	0.057	0.084	2.98	111.5	3970	0.08	241	6.19	0.09	0.224	0.019
UMT094-1365	0.18	0.28	9	0.13	0.214	0.135	6.68	97.4	6940	0.14	542	4.08	0.08	0.608	0.025
UMT094-1384	0.247	0.73	54	0.14	0.495	0.226	6.6	71.6	111.5	0.45	496	11	0.06	0.916	0.039
UMT094-1402	0.172	0.67	29	0.11	0.24	0.09	9.51	79.7	7900	1.11	514	9.91	0.09	1.215	0.036

Table 3B-3. Trace Elements (ME-MS61L).

D.L. ppm	La	Li	Mn	Mo	Nb	Ni	Pb	Rb	Re	Sb	Sc	Se	Sn	Sr	Ta
	0.005	0.2	0.2	0.02	0.005	0.08	0.01	0.02	0.002	0.02	0.01	0.2	0.02	0.02	0.01
UMT094-1096	4.69	8.5	719	0.45	1.38	151.5	2.75	3.32	<0.002	0.07	11.8	<0.2	0.36	269	0.1
UMT094-1111	5.61	8.2	841	0.31	0.965	197.5	2.08	4.38	<0.002	0.06	17.2	<0.2	0.29	242	0.08
UMT094-1135	4.99	11.6	839	0.44	2.08	177	2.6	10.15	<0.002	0.19	14.45	<0.2	0.37	259	0.15
UMT094-1165	4.59	14.3	1020	0.48	0.927	204	20.1	7.73	<0.002	0.23	15.25	<0.2	0.28	252	0.06
UMT094-1184	1.97	4.6	631	0.33	0.242	134	1.53	0.19	<0.002	0.03	11.55	<0.2	0.13	287	0.02
UMT094-1213	2.25	3.9	638	0.33	0.614	122	1.9	1.11	<0.002	0.07	9.48	<0.2	0.18	293	0.05
UMT094-1218	2.69	6.3	883	0.32	0.199	276	1.52	2.65	<0.002	0.05	12.85	<0.2	0.16	239	0.02
UMT094-1226	1.305	9.1	334	0.43	0.201	91.8	2.31	2.09	<0.002	0.14	4.73	<0.2	0.2	305	0.01
UMT094-1228	2.55	7.9	1650	0.39	0.4	581	2.44	2.07	<0.002	0.1	28.7	<0.2	0.24	61.6	0.03
UMT094-1232	1.36	9.1	1715	0.23	0.095	2460	2.68	1.84	0.005	0.22	31.7	2.4	0.3	55.5	<0.01
UMT094-1233	2.05	7.9	1460	0.28	0.13	3440	4.6	5.3	0.007	0.09	25	3.6	0.3	113	0.01
UMT094-1238	2.98	5.9	1480	0.35	0.374	1800	2.88	8.26	0.003	0.06	27.5	1.5	0.24	65.5	0.03
UMT094-1245	1.425	6.1	1575	0.35	0.125	862	2.29	10.2	<0.002	0.05	24	0.3	0.16	78.9	0.01
UMT094-1252	2.47	8.2	1560	0.25	0.351	1300	2.08	6.14	0.003	0.08	27.3	0.7	0.25	44.6	0.02
UMT094-1254	2.06	5.8	1695	0.47	0.403	1800	4.65	6.52	0.004	0.11	28.5	1.6	0.41	25.3	0.03
UMT094-1258	1.48	6.9	1605	0.15	0.215	2180	3.03	4.12	0.004	0.08	27.6	2	0.27	27.8	0.01
UMT094-1265	2.26	6.1	1540	0.2	0.33	1265	3.36	8.6	0.003	0.13	29.1	0.5	0.27	34.1	0.02
UMT094-1273	6.75	10.2	1050	0.55	0.981	1680	7.61	23.5	0.004	0.16	21.5	2.4	0.47	192	0.07
UMT094-1277	1.22	5.7	1705	0.24	0.204	1695	5.08	3.59	0.002	0.11	30.7	1.2	0.32	25.2	0.02
UMT094-1282	1.815	16.2	1615	0.27	0.274	1620	4.22	3.64	0.003	0.06	26.6	1	0.26	62.1	0.02
UMT094-1285	2.87	6.2	1630	0.42	0.918	3940	9.95	6.56	0.009	0.11	25.8	4.2	0.52	31.8	0.06
UMT094-1286	3.38	7.3	1345	0.24	0.186	2750	9.74	3.4	0.004	0.11	29.4	2.2	0.62	45.8	0.02
UMT094-1288	6.26	10.5	1225	0.27	0.454	2150	5.52	1.65	0.005	0.12	42.8	2.4	0.56	116.5	0.06
UMT094-1289	6.91	14.2	1080	0.3	0.695	2300	20.8	6.63	0.004	0.19	36.5	2.9	0.63	186.5	0.05
UMT094-1291A	3.53	10.1	987	0.23	0.275	2120	7.66	2.68	0.004	0.06	38.5	2	0.49	118	0.02
UMT094-1291B	0.88	2.7	1110	0.21	0.123	3570	3.64	1.46	0.003	0.04	9.58	2.1	0.27	71.7	0.02
UMT094-1292A	0.774	6.1	232	0.34	0.163	3880	11.75	4.08	0.011	0.07	2.17	4.2	0.47	499	0.01
UMT094-1292B	0.717	4.1	370	0.31	0.178	111	2.64	1.16	<0.002	0.09	4.3	<0.2	0.12	405	0.02
UMT094-1294	0.677	3.5	208	0.35	0.216	66.1	2.04	1.12	<0.002	0.14	2.8	<0.2	0.14	416	0.01
UMT094-1296	1.425	3.7	618	0.34	0.208	1030	4.14	1.68	0.002	0.07	9	1	0.16	368	0.01
UMT094-1300	1.38	3.7	645	0.31	0.22	236	1.32	1.12	<0.002	0.04	10.55	<0.2	0.13	330	0.02
UMT094-1311	3.72	4.7	921	0.4	0.397	1835	8.94	11.35	0.005	0.08	19	1.6	0.35	275	0.03
UMT094-1319	2.24	4.6	1485	0.24	0.282	1140	6.14	5.81	<0.002	0.29	27.9	0.5	0.29	118.5	0.02
UMT094-1325A	1.85	3.4	1615	0.25	0.474	1745	6.84	5.08	<0.002	0.07	28.1	1.2	0.3	78.9	0.03
UMT094-1325B	2	2.9	1130	0.29	0.179	437	1.48	2.01	<0.002	0.05	19.35	<0.2	0.15	209	0.01
UMT094-1326A	2.24	7.9	1525	0.3	0.423	991	3.36	4.5	<0.002	0.06	30.2	<0.2	0.25	62.9	0.03
UMT094-1326B	0.45	2.6	1650	0.29	0.069	2030	3.81	0.51	0.004	0.05	29	1.9	0.21	52.6	0.01
UMT094-1327	2.42	3.7	1540	0.22	0.279	729	2.2	2.75	<0.002	0.06	28.1	<0.2	0.17	105.5	0.02
UMT094-1329	0.97	3.4	1705	0.28	0.171	1000	2.36	1.12	0.002	0.04	28.7	0.4	0.16	52.7	0.01

Table 3B-3. Trace Elements (ME-MS61L) continued.

D.L. ppm	La 0.005	Li 0.2	Mn 0.2	Mo 0.02	Nb 0.005	Ni 0.08	Pb 0.01	Rb 0.02	Re 0.002	Sb 0.02	Sc 0.01	Se 0.2	Sn 0.02	Sr 0.02	Ta 0.01
UMT094-1332	1.92	4.1	1480	0.23	0.258	1320	3.3	2.75	0.003	0.05	27.6	0.7	0.16	96	0.02
UMT094-1335	4.19	5.9	986	0.27	0.35	2100	12	3.87	0.002	0.09	24.5	2	0.88	74.2	0.04
UMT094-1336	1.05	5.7	1360	0.2	0.116	1700	6.37	4.17	0.004	0.06	20.8	1.2	0.25	126	0.01
UMT094-1337	1.06	2.8	1650	0.25	0.18	2820	8.88	1.62	0.006	0.05	27.6	2.5	0.34	62.2	0.01
UMT094-1339	1.295	4.1	1720	0.15	0.268	823	3.5	2.63	<0.002	0.04	30.7	<0.2	0.21	40.6	0.02
UMT094-1340	1.215	4.7	1525	0.19	0.163	787	3.27	3.18	<0.002	0.03	26.7	<0.2	0.15	72.7	0.01
UMT094-1343	1.135	3.6	1590	0.18	0.157	526	2.06	1.69	<0.002	0.03	23.3	<0.2	0.14	81.7	0.01
UMT094-1351	1.39	5.5	1580	0.25	0.247	1105	1.94	1.63	<0.002	0.05	20.4	<0.2	0.13	97.4	0.02
UMT094-1365	2.89	4	1225	0.19	0.534	858	4.9	0.54	<0.002	0.09	9.42	0.3	0.44	33.1	0.06
UMT094-1384	2.89	8.4	1040	0.12	0.389	573	4.91	3.05	<0.002	0.17	14.25	0.6	0.41	116.5	0.04
UMT094-1402	3.42	3.4	876	0.21	0.365	764	3.8	12.8	<0.002	0.18	15.2	0.3	0.6	37	0.04

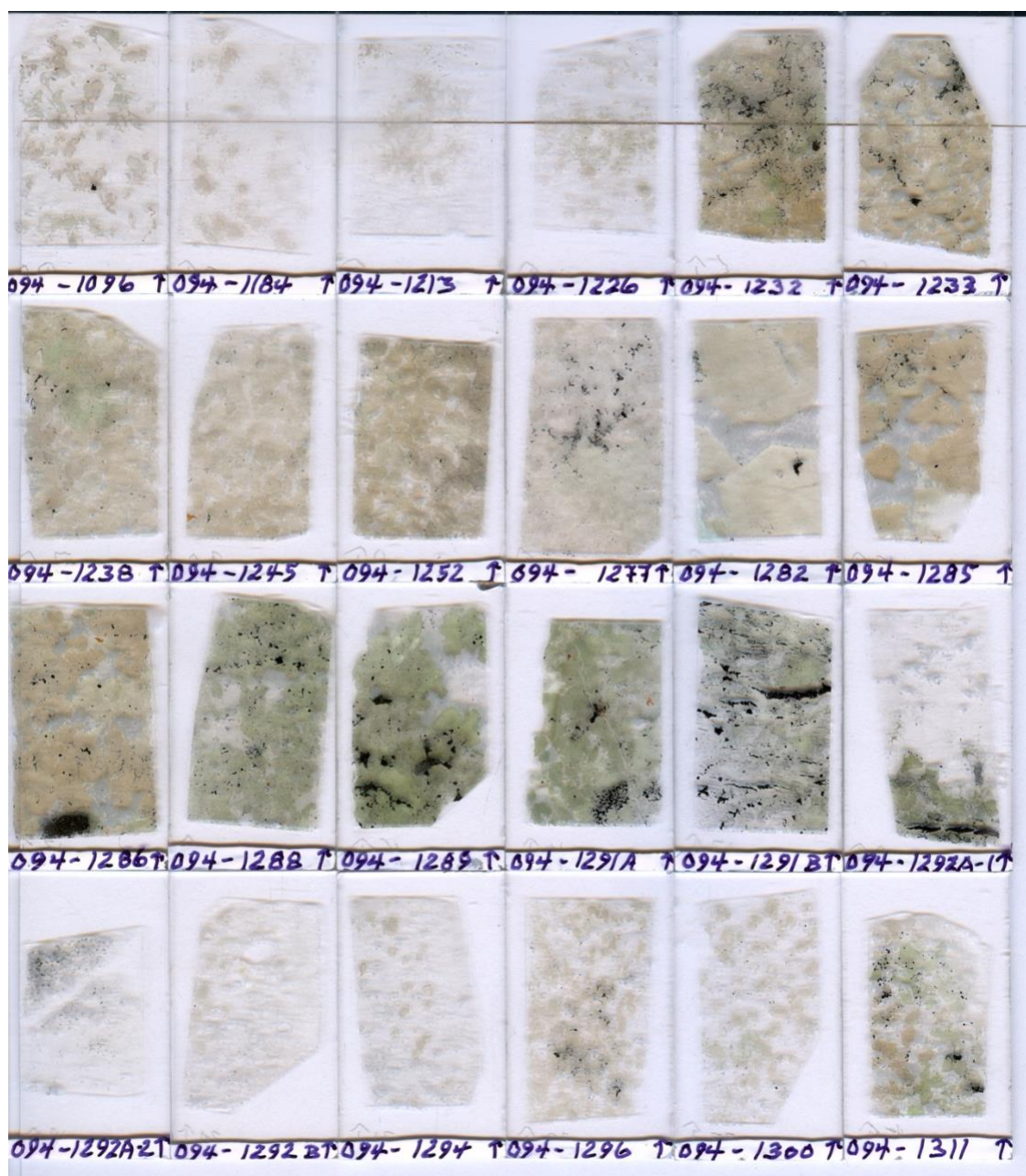
Table 3B-4. Trace Elements (ME-MS61L).

D.L. ppm	Te	Th	Tl	U	V	W	Y	Zn	Zr
	0.04	0.004	0.004	0.01	0.1	0.008	0.01	0.2	0.1
UMT094-1096	<0.04	0.869	0.049	0.3	89.3	0.118	4.46	46	25
UMT094-1111	<0.04	0.784	0.035	0.2	109.5	0.256	6.55	53.4	23.4
UMT094-1135	<0.04	1.375	0.099	0.45	101.5	0.142	5.95	55.6	28
UMT094-1165	<0.04	0.626	0.078	0.18	102.5	0.241	5.07	91.9	20.2
UMT094-1184	<0.04	0.197	0.01	0.06	81.1	0.029	2.52	40.4	8.3
UMT094-1213	<0.04	0.313	0.043	0.11	73.9	0.058	3.06	40.9	12.1
UMT094-1218	<0.04	0.225	0.027	0.07	75.4	0.029	3.14	52.3	7
UMT094-1226	<0.04	0.077	0.107	0.03	33.1	0.092	1.36	25.6	5.2
UMT094-1228	<0.04	0.392	0.018	0.14	125.5	0.07	5.65	94.2	13.4
UMT094-1232	0.58	0.059	0.072	0.02	118.5	0.022	5.09	81.8	6
UMT094-1233	2.88	0.152	0.095	0.03	102.5	0.03	3.91	75.7	7.3
UMT094-1238	0.8	0.913	0.052	0.09	117	0.035	5.02	79.3	11.1
UMT094-1245	0.13	0.116	0.044	0.03	101.5	0.025	2.85	73.1	5.3
UMT094-1252	0.22	0.662	0.037	0.12	110	0.047	4.79	82.1	10.2
UMT094-1254	0.35	0.827	0.061	0.19	119	0.245	4.7	94.9	11.6
UMT094-1258	0.44	0.19	0.04	0.04	111.5	0.045	3.59	87	7.9
UMT094-1265	0.18	0.559	0.056	0.14	109	0.143	4.85	80.2	11.6
UMT094-1273	1.61	1.275	0.11	0.33	84.1	0.296	5	57.2	12.3
UMT094-1277	0.28	0.213	0.054	0.05	114.5	0.262	4.85	96.1	8.1
UMT094-1282	0.14	0.418	0.074	0.08	133	0.184	3.49	91.7	6.7
UMT094-1285	1.04	0.881	0.104	0.25	125	0.14	4.53	96.2	15.9
UMT094-1286	0.35	0.237	0.06	0.06	127	0.041	9.93	68.4	24.7
UMT094-1288	0.36	0.664	0.12	0.16	191	0.048	11.35	57.7	46.8
UMT094-1289	0.4	0.601	0.14	0.14	159	0.135	12	47.3	47.9
UMT094-1291A	0.31	0.197	0.098	0.06	151	0.048	8.61	35.1	21
UMT094-1291B	0.49	0.169	0.061	0.02	51.1	0.024	2.61	78.3	7.9
UMT094-1292A	1.02	0.081	0.409	0.02	15.5	0.029	0.65	20.1	3.3
UMT094-1292B	<0.04	0.075	0.137	0.02	25.9	0.046	0.78	26.3	4.1
UMT094-1294	<0.04	0.063	0.106	0.02	18.8	0.047	0.62	17.2	3.6
UMT094-1296	0.08	0.114	0.085	0.04	41.8	0.038	1.34	38.2	5.4
UMT094-1300	<0.04	0.113	0.037	0.04	51.7	0.027	1.51	38.4	5.7
UMT094-1311	0.32	0.384	0.086	0.1	120.5	0.074	2.95	71.1	11.5
UMT094-1319	0.3	0.239	0.048	0.07	120.5	0.109	3.53	88.3	9.6
UMT094-1325A	0.32	0.472	0.041	0.13	114	0.113	3.98	93.4	13
UMT094-1325B	<0.04	0.144	0.013	0.04	93.2	0.03	3.06	66.9	6.4
UMT094-1326A	0.13	0.498	0.036	0.13	128.5	0.063	4.4	92.7	13.4
UMT094-1326B	0.37	0.043	0.009	0.01	104.5	0.017	2.07	91.4	3.3
UMT094-1327	0.04	0.33	0.019	0.08	117.5	0.036	3.8	88.5	10.3
UMT094-1329	0.07	0.131	0.013	0.04	103	0.031	2.89	93.8	5.9
UMT094-1332	0.15	0.217	0.028	0.06	98.5	0.032	3.59	84.1	7.7
UMT094-1335	0.55	0.33	0.079	0.07	88.5	0.043	10.05	69.7	48.3
UMT094-1336	0.39	0.096	0.043	0.03	74.8	0.026	2.19	86.3	4.4
UMT094-1337	0.49	0.111	0.033	0.04	160.5	0.026	3.25	116.5	6
UMT094-1339	0.08	0.233	0.031	0.06	144	0.029	4.11	110.5	8.5
UMT094-1340	0.06	0.112	0.023	0.03	121.5	0.02	3.35	92.1	6.8
UMT094-1343	<0.04	0.122	0.016	0.03	130.5	0.021	3.11	103.5	6.1
UMT094-1351	<0.04	0.218	0.016	0.05	95.8	0.038	2.98	105.5	7.8
UMT094-1365	0.04	0.467	0.036	0.11	64.8	0.031	3.75	55.5	25.8
UMT094-1384	0.23	0.276	0.083	0.07	74.2	0.074	5.57	155	25
UMT094-1402	0.05	0.296	0.14	0.08	114.5	0.096	8.29	110.5	33.5

Table 4B. Pt-Pd-Au (PGM-MS23L, PGM-ICP27).

D.L. ppb	Au 1	Pt 0.1	Pd 0.2	D.L. ppm	Au 0.01	Pt 0.01	Pd 0.01
UMT094-1096	1	1.7	0.8				
UMT094-1111	2	0.9	0.8				
UMT094-1135	1	2.4	1.1				
UMT094-1165	2	2.7	1.1				
UMT094-1184	1	1.9	1.1				
UMT094-1213	2	16.6	1.4				
UMT094-1218	2	2.9	2.1				
UMT094-1226	2	2.4	0.5				
UMT094-1228	2	1.7	0.8				
UMT094-1232	290	603	323				
UMT094-1233	598	>1000	>1000		1.23	1.46	1.27
UMT094-1238	229	538	217				
UMT094-1245	52	90.3	26.9				
UMT094-1252	126	326	119				
UMT094-1254	213	>1000	>1000		0.18	1.44	1.18
UMT094-1258	144	>1000	>1000		0.14	1.25	1.1
UMT094-1265	78	630	664				
UMT094-1273	111	>1000	>1000		NSS	NSS	NSS
UMT094-1277	115	>1000	>1000		0.14	1.06	1.08
UMT094-1282	40	287	311				
UMT094-1285	294	>1000	>1000		0.36	1.76	2.03
UMT094-1286	155	956	946				
UMT094-1288	139	699	615				
UMT094-1289	130	>1000	>1000		0.17	0.93	1.03
UMT094-1291A	188	969	>1000		0.2	0.91	1.06
UMT094-1291B	190	979	944				
UMT094-1292A	347	877	769				
UMT094-1292B	2	113.5	39.5				
UMT094-1294	2	47.3	6.7				
UMT094-1296	20	46.4	63.4				
UMT094-1300	4	65.3	29.1				
UMT094-1311	102	581	657				
UMT094-1319	110	488	432				
UMT094-1325A	143	>1000	910		0.13	1.06	0.86
UMT094-1325B	11	55.7	36.6				
UMT094-1326A	63	483	313				
UMT094-1326B	97	>1000	921		0.1	1.29	0.92
UMT094-1327	12	115.5	173.5				
UMT094-1329	25	312	263				
UMT094-1332	63	290	354				
UMT094-1335	380	724	854				
UMT094-1336	207	>1000	>1000		0.25	1.57	1.57
UMT094-1337	240	>1000	>1000		0.19	3.17	2.11
UMT094-1339	30	250	203				
UMT094-1340	22	137.5	149.5				
UMT094-1343	6	22.4	19.7				
UMT094-1351	12	58.4	71.4				
UMT094-1365	16	173.5	194				
UMT094-1384	63	96.3	198.5				
UMT094-1402	18	203	307				

Appendix C: Thin section descriptions



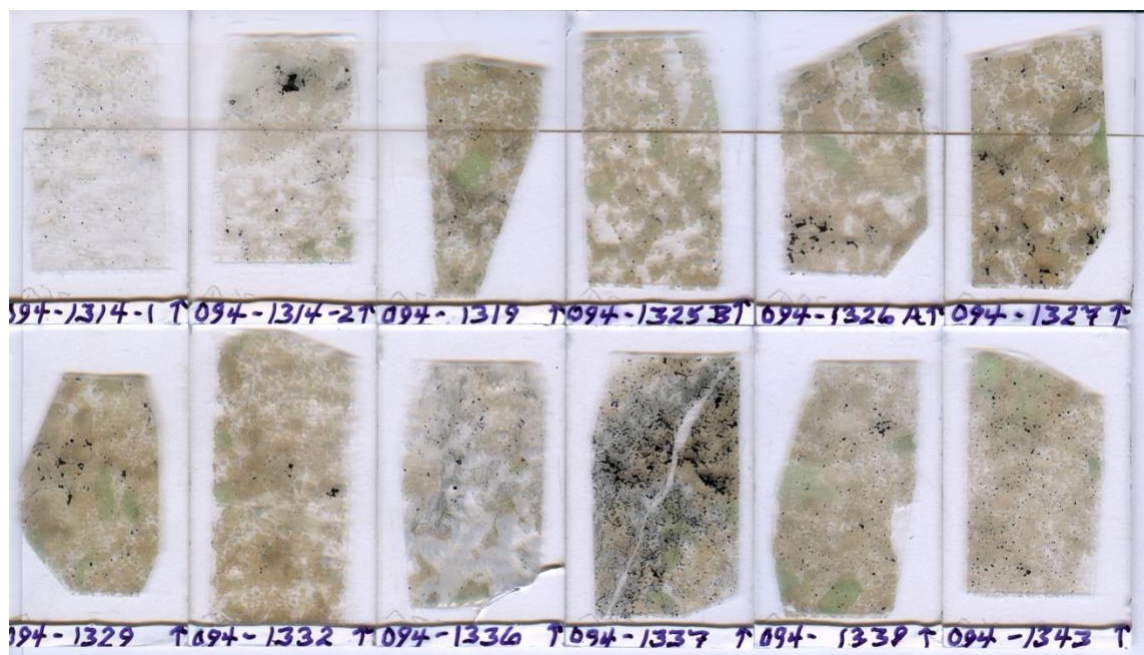


Figure C 1. Scanned thin sections associated with thin section descriptions below.

Table C 1. Thin section mineralogy of individual samples.

Thin Section	Main Minerals					Sulfides				Alteration Minerals						
	Opx	Cpx	Pl	Ol	Chr	Po	Ccp	Pn	Py	Mag	Bt	Amp	WM	Chl	Srp	Cal
094-1096	30	15	55	-	-	tr	tr	-	tr	tr	tr	-	tr	-	-	-
094-1184	30	5	65	-	-	-	tr	-	tr	tr	-	-	tr	-	-	-
094-1213	25	3	70	-	-	tr	tr	-	tr	tr	tr	-	2	-	-	-
094-1226	20	20	57	-	-	tr	tr	-	tr	-	-	-	3	-	-	-
094-1232	52	18	16	5	1	1	2	tr	-	tr	1	-	4	tr	-	-
094-1233	63	5	25	-	-	1	2	tr	-	tr	tr	-	4	-	-	-
094-1238	64	15	15	-	-	1	1	tr	-	tr	1	-	3	-	-	-
094-1245	72	3	20	-	-	tr	tr	-	-	tr	1	-	4	tr	-	-
094-1252	71	10	15	-	-	1	tr	tr	-	tr	1	-	2	-	-	-
094-1277	73	8	10	-	tr	2	1	tr	-	tr	1	tr	4	1	-	-
094-1282	65	10	17	-	-	1	1	tr	-	tr	tr	-	5	1	-	-
094-1285	10	45	25	-	tr	1	tr	tr	-	tr	1	-	15	3	-	2
094-1286	56	20	10	-	1	-	2	2	-	tr	tr	-	8	1	-	tr
094-1288	5	56	20	-	3	2	1	tr	-	tr	1	-	12	tr	-	-
094-1289	1	67	20	-	1	1	2	2	-	tr	tr	-	6	tr	-	-
094-1291A	5	71	15	-	2	1	1	tr	-	tr	2	-	3	tr	-	tr
094-1291B	3	15	8	20	1	1	1	1	-	3	tr	-	3	-	44	-
094-1292A-1	2	15	61	10	tr	tr	tr	-	-	2	-	-	2	-	8	-
094-1292A-2	4	1	91	-	-	1	tr	tr	-	-	-	-	2	1	-	-
094-1292B	12	5	81	-	-	tr	tr	-	-	-	-	-	2	-	-	-
094-1294	8	4	87	-	tr	tr	tr	-	-	-	-	-	1	tr	-	-
094-1296	40	5	50	-	tr	1	1	tr	-	-	tr	-	3	-	-	-
094-1300	30	5	63	-	1	tr	tr	-	-	-	-	-	1	-	-	-
094-1311	10	40	44	-	2	1	tr	tr	-	tr	tr	-	3	-	-	-
094-1314-1	15	2	80	-	1	tr	tr	-	tr	tr	tr	-	2	-	-	-
094-1314-2	55	5	36	-	1	1	1	tr	tr	-	tr	tr	1	-	-	-
094-1319	57	18	20	-	1	tr	1	tr	-	-	1	-	2	-	-	-
094-1325B	38	25	35	-	1	tr	tr	-	-	-	tr	-	1	tr	-	-
094-1326A	51	25	20	-	tr	1	1	1	-	-	tr	-	1	-	-	-
094-1327	48	30	15	-	2	1	1	1	-	tr	tr	-	2	-	-	-
094-1329	43	35	20	-	tr	1	tr	tr	tr	tr	tr	-	1	-	-	-
094-1332	63	20	15	-	tr	1	tr	tr	-	tr	tr	-	1	-	-	-
094-1336	30	4	38	20	tr	1	tr	tr	-	tr	tr	-	5	-	2	-
094-1337	31	7	20	25	8	2	1	1	-	1	tr	-	2	-	2	-
094-1339	61	16	18	-	2	1	tr	tr	-	-	tr	-	2	-	-	-
094-1343	60	15	20	-	5	tr	tr	-	-	-	tr	-	tr	-	-	-

Amp = Amphibole, Bt = Biotite, Cal = Calcite, Ccp = Chalcopyrite, Chl = Chlorite, Chr = Chromite, Cpx = Clinopyroxene, Mag = Magnetite, Ol = Olivine, Opx = Orthopyroxene, Pl = Plagioclase, Pn = Pentlandite, Po = Pyrrhotite, Py = Pyrite, Srp = Serpentine, tr = trace and WM = White Mica.

Table C 2. Thin section rock classification, mineral textures and alteration in individual samples.

Thin Section	Rock Classification		Mineral Textures				Alteration				
	Rock Type	Color Index	Pl	Opx	Cpx	Ol	Amp	Cal	Chl	WM	Srp
094-1096	Gabbronorite	Meso	A	O	H	-	-	-	-	VW	-
094-1184	Norite to Gabbronorite	Leuco-Meso	A	O	H	-	-	-	-	VW	-
094-1213	Norite	Leuco	A	H	H	-	-	-	-	M	-
094-1226	Gabbronorite	Meso	A	O	H	-	-	-	-	M	-
094-1232	Olivine Gabbronorite	Mela	H	C	C	C	-	-	W	S	-
094-1233	Gabbronorite to Norite	Mela	H	C	C	-	-	-	-	M	-
094-1238	Gabbronorite	Mela	H	C	C/P	-	-	-	-	M	-
094-1245	Norite	Mela	H	C	C	-	-	-	-	M-S	-
094-1252	Gabbronorite	Mela	H	C	C	-	-	-	-	M	-
094-1277	Orthopyroxenite - Gabbronorite	Mela	I	C	H/P	-	W	-	S	M-S	-
094-1282	Pegmatitic Gabbronorite	Mela	I	C	C	-	-	-	W	S	-
094-1285	Gabbronorite	Mela	I	-	C	-	-	W	W	VS	-
094-1286	Gabbronorite/Pyroxenite	Mela	I	C	C	-	-	W	S	S	-
094-1288	Gabbronorite	Mela	I	A	A	-	-	-	W	S	-
094-1289	Gabbro to Gabbronorite	Mela	I	C	A	-	-	-	W	S	-
094-1291A	Gabbro to Gabbronorite	Mela	I	C	A/H	-	-	-	-	M	-
094-1291B	Olivine Gabbronorite - Olivine Norite	Mela	I/C	C	A	C	-	-	-	M	VS
094-1292A-1	Olivine Gabbronorite/Anorthosite	Meso	I/A	I	H	C	-	-	-	W	VS
094-1292A-2	Anorthosite	Leuco	A	I	I	-	-	-	-	W	-
094-1292B	Gabbronorite to Norite	Leuco	A	C	I	-	-	-	-	M	-
094-1294	Norite	Leuco	A	C	I	-	-	-	-	M	-
094-1296	Norite to Gabbronorite	Meso	A	C	I	-	-	-	-	M	-
094-1300	Gabbronorite	Meso	A	C/I	I	-	-	-	-	W	-
094-1311	Gabbronorite	Meso	A	C/A	A/I	-	-	-	-	M-S	-
094-1314-1	Norite	Leuco	C/A	C	I	-	-	-	-	M	-
094-1314-2	Norite - Gabbronorite	Meso	A/I	C	I	-	W	-	-	M	-
094-1319	Gabbronorite	Mela	H/I	C	I/H	-	-	-	-	M-S	-
094-1325B	Gabbronorite	Meso-Mela	A	C	H	-	-	-	-	M	-
094-1326A	Gabbronorite	Mela	H	C	C/H	-	-	-	-	M	-
094-1327	Gabbronorite	Mela	H	C	C/H	-	-	-	-	M	-
094-1329	Gabbronorite	Mela	H	C	C/H	-	-	-	-	W	-
094-1332	Gabbronorite	Mela	H	C	A	-	-	-	-	W-M	-
094-1336	Olivine Norite	Meso	H	H/C	H	C	-	-	-	S	W
094-1337	Olivine Gabbronorite	Mela	H	C	A	C	-	-	-	W	W
094-1339	Gabbronorite	Mela	H	C	C/P	-	-	-	-	W	-
094-1343	Gabbronorite	Mela	H	C	H	-	-	-	-	W	-

Leuco = Leucocratic, Meso = Mesocratic, Mela = Melanocratic, A = Adcumulate, C = Cumulate, H = Heteradcumulate, I = Intercumulate, O = Orthocumulate, P = Poikilitic, VW = Very Weak, W = Weak, M = Moderate, S = Strong, VS = Very Strong, Amp = Amphibole Cal = Calcite, Chl = Chloritization, Srp = Serpentinization and WM = White Mica.

Curriculum Vitae

Name: Cedric Mayer

Post-secondary Education and Degrees:

Laurentian University, Sudbury, Ontario Canada, 2011-2015 H.B.Sc.

Laurentian University, Sudbury, Ontario Canada, 2016-2018 M.Sc.

Honours and Awards:

Dennis David Travioli Memorial Scholarship, Undergraduate Scholarship, 2014

Pada Memorial Scholarship, Undergraduate Scholarship, 2014

Queen Elizabeth II Diamond Jubilee Scholarship, Graduate Scholarship – 8000\$, 2016 January-July

Ivanplats – an Ivanhoe Mines company, Graduate Scholarship – 70 000\$, 2016-2018

Related Work Experience:

Lecturer (Geochemistry), University of Limpopo, 2016 January-March

Teaching Assistant, Laurentian University, 2016-2018

Publications:

C.C. Mayer, P.J. Jugo, M.I. Leybourne (2017). Strontium isotope stratigraphy of the Platreef: a tool for correlation with the rest of the Bushveld Igneous Complex. Extended Abstract, 14th SGA Biennial Meeting 2017, Volume 2, p. 547-550.

C. Mayer, P.J. Jugo, M. Leybourne (2017). Strontium isotope stratigraphy of the Platreef: a tool for correlation with the rest of the Bushveld Igneous Complex. Poster Abstract, PDAC-SEG Student Minerals Colloquium 2017.

B. Azar, S.A. Ferguson, C. Mayer (2016). Precambrian Geology of the Attwood Lake Area, Fort Hope Greenstone Belt; Ontario Geological Survey, Preliminary Map P.3800, scale 1:50 000.

M. Duguet, Q. Duparc, C. Mayer (2015). Geology and Mineral Potential of the Centennial Lake Area, Northeastern Central Metasedimentary Belt, Grenville Province; Ontario Geological Survey, Open File Report 6313.19.

C. Mayer, M. Lesher, B. Azar (2015). Geochemistry and Petrogenesis of the Weese Lake Mafic Intrusion in the Fort Hope Greenstone Belt, Uchi Subprovince, and Its Relationship to Regional Mafic Intrusions. Poster Abstract, PDAC-SEG Student Colloquium 2015.